Optimal processes in Stochastic Thermodynamics

Von der Fakultät Mathematik und Physik der Universität Stuttgart
zur Erlangung der Würde eines Doktors der
Naturwissenschaften (Dr. rer. nat.) genehmigte Abhandlung

vorgelegt von

Tim Schmiedl

aus Zweibrücken

Hauptberichter: Prof. Dr. Udo Seifert
Mitberichter: Prof. Dr. Günter Mahler

Tag der mündlichen Prüfung: 29.04.2009

II. Institut für Theoretische Physik der Universität Stuttgart
2009

Ehrenwörtliche Erklärung

Ich erkläre, dass ich diese Arbeit selbständig verfasst und keine anderen als die angegebenen Quellen und Hilfsmittel benutzt habe.

Stuttgart, 30. April 2009 Tim Schmiedl

Contents

Summary **7**

Zusammenfassung **15**

1 Introduction **25**

2 Stochastic Thermodynamics **31**

3 Optimal protocols **35**

- 3.1 Introduction 35
- 3.2 Overdamped Langevin dynamics 38
  - 3.2.1 The model 38
  - 3.2.2 Case study I: Moving harmonic potential 39
  - 3.2.3 Case study II: Harmonic potential with time-dependent stiffness 43
  - 3.2.4 General case 46
- 3.3 Underdamped Langevin dynamics 48
  - 3.3.1 Case Study I: Moving harmonic potential 49
  - 3.3.2 Case Study II: Harmonic potential with time-dependent stiffness 53
  - 3.3.3 Discussion 57
- 3.4 Hamiltonian dynamics 58
  - 3.4.1 Case Study I: Moving harmonic potential 58
  - 3.4.2 Case Study II: Harmonic potential with time-dependent stiffness 60
  - 3.4.3 Quartic anharmonic potential 63
- 3.5 Quantum Systems 64
  - 3.5.1 Case Study I: Moving harmonic potential 65
  - 3.5.2 Case Study II: Harmonic potential with time-dependent frequency 66
  - 3.5.3 Two-level system 68
- 3.6 Benefits for free energy reconstruction 70

3.6.1 Harmonic potentials 71
3.6.2 Anharmonic potentials 71
3.6.3 Sampling of initial conditions 74
3.6.4 Discussion 77

4 Optimization of Brownian motors 81
4.1 Introduction 81
4.2 Cyclic Brownian heat engine 83
4.2.1 The model 84
4.2.2 Example 87
4.2.3 General Case 90
4.2.4 Role of kinetic energy 94
4.3 Molecular motor at maximum power 94
4.3.1 Model I 95
4.3.2 Model II 99
4.3.3 Discussion 102

5 Optimization of kinetic proofreading in translation 105
5.1 Introduction 105
5.2 The model 108
5.2.1 Dependence of the error rate on the backward rate constants 112
5.3 Optimization results 114
5.3.1 Maximization of Incorporation rate at given error rate . 114
5.3.2 Role of dissipation 115
5.3.3 Robustness of the results 115
5.3.4 Effect of allowing for more than one non-cognate codon 117
5.4 Discussion 119

6 Perspectives 121

A Solution of the underdamped optimization problem (case study II) 123

Bibliography 127

List of publications 143

Lebenslauf 145

Acknowledgement 147

List of symbols

β	Boltzmann factor
$\Delta\mu$	Chemical potential difference
ΔF	Free energy difference between two equilibrium states
ΔF^{est}	Estimate for the free energy difference
ΔS	Mean difference in the system entropy
δ	Transition state position
$\mathcal{E}$	Stochastic internal energy
η	Efficiency
η^*	Efficiency at maximum power
η_{C}	Carnot efficiency
η_{CA}	Curzon-Ahlborn efficiency
η_{qs}	Efficiency for quasistatic driving
F^{st}	Stall force
γ	Friction coefficient
$\lambda(\tau)$	Control parameter for the transition between equilibrium states
$\lambda^*(\tau)$	Optimal protocol
λ_f	Final value of the control parameter
λ_i	Initial value of the control parameter
μ	Mobility or mobility matrix
ω	Frequency
$\mathcal{Q}$	Stochastic nonequilibrium heat
τ	Time
T_{c}	Temperature of the colder heat bath coupled to a heat engine
T_{h}	Temperature of the hotter heat bath coupled to a heat engine
W_{chem}	Chemical work
W^*	Minimal mean work
$\mathcal{W}$	Stochastic nonequilibrium work
$\mathcal{W}_{\mathrm{irr}}$	Stochastic irreversible work
ζ	Gaussian white noise

a, $a^\dagger$	Annihilation and creation operators for a quantum harmonic oscillator
$c_{\mathrm{ATP}}, c_{\mathrm{ADP}}, c_{\mathrm{P}}$	Dimensionless concentrations of ATP, ADP, and P molecules
E	Mean internal energy
F	Load force
F^*	Optimal load force
H	Hamiltonian
k^+, k^-	Bare reaction rate constants for forward and backward steps
l	Distance between two neighbouring motor sites
m	Mass
$p(x, \tau)$	Probability distribution for the coordinate x at time τ
p_i^s	Steady state probability of state i
Q	Mean nonequilibrium heat
T	Temperature
t	Total transition time
$u(\tau)$	Mean particle position in a moving harmonic potential
v	Velocity
$V(x, \tau)$	Time-dependent potential
W	Mean nonequilibrium work
$w(\tau)$	Variance of the particle position in a harmonic potential with time-dependent stiffness
w^+, w^-	Reaction rate constants for forward and backward steps
W^{ad}	Adiabatic work
W^{qs}	Quasistatic work
W_{irr}	Mean irreversible work
$y(\tau)$	Position-momentum correlation
$z(\tau)$	Mean squared momentum
$\mathbf{j}$	Probability current
$\boldsymbol{\sigma}$	Vector of Pauli matrices
$\boldsymbol{B}$	Magnetic field
$\rho(\tau)$	Density operator
RMSE	Root mean squared error
k	Stiffness of the moving harmonic potential

Summary

The concept of Stochastic Thermodynamics deals with the question how to define thermodynamic quantities for mesoscopic systems. One important goal is the thermodynamic description of processes in the biological cell. There are two major challenges in this regime. First, most processes in the cell are driven far out of equilibrium. Second, binding energies are typically of the order of the thermal energy $k_B T$ (at room temperature), and fluctuations are thus important.

During the last decade, there has been considerable progress in this field. It has been shown how to consistently define stochastic analogues of typical thermodynamic quantities such as work, heat, or entropy. While the second law of thermodynamics is valid only on average, a class of fascinating exact nonequilibrium work and fluctuation relations have been found. The Jarzynski relation connects the equilibrium free energy difference ΔF between two equilibrium states with a nonequilibrium average over (stochastic) work values $\mathcal{W}$ obtained from a nonequilibrium transition between these states. While such relations are intruiging from a theoretical point of view, they also offer a new class of methods for free energy calculations. However, the straightforward application of the Jarzynski relation is plagued by a systematic bias for any finite number of nonequilibrium trajectories. Particularly for nonequilibrium transitions with large typical values of the irreversible work $\mathcal{W}_{\mathrm{irr}} \equiv \mathcal{W} - \Delta F$, a correct estimate of the free energy difference requires a huge number of trajectories.

The main objective of this thesis is the analysis of optimization problems in the context of Stochastic Thermodynamcis. A quite natural optimization principle for nonequilibrium processes is the requirement that a defined result should be achieved with the smallest possible amount of dissipation. For a transition between two given equilibrium states in a given finite time t, this is directly linked to a process schedule which leads to a minimal (mean) work.

Such an optimization is also relevant from a practical point of view. A variety of strategies has been proposed in order to improve free energy calculations via the Jarzynski relation, e.g. by biasing the dynamics for trajectories with low work values. Although very unlikely for unbiased dynamics, these trajectories contribute strongly in the average in the Jarzynski relation and therefore are

important for a correct estimate of the free energy difference. As an alternative approach which may also be combined with other strategies, we exploit the fact that the Jarzynski relation is valid for any time-dependent driving scheme between two equilibrium states. Quite generally, the quality of the Jarzysnki estimate improves with decreasing dissipation during the transition. We therefore ask for the driving scheme which yields the minimal mean work W for a transition between two given equilibrium states in a given finite time t. Such an optimization is equivalent to the mininization of the mean irreversible work $W_{\rm irr} \equiv W - \Delta F$ since the free energy difference is determined by the (given) equilibrium states.

In order to study optimal protocols, we need to specify the dynamics of the considered system. For the correct description of the dynamics of biomolecules, e. g. in protein pulling experiments or protein folding simulations, it is crucial to include dissipative effects and fluctuations induced by the surrounding fluid in the cell which acts as a heat bath. A variety of different thermostats are used in molecular dynamics simulation. If only a few degrees of freedom are considered, a Langevin equation with Gaussian white noise is often a good description of the dynamics. If the momentum relaxation times are short compared to other typical times in the system, one can use overdamped Langevin dynamics. For such dynamics, we calculate optimal driving schemes (protocols) using two different time-dependent model potentials.

First, we consider a harmonic potential where the minimum of the potential is moved time-dependently from a given initial position $\lambda_i = 0$ to a given final position λ_f during a finite time t. This situation corresponds to a colloidal particle in an optical trap where the focus of the laser is moved from a given initial position $\lambda_i = 0$ to a given final position λ_f. In this example, the free energy difference between initial and final states vanishes. For any given protocol $\lambda(\tau)$ for the focus of the laser at time τ, the mean work applied to the colloidal particle by changing the potential time-dependently can be calculated. The mean work is generally a non-local functional of the protocol. However, it can be transformed into a local functional of the mean particle position in this particular case. At the beginning, the system is in equilibrium and the mean particle position is at the minimum of the potential $\lambda_i = 0$. The mean particle position at the end of the process, however, is not determined by the boundary conditions $\lambda(0) = 0$, $\lambda(t) = \lambda_f$ which can be met by jumps of the protocol $\lambda(\tau)$ at beginning and end of the process for any given time evolution of the mean particle positions. The minimization therefore is performed in two distinct steps: First, the optimal time evolution for the mean particle position subject to given boundary values is calculated using an Euler-Lagrange equation. In a second step, the optimal final value for the mean particle position is determined. The optimal protocol $\lambda^*(\tau)$ then exhibits jumps at the beginning and end of the process. These jumps correspond to instantaneous changes of the position of the trap. Such discontinuities can be rationalized by the requirement of a constant velocity of the particle. Since the particle has a vanishing mean velocity in the initial equilibrium state, the optimal mean velocity jumps to the required finite value at the beginning of the process. This jump in the velocity can only be achieved by a jump in the protocol. In this simple model, jumps could have also been obtained in a damped dynamics without fluctuations. Indeed, such a behaviour has previously been found in the context of optimized macroscopic heat engines.

Therefore, it is interesting to consider a second case study whith a finite free energy difference and with fluctuations affecting also the mean work. Since the analytic solution of the dynamic equations is out of scope for anharmonic potentials, we study a harmonic potential with time dependent stiffness. Here, the free energy change is due to entropic contributions, which indicates that fluctuations play a crucial role in the system. Again, the mean work is not a time-local functional of the protocol. However, the mean work can be transformed into a local functional of the variance of the particle position. The optimization then can be done in complete analogy to the moving harmonic potential and yields non-linear optimal protocols which also show jumps at beginning and end. We thus conjecture that jumps quite generally occur in optimal protocols for overdamped Langevin dynamics.

It is important to keep in mind that the overdamped Langevin equation is only an approximation valid to describe dynamics if the momentum relaxation times are short compared to other typical times in the system. The observed jumps may therefore be an artefact of this overdamped limit. Inertial effects also play an important role in molecular dynamics simulations. Thus, it is helpful to consider both harmonic case studies introduced above also for underdamped Langevin dynamics, where inertia effects are taken into account.

For the moving harmonic potential, the mean work can again be written as a time-local functional of the mean particle position. The minimization then can be performed in analogy to the overdamped case. The minimal work is given by exactly the same expression as in the overdamped case. However, the optimal protocol does not only involve jumps but also delta-type singularities at beginning and end. A posteriori, this behaviour can be rationalized again by the requirement of a constant velocity throughout the transition. In the underdamped regime, a jump in the velocity can only be achieved by a delta-peak in the force which directly transfers to a delta-peak in the protocol. For large masses of the particle and appropriate transition times, the minimal mean work is much smaller than for a linear protocol.

In the second case study of a harmonic potential with time-dependent stiffness, the mean work can no longer be transformed in a time-local functional of the variance of the particle position alone. Rather, it is a local functional of the covariance matrix of position and momentum. The entries of the covariance matrix are linked by contraints imposed by the dynamics of the system. A variation under these constraints leads to coupled Euler-Lagrange equations which cannot be solved analytically. Therefore, the shape of the optimal protocol can only be calculated numerically, involving also a numerical minimum search for the optimal boundary values. Again, the optimal protocol shows jumps and delta-type singularities at beginning and end. Optimizing a protocol with only one free parameter but allowing for additional singularities at the boundaries, we show that the resulting mean work is already very close to the optimal value. Thus, singularities are crucial to obtain a small value for the mean work.

From a theoretical point of view, it is also interesting to consider purely Hamiltonian or Schrödinger dynamics with initial canonical distribution, without any thermostat coupled to the system during the transition. This procedure corresponds to an experiment where the thermal bath is decoupled from the system at time $\tau = 0$ and recoupled to the system after the transition at time $\tau = t$. It is important to note that due to the lack of thermalization during the process, the work for quasistatic (infinitely slow) driving is not given by the free energy difference ΔF but by the adiabatic work $W^{\mathrm{ad}} \geq \Delta F$. For both previously introduced harmonic case studies and for Hamiltonian as well as Schrödinger dynamics, the adiabatic work can be reached in any finite transition time t. Naively, one would have expected to obtain the work for an instantaneous jump in the limit $t \to 0$, which is considerably larger than the adiabatic work. For both case studies and both types of dynamics, the optimal protocol is highly degenerate.

In order to probe whether these features persist for an anharmonic potential, we study a quartic potential with Hamiltonian dynamics. A numerical minimization shows that work values well below the work for an instantaneous jump can be achieved even for very fast transitions. However, it is hard to decide from the numerics whether the adiabatic work can be achieved in a finite transition time t.

For a quantum two-level system, the answer to the question whether the adiabatic work can be reached in any given time t depends on the allowed range of absolute values for the magnetic field. If the absolute value of the magnetic field is restricted, a finite time t_c is necessary to obtain the adiabatic work. For any larger time, the adiabatic work can also be reached while for $t < t_c$, the optimal work is larger than the adiabatic work. If any absolute value of the magnetic field is allowed, the adiabatic work can be reached in an arbitrarily short time.

Beyond the theoretical importance of minimal dissipation processes, optimal protocols may become important for free energy calculations. In the case studies mentioned above, free energy calculations are indeed improved if the optimal protocol rather than a linear protocol is used. We explicitly show that the error in the free energy estimate can be reduced by approximately 15% for a harmonic potential with time-dependent stiffness and given model parameters subject to underdamped Langevin dynamics. For a simple anharmonic potential, singularities as found in the optimal protocols in the harmonic case studies also improve free energy estimates. We thus conjecture that using appropriate singularities in the protocol will generically improve free energy calculations via the Jarzynski relation.

When comparing different free energy methods, the computational cost to create an equilibrated initial state is often neglected. We study the error in free energy estimates for a given total computational cost as a function of the time used for equilibration t_r and the total transition time t. For slow transtions and long equilibration times t_r, only few trajectories can be sampled at the given computational cost. However, for a model potential, few slow trajectories lead to better estimates of the free energy difference than many fast trajectories. If we had neglected the computational cost of equilibration, many fast trajectories would have yielded a better result. This example shows that it is important to take the computational cost of equilibration into account when comparing different free energy methods.

Until now, we have studied transitions between equilibrium states. Most processes in the biological cell, however, cannot be described by a nonequilibrium transition between equilibrium states. Rather, these systems are permanently driven out of equilibrium, e. g. by chemical potential differences. An important model class of such dynamics are Brownian motors which transfer either chemical or thermal energy into mechanical work leading to directed transport against a load force. The dynamics of these motors is stochastic due to thermal fluctuations.

Heat engines as well as thermodynamic machines can quite generally be characterized by two important quantities: (i) their efficiency and (ii) their power output. It is well known that the efficiency for heat engines operating between two thermal baths with temperatures $T_h > T_c$ is bounded from above by the Carnot efficiency $\eta_{\mathrm{C}} \equiv 1 - T_{\mathrm{c}}/T_{\mathrm{h}}$. The efficiency of molecular motors which transfer chemical energy into directed motion is bounded by $\eta_{\text{max}} = 1$. However, these upper bounds can only be reached for reversible "quasi-equilibrium" processes which require infintely slow driving and thus lead to a vanishing power output. It thus has been argued that it is more meaningful to characterize such thermodynamic machines by their performance at maximum power output. For heat engines in the endoreversible approximation, where dissipation is assumed to occur only due to a finite heat conductivity, the efficiency at maximum power is given by the Curzon-Ahlborn efficiency $\eta_{\text{CA}} \equiv 1 - \sqrt{T_{\text{c}}/T_{\text{h}}}$. For real macroscopic heat engines, it has indeed been found that their efficiency is close to the Curzon-Ahlborn value. It has been claimed that the Curzon-Ahlborn efficiency is somewhat universal beyond the endoreversible approximation.

In order to study this apparent universality, we consider a Carnot engine on the mesoscale which can be constructed by using a Brownian particle instead of the working gas and a time-dependent trapping potential instead of the confining vessel. The variance of the probability distribution for the position of the particle then corresponds to the pressure of the gas. For quasistatic driving where the isothermal transitions are performed infinitely slowly, it can be shown that the Carnot efficiency can indeed be reached in the overdamped regime (neglecting contributions from the kinetic energy). For a given variance of the particle position at beginning and end of the isothermal transitions, the driving scheme as well as the times used for the isothermal transitions can be adjusted to yield a maximum power output. The efficiency at this operational point of maximum power output can be calculated analytically. Surprisingly, it is given by a quite universal expression which does only depend on the viscosity (or more generally on the mobility matrices) at the temperatures T_{h} and T_{c}. This result is independent of the shape of the potential used to trap the particle. If contributions from the kinetic energy are taken into account, the efficiency generally decreases. The maximum attainable efficiency then is smaller than the Carnot value. However, the universal result for the efficiency at maximum power persists with slight modifications.

In contrast to heat engines, molecular motors in the biological cell are mostly driven by chemical potential differences. Such motors can be modeled by a master equation on a discrete state space. The stochastic dynamics then involves transitions between these discrete motor states along a track with given rate constants. We assume that the motor acts against a load force F. The rate constants then are constrained by thermodynamic consistency relations. For processive motors which perform many subsequent steps before they detach from their track, the system reaches a non-equilibrium steady state (NESS) with time-constant occupation probabilities for the sites. For a given load force F, thermodynamic quantities such as the (chemical) work input, the (mechanical) work output, and the efficiency can be calculated. For a simple linear motor model, all relevant quantities can be expressed as a function of only three relevant quantities: the chemical potential difference $\Delta\mu$, the load force F, and the position of the transition state δ between two neighbouring sites. For zero load force $F = 0$, the motor produces no power output and the efficiency vanishes. For the stall force, where the directed motion ceases, the power output also vanishes. Therefore, the load force F can be tuned to reach a maximum power output of the motor. The efficiency of the molecular motor in this maximum power regime shows two unexpected features: (i) Both the power output and the efficiency increase when the transition state position is moved closer to the initial motor position and (ii) for appropriate parameters, the efficiency increases when the system is driven further out of equilibrium by a higher chemical potential difference.

Recent experiments have shown that simple linear models might not be appropriate to explain all features of molecular motors. It seems to be necessary to include a second motor cycle which allows for dissipation even at the stall force. In such a model, mechanical backsteps may also involve the consumption of chemical energy. Thus, the chemical and the mechanical cycle are no longer tightly coupled, *i. e.* the hydrolyzation of ATP does not necessarily involve a mechanical forward step of the motor. In a motor model with two cycles, the qualitative results for the efficiency at maximum power are confirmed. Moreover, there is experimental evidence that the transition state position in real molecular motors is compatible with a high efficiency at maximum power.

Beyond their relevance for directed transport within the cell, molecular motors are also important for the synthesis of proteins. Most processes within the cell involve proteins or protein complexes. Proteins are assembled from the information stored in the genetic code during a process called gene expression. It is crucial for the cell to ensure a high protein production rate in combination with a low error rate. In order to achieve the low error rates observed in living cells, a mechanism called kinetic proofreading has evolved. However, it has been found experimentally that the proofreading scheme is not fully exploited and that the error rate can be reduced in mutant organisms. It has been speculated that a low error rate is sacrificed for a high rate of protein production. This conjecture can be probed within a recently introduced model for the second stage of gene expression (translation) which dominates the total error of gene expression. We find that for a given error rate equivalent to the experimentally observed value, the protein production rate is not at its theoretical maximum either. We therefore conjecture that other evolutionary goals or structural reasons are responsible for the observed rate constants.

Zusammenfassung

Die Stochastische Thermodynamic beschäftigt sich mit der Fragestellung, wie thermodynamische Größen auch für mesoskopische Systeme definiert werden können. Ein wichtiges Ziel ist es dabei, die thermodynamischen Prozesse in der biologischen Zelle zu beschreiben. Dabei entstehen im Vergleich zur makroskopischen Gleichgewichts-Thermodynamik zwei wesentliche neue Herausforderungen. Zum einen laufen Prozesse in der Zelle meist fern vom thermodynamischen Gleichgewicht ab. Zum anderen sind die typischen Binde-Energien für Biomoleküle vergleichbar mit der thermischen Energie k_BT bei Raumtemperatur. Deshalb müssen thermische Fluktuationen bei der Beschreibung dieser Systeme berücksichtigt werden.

Im letzten Jahrzehnt gab es entscheidende Fortschritte im Bereich der Stochastischen Thermodynamik. Für verschiedene Formen der stochastischen Dynamik gelang es, stochastische Analoga für konventionelle thermodynamische Größen wie Arbeit, Wärme oder Entropie zu definieren. Auf dieser mesoskopischen Skala gilt der zweite Hauptsatz der Thermodynamik nur noch für die Mittelwerte der stochastischen thermodynamischen Größen. Darüber hinaus gelten aber in großer Allgemeinheit neue, faszinierende Arbeits- und Fluktuationstheoreme im Nichtgleichgewicht wie zum Beispiel die Jarzynski-Relation, die eine Verknüpfung zwischen der freien Energiedifferenz zwischen zwei Gleichgewichtszuständen und einem nichtlinearen Mittelwert der Arbeit beim Übergang zwischen diesen beiden Zuständen herstellt. Diese Relation ist nicht nur aus theoretischer Sicht interessant, sondern ermöglicht auch die Berechnung von freien Energiedifferenzen aus Nichtgleichgewichts-Trajektorien. Die direkte Anwendung der Jarzynski-Relation führt jedoch bei jeder endlichen Anzahl von Nichtgleichgewichts-Trajektorien zu einem systematischen Fehler, der durch den nichtlinearen Mittelwert entsteht. Vor allem für schnelle Übergänge, bei denen die typische irreversible Arbeit $\mathcal{W}_{\text{irr}} \equiv \mathcal{W} - \Delta F$ wesentlich größer als die thermische Energie k_BT ist, benötigt man sehr viele Trajektorien, um eine gute Abschätzung der freien Energie zu erhalten.

Das Hauptziel der vorliegenden Arbeit ist die Analyse von Optimierungs-Problemen im Umfeld der Stochastischen Thermodynamik. Ein natürliches Optimierungsprinzip für Nichtgleichgewichtsprozesse ist die Forderung, dass ein definiertes Ziel mit einem Minimum an benötigter Dissipation erreicht wird. Für einen Übergang zwischen zwei Gleichgewichtszuständen is dies eng verknüpft mit der Frage nach einer Prozessführung, die zu einer minimalen mittleren Arbeit führt.

Die Optimierung eines solchen Prozesses ist aber auch aus praktischen Gesichtspunkten interessant. Um die Berechnung von Differenzen in der freien Energie ΔF mit Hilfe der Jarzynski-Relation zu verbessern, wurden verschiedene Strategien vorgeschlagen. Zum Beispiel kann die physikalische Dynamik in Computer-Simulationen so abgeändert werden, dass mehr Trajektorien mit niedriger Arbeit $\mathcal{W}$ auftreten. Diese Trajektorien liefern einen großen Beitrag zum Mittelwert in der Jarzynski-Relation und sind deshalb wichtig für eine korrekte Abschätzung der freien Energie. Alternativ oder auch in Kombination zu diesem Vorgehen kann auch ausgenutzt werden, dass die Jarzynski-Relation für jedes beliebige Protokoll gilt, mit dem das betrachtete System von einem in den anderen Gleichgewichtszustand getrieben wird. Da erwartet werden kann, dass sich der Schätzwert für die freie Energiedifferenz mit sinkender Dissipation verbessert, suchen wir für eine feste Übergangszeit t nach dem Protokoll, das zu einer minimalen mittleren Arbeit W für den Übergang zwischen den betrachteten Gleichgewichtszuständen führt. Diese Optimierung ist äquivalent zur Minimierung der mittleren irreversible Arbeit $W_{\text{irr}} \equiv W - \Delta F$, da die freie Energie durch die (gegebenen) Gleichgewichtszustände bestimmt ist und nicht vom Protokoll abhängt.

Um die Dynamik von Biomolekülen in der Zelle korrekt wiedergeben zu können (z. B. in Zieh-Experimenten an Proteinen oder in Simulationen zur Proteinfaltung), muss die verwendete Dynamik Dissipation und Fluktuationen berücksichtigen. Diese beiden Effekte werden durch die Zellflüssigkeit, die als Wärmebad für das betrachtete System wirkt, hervorgerufen. Alternativ können die Wassermoleküle auch explizit in die Simulation eingebunden werden. Wenn nur einige wenige Freiheitsgrade von Interesse sind, kann die Dynamik des betrachteten Systems meist in guter Näherung durch eine Langevin-Gleichung mit weißem, Gauß'schem Rauschen beschrieben werden. Wenn die Impulsrelaxation zusätzlich schnell im Vergleich zu anderen Zeitskalen im System ist, kann die überdämpfte Langevin-Gleichung verwendet werden. Für eine solche Dynamik berechnen wir optimale Protokolle für zwei verschiedene Fallstudien mit unterschiedlichen zeitabhängigen Potentialen.

Zunächst betrachten wir ein harmonisches Potential mit zeitabhängiger Verschiebung des Potentialminimums von einer Anfangsposition $\lambda_i = 0$ zu einer Endposition λ_f in einer gegebenen endlichen Zeit t. Dies entspricht z. B. einem kolloidalen Teilchen in einer optischen Pinzette, deren Laser-Fokus zeitabhängig von der Anfangsposition bei λ_i zur Endposition bei λ_f verschoben wird. Dabei sei die Position des Laser-Fokus zur Zeit τ durch das Protokoll $\lambda(\tau)$ gegeben. In dieser einfachen Fallstudie ist die freie Energiedifferenz $\Delta F = 0$. Die mittlere Arbeit, die durch die zeitliche Änderung des Potentials auf das kolloidale Teilchen ausgeübt wird, kann dann für jedes gegebene Protokoll berechnet werden. Die mittlere Arbeit ist allerdings ein zeitlich nicht-lokales Funktional des Protokolls, welches jedoch mit Hilfe einer Substitution in ein zeitlich lokales Funktional der mittleren Teilchenposition überführt werden kann. Am Anfang des Prozesses befindet sich das betrachtete System im Gleichgewicht und die mittlere Position des Teilchens ist deshalb bei 0. Die mittlere Teilchenposition am Ende des Prozesses ist jedoch nicht vorgegeben. Die Minimierung erfolgt deshalb in zwei Schritten: Zunächst wird für gegebene Randwerte der mittleren Teilchenposition mit Hilfe einer Euler-Lagrange-Gleichung die optimale Zeitentwicklung bestimmt. In einem zweiten Schritt wird dann der optimale Endwert der mittleren Teilchenposition bestimmt. Die Randbedingungen an das Protokoll $\lambda(0) = 0$ und $\lambda(t) = \lambda_f$ können dann bei gegebener Zeitentwicklung der mittleren Teilchenposition immer durch Sprünge des Protokolls zu Beginn und Ende des Prozesses erreicht werden. Die Minimierung der mittleren Arbeit führt deshalb auf ein optimales Protokoll $\lambda^*(\tau)$, welches Sprünge zu Beginn und Ende des Übergangs aufweist. Diese Sprünge entsprechen einer instantanen Änderung der Position des Laser-Fokus. Diese Unstetigkeiten können erklärt werden durch die Forderung, dass das kolloidale Teilchen über die gesamte Dauer des Prozesses eine möglichst konstante Geschwindigkeit aufweisen sollte, um die Dissipation niedrig zu halten. Da die mittlere Geschwindigkeit im Gleichgewicht Null ist, muss diese somit zu Beginn des Prozesses auf diesen konstanten Wert springen. Eine Unstetigkeit in der Geschwindigkeit kann nur durch einen Sprung im Protokoll erreicht werden. In diesem einfachen Beispiel wären Sprünge im optimalen Protokoll auch schon in einer gedämpften Dynamik ohne Fluktuationen aufgetreten. Ein ähnliches Verhalten wurde tatsächlich bei der Optimierung von makroskopischen Wärme-Kraft-Maschinen gefunden.

Es ist deshalb interessant, eine zweite Fallstudie zu betrachten, in der die freie Energie nicht verschwindet und sich die thermischen Fluktuationen auch auf die mittlere Arbeit auswirken. Da selbst die Lösung der Bewegungsgleichungen für ein anharmonisches Potential nur numerisch möglich ist, betrachten wir ein harmonisches Potential mit zeitabhängiger Federkonstante. In diesem System wird die freie Energiedifferenz allein durch entropische Effekte hervorgerufen. Fluktuationen spielen deshalb eine wichtige Rolle für die Thermodynamik dieses Systems. Die mittlere Arbeit ist auch hier ein zeitlich nicht-lokales Funktional des Protokolls. Allerdings kann die mittlere Arbeit als lokales Funktional der Varianz der Teilchenposition geschrieben werden. Die Optimierung dieses Funktionals kann dann analog zum harmonischen Potential mit zeitabhängiger Position des Minimums durchgeführt werden. Es ergeben sich nicht-lineare optimale Protokolle, die wieder Sprünge am Anfang und am Ende des Prozesses aufweisen. Es kann daher vermutet werden, dass solche Sprünge sehr allgemein in optimalen Protokollen für eine überdämpfte Langevin-Dynamik auftreten.

Man muss sich bewusst sein, dass die überdämpfte Langevin-Gleichung eine Näherung für den Fall ist, dass die Impulsrelaxation schnell im Vergleich zu anderen charakteristischen Zeiten im System ist. Die beobachteten Sprünge im optimalen Protokoll könnten deshalb ein Artefakt des überdämpften Grenzfalls sein. Trägheitseffekte spielen auch in Molekulardynamik-Simulationen eine wichtige Rolle. Wir betrachten die beiden oben eingeführten Fallstudien deshalb auch für eine unterdämpfte Langevin-Dynamik, welche Trägheitseffekte berücksichtigt.

Für die erste Fallstudie eines harmonischen Potential mit zeitabhängiger Position des Minimums kann die mittlere Arbeit wieder als zeitliche lokales Funktional der mittleren Teilchenposition geschrieben werden. Die Optimierung kann dann analog zum überdämpften Fall ausgeführt werden. Für die minimale Arbeit ergibt sich der gleiche Ausdruck wie im überdämpften Fall. Es zeigt sich jedoch, dass nun nicht nur Sprünge sondern auch Delta-Singularitäten am Anfang und am Ende des optimalen Protokolls auftreten. Im Nachhinein kann man dieses Verhalten verstehen, wenn man wieder fordert, dass die mittlere Teilchengeschwindigkeit während des Prozesses konstant ist. Im unterdämpften Fall kann eine Unstetigkeit in der Geschwindigkeit nur durch einen Delta-Peak in der Kraft auf das Teilchen erreicht werden. Dieser Delta-Peak in der Kraft überträgt sich direkt auf einen Delta-Peak im Protokoll. Die minimale mittlere Arbeit ist für große Massen und geeignete Übergangszeiten um ein Vielfaches kleiner als die entsprechende mittlere Arbeit für ein lineares Protokoll.

Wir betrachten die zweite Fallstudie eines harmonischen Potentials mit zeitabhängiger Federkonstante. Die mittlere Arbeit kann nun nicht mehr allein als ein Funktional der Varianz der Teilchenposition geschrieben werden, sondern ist nun ein Funktional der Kovarianzmatrix für Ort und Impuls des Teilchens. Die Einträge dieser Matrix sind durch Nebenbedingungen verknüpft, die durch die Dynamik des Systems gegeben sind. Eine Variation unter Nebenbedingungen führt auf gekoppelte Euler-Lagrange-Gleichungen, die nicht analytisch gelöst werden können. Damit kann das optimale Protokoll nur numerisch berechnet werden, wobei zusätzlich eine numerische Minimumsuche für Randwerte nötig ist. Analog zur ersten Fallstudie ergeben sich wieder Sprünge und Delta-

Peaks im optimalen Protokoll. Es zeigt sich, dass schon die Optimierung eines Protokolls mit nur einem freien Parameter auf eine mittlere Arbeit führt, die sehr nahe beim optimalen Wert liegt, sofern man Singularitäten am Anfang und Ende des Protokolls zulässt. Dies verdeutlicht, dass solche Singularitäten entscheidend sind, um eine niedrige mittlere Arbeit zu erzielen.

Aus einer theoretischen Perspektive ist es auch interessant, optimale Protokolle für Hamilton'sche Dynamik und für eine Schrödingerdynamik mit jeweils kanonischen Anfangsbedingungen zu berechnen. Während des Prozesses ist dann kein Wärmebad an das System gekoppelt. In einem entsprechenden Experiment müsste also das Wärmebad am Anfang des Übergangs zur Zeit $\tau = 0$ vom System abgekoppelt und am Ende des Übergangs zur Zeit $\tau = t$ wieder angekoppelt werden. Für eine solche Dynamik ist die Arbeit bei unendlich langsamer (quasistatischer) Prozessführung im Unterschied zur Langevin-Dynamik nicht durch die freie Energiedifferenz ΔF sondern durch die adiabatische Arbeit $W^{\text{ad}} \geq \Delta F$ gegeben. Für die beiden harmonischen Fallstudien ergeben sich sowohl für eine Hamilton'sche Dynamik als auch für Schrödingerdynamik hochgradig entartete optimale Protokolle. Dabei ist die optimale Arbeit für jede endliche Übergangszeit durch die adiabatische Arbeit gegeben. Dies ist überraschend, da man für kleine Übergangszeiten $t \to 0$ eigentlich die mittlere Arbeit für einen istantanen Sprung des Protokolls erwartet, welche wesentlich größer als die adiabatische Arbeit ist.

Um zu überprfüfen, ob die adiabatische Arbeit generell in beliebig kurzer Zeit erreicht werden kann, untersuchen wir ein anharmonisches quartisches Potential für Hamilton'sche Dynamik. Eine numerische Minimierung zeigt, dass selbst für sehr kurze Übergangszeiten schon Werte der mittleren Arbeit erzielt werden können, die deutlich unterhalb der mittleren Arbeit für einen instantanen Sprung liegen. Die numerische Minimierung lässt allerdings keinen eindeutigen Schluß zu, ob die adiabatische Arbeit schon in einer endlichen Übergangseit t erreicht werden kann.

Für ein quantenmechanisches Zwei-Niveau-System hängt die Beantwortung dieser Frage davon ab, ob beliebig große Absolutwerte für das magnetische Feld erlaubt sind. Falls der Betrag des magnetischen Feldes beschränkt ist, ergibt sich eine kritische Zeit t_c, ab der die adiabatische Arbeit erreichbar ist. Für kleinere Zeiten $t < t_c$ liegt die optimale Arbeit oberhalb der adiabatischen Arbeit. Für ein unbeschränkt beliebig wählbares magnetisches Feld kann die adiabatische Arbeit in jeder beliebigen Übergangszeit t erreicht werden.

Abgesehen von der theoretischen Relevanz von Prozessen mit minimaler Dissipation könnten optimale Protokolle auch für die Berechnung von freien Energiedifferenzen wichtig werden. In den untersuchten Fallstudien kann der

Fehler in der Abschätzung der freien Energiedifferenz tatsächlich durch die Verwendung des optimalen Protokolls im Vergleich zu einem linearen Protokoll verbessert werden. Dies untersuchen wir exemplarisch für ein harmonisches Potential mit zeitabhängiger Federkonstante für unterdämpfte Langevin-Dynamik. Dort ergibt sich für die untersuchten Modellparameter eine Verringerung des Fehlers um ca. 15%. Für eine unterdämpfte Langevin-Dynamik in einem einfachen anharmonisches Potential verbessern Singularitäten zu Beginn und Ende des Protokolls ebenfalls die Abschätzung der freien Energiedifferenz. Es lässt sich daher vermuten, dass geeignete Singularitäten sehr allgemein den Fehler bei der Berechnung von freien Energiedifferenzen mit Hilfe der Jarzynski-Relation verringern können.

Beim Vergleich verschiedener Methoden zur Berechnung von freien Energiedifferenzen wird oft der Zeitbedarf für die Erzeugung des benötigten Anfangs-Gleichgewichtszustandes vernachlässigt. Wir untersuchen für ein einfaches anharmonisches Modellpotential den Fehler in der Abschätzung der freien Energiedifferenz bei gegebener Gesamtrechenzeit für verschiedene Übergangszeiten t und verschiedene Zeiten t_r, die für die Anfangsrelaxation ins Gleichgewicht verwendet werden. Für langsame Übergänge und lange Relaxationszeiten t_r können dann nur wenige Trajektorien berechnet werden. Es zeigt sich dennoch, dass die Verwendung von wenigen langsamen Trajektorien bessere Ergebnisse als die Verwendung von vielen schnellen Trajektorien liefert. Ohne die Berücksichtigung der Relaxationszeit t_r wäre das Urteil genau andersherum ausgefallen. Es ist deshalb wichtig, bei einem Vergleich verschiedener Verfahren zur Berechnung der freien Energiedifferenz auch die “Kosten” für die Relaxation ins Gleichgewicht zu berücksichtigen.

Bis jetzt haben wir Übergänge zwischen Gleichgewichtszuständen untersucht. Die meisten Prozesse in der biologischen Zelle können jedoch nicht durch einfache Nichtgleichgewichts-Übergänge zwischen Gleichgewichtszuständen beschrieben werden. Viele Systeme werden z. B. durch chemische Potentialdifferenzen permanent aus dem Gleichgewicht getrieben. Eine wichtige Klasse solcher Prozesse sind Brown’sche Motoren, die entweder durch chemische oder thermische Energie getrieben werden und diese in mechanisch Arbeit umwandeln.

Sowohl Wärme-Kraft-Maschinen als auch durch chemische Energie getriebene Motoren können allgemein durch ihren Wirkungsgrad und ihre Leistung charakterisiert werden. Für eine Wärme-Kraft-Maschine, die zwischen zwei Wärmebädern mit Temperaturen $T_h > T_c$ betrieben wird, ist der maximal erreichbare Wirkungsgrad der Carnot-Wirkungsgrad $\eta_{\mathrm{C}} \equiv 1 - T_{\mathrm{c}}/T_{\mathrm{h}}$. Für molekulare Motoren, die durch chemische Energie getrieben werden, ist der maximal Wirkungsgrad $\eta_{\max} = 1$. In beiden Fällen können diese oberen

Schranken allerdings nur für unendlich langsame, reversible Prozessführung erreicht werden. Dann geht allerdings auch die Leistung gegen Null. Deshalb ist es sinnvoller, statt des Wirkungsgrades die Leistung einer solchen Maschine zu maximieren. Der Wirkungsgrad bei dieser maximalen Leistung wurde als Erstes von Curzon und Ahlborn für eine Wärme-Kraft-Maschine in der sogenannten endoreversiblen Näherung berechnet. Dabei wird eine Carnot-Maschine angenommen, bei der Dissipation nur durch eine endliche Wärmeleitfähigkeit auftritt. Der Wirkungsgrad bei maximaler Leistung ist dann durch den Curzon-Ahlborn Wirkungsgrad $\eta_{\mathrm{CA}} \equiv 1 - \sqrt{T_{\mathrm{c}}/T_{\mathrm{h}}}$ gegeben. Ein Vergleich mit verschiedenen existierenden Wärme-Kraft-Maschinen zeigt, dass deren Wirkungsgrad gut mit dem Curzon-Ahlborn-Wirkungsgrad übereinstimmt. Es wurde vermutet, dass der Curzon-Ahlborn Ausdruck für den Wirkungsgrad bei maximaler Leistung über die endoreversible Näherung hinaus eine relativ universelle Gültigkeit besitzt.

Um diese vermeintliche Universalität näher zu untersuchen, wollen wir das Analogon zu einer Carnot-Maschine auf einer mesoskopischen Skala betrachten. Dabei kann ein Brown'sches Teilchen als Arbeitsgas und ein zeitabhängiges Potential anstatt eines Zylinders verwendet werden. Die Breite des Wahrscheinlichkeitsdichte für die Position des Brown'schen Teilchens entspricht dann dem Druck des Gases. Für sehr langsam (reversibel) getriebene Isothermen kann der Carnot-Wirkungsgrad (zumindest im überdämpften Regime) tatsächlich erreicht werden. Dabei werden allerdings Beiträge der kinetischen Energie des Brown'schen Teilchens zu Wärme und Arbeit nicht berücksichtigt. Geben wir nun die Randwerte für die Varianz der Wahrscheinlichkeitsdichte für das Brown'sche Teilchen vor, können sowohl das Protokoll für die isothermen Übergänge als auch die Zykluszeit variiert werden, um eine maximale Leistung der Maschine zu erreichen. Der Wirkungsgrad an diesem Arbeitspunkt mit maximaler Leistung kann dann analytisch berechnet werden. Überraschenderweise ergibt sich ein sehr universeller Ausdruck, der nur von den Viskositäten (oder allgemein in mehreren Dimensionen von den Mobilitätsmatrizen) der umgebenden Flüssigkeit bei den beiden Temperaturen T_{h} und T_{c} abhängt. Insbesondere ist dieses Ergebnis unabhängig von der Form des verwendeten zeitabhängigen Potentials. Berücksichtigt man die Beiträge der kinetische Energie, so sinkt der Wirkungsgrad allgemein. Der maximal mögliche Wirkungsgrad ist dann kleiner als der Carnot-Wirkungsgrad. Das universelle Ergebnis für den Wirkungsgrad bei maximaler Leistung bleibt jedoch nach einer kleinen Anpassung erhalten.

Molekulare Motoren in der Zelle werden meist nicht durch Temperaturdifferenzen sondern durch chemische Potentialdifferenzen angetrieben. Solche Motoren können z. B. durch eine stochastische Master-Gleichung auf einem diskreten Zustandsraum modelliert werden. Dabei finden Übergänge zwischen den diskreten Zuständen des Systems mit gegebenen Raten (Wahrscheinlichkeit pro Zeitintervall) statt. Wir nehmen an, dass der Motor eine gerichtete Bewegung gegen eine Last F ausführt. Die Übergangsraten zwischen den Zuständen müssen dann thermodynamische Konsistenzbedingungen erfüllen. Wir betrachten sogenannte prozessive molekulare Motoren, die sehr viele Motorschritte ausführen, bevor sie sich von ihrer Schiene lösen. Für gegebene Last F können in solch einem Modell thermodynamische Größen wie die den Motor antreibende chemische Arbeit, die vom Motor geleistete mechanische Arbeit und der Wirkungsgrad berechnet werden. In einem sehr einfachen linearen Motor-Modell können alle Größen als Funktion von drei relevanten Parametern ausgedrückt werden: die chemische Potentialdifferenz $\Delta\mu$, die Last F und die Position des Übergangszustands δ zwischen zwei benachbarten Motorzuständen. Die Leistung als Funktion der Last F zeigt dann folgendes Verhalten: Bei verschwindender Last F verschwindet auch die Leistung des Motors. Ebenso verschwindet die Leistung bei der Halt-Last ("stall force"), wo die Last F gerade so groß ist, dass der Motor keine gerichtete Bewegung mehr ausführt. Deswegen muss es zwischen diesen beiden Werten eine optimale Last F^* geben, bei der die Leistung des Motors maximal wird. Der Wirkungsgrad des molekularen Motors bei dieser optimalen Last als Funktion der anderen beiden Parameter zeigt dann folgendes überraschendes Verhalten: (i) Der Wirkungsgrad und die Leistung nehmen gleichzeitig zu, wenn die Position des Übergangszustands δ näher an den ursprünglichen Zustand rückt. (ii) Bei geeigneter Parameterwahl wächst der Wirkungsgrad, wenn das System durch eine wachsende chemische Potentialdifferenz weiter aus dem Gleichgewicht getrieben wird.

Neuere Experimente zeigen, dass einfache lineare Modell möglicherweise nicht alle Eigenschaften von molekularen Motoren korrekt beschreiben können. Insbesondere gibt es wohl auch Dissipation, wenn der Motor genau bei der Halt-Kraft arbeitet. Um dies zu gewährleisten, muss ein Motor-Modell mindestens einen zweiten Motor-Zyklus enthalten. In solch einem Modell können mechanische Rückwärtsschritte auch mit einem Verbrauch von chemischer Energie einhergehen. Der chemischer und der mechanische Motor-Zyklus sind dann nicht mehr eng gekoppelt, d. h. die Hydrolyse von ATP führt nicht notwendigerweise immer zu einem Vorwärtsschritt. In einem Motor-Modell mit zwei Zyklen können die gewonnenen Resultate für den Wirkungsgrad bei maximaler Leistung bestätigt werden. Darüberhinaus gibt es Anhaltspunkte, dass der Übergangszustand in biologischen Motoren tatsächlich in der Nähe des Anfangszustands liegt und deshalb zu einem hohen Wirkungsgrad bei maximaler Leistung führt.

Molekularen Motoren sorgen nicht nur für gerichteten Transport in der Zelle sondern sind auch an der Synthese von Proteinen beteiligt. Für viele Prozesse, die in der Zelle ablaufen, sind Proteine oder Komplexe aus Proteinen essentiell. Bei der Proteinsynthese wird die genetische Information, die in der DNA gespeichert ist, in einem zweistufigen Prozess in entsprechende Proteine übersetzt. Für die Zelle ist es entscheidend, Proteine mit hoher Rate und mit niedriger Fehlerrate herzustellen. Um die in lebenden Zellen beobachtete niedrige Fehlerrate zu gewährleisten, hat die Zelle einen speziellen Fehlerkorrektur-Mechanismus entwickelt. Es zeigt sich jedoch experimentell, dass dieser Mechanismus nicht voll ausgechöpft wird und Mutationen zu einer noch niedrigeren Fehlerrate führen können. Es wurde deshalb vermutet, dass eine erhöhte Fehlerrate in Kauf genommen wird, um eine hohe Protein-Produktionsrate zu erreichen. Diese Vermutung kann in einem kürzlich eingeführten Modell der zweiten Phase der Protein-Produktion (”translation“) getestet werden. Diese zweite Phase dominiert den Gesamt-Fehler in der Protein-Herstellung. Wir untersuchen deshalb die Produktionsrate für Proteine bei einer gegebenen Fehlerrate. Dabei zeigt sich, dass die Protein-Produktionsrate selbst bei einer festgehaltenen (durch den experimentellen Wert gegebenenen) Fehlerrate nicht maximal ist. Deshalb kann vermutet werden, dass andere evolutionäre Ziele oder strukturelle Gründe für die beobachten Ratenkonstanten verantwortlich sind.

1 Introduction

Recently, there has been considerable progress in the thermodynamic description of small (bio-) systems [1, 2]. Typically, processes within the biological cell occur at a constant temperature T. Still, these processes occur neither in equilibrium nor in the linear response regime but are driven far out of equilibrium by chemical potential differences between reacting species within the cell. A prominent example is the hydrolyzation of ATP into ADP + P which is the driving force for a variety of different molecular motors.

In contrast to the macroscopic heat engines considered in conventional thermodynamics, processes in the cell typically involve energy scales of the order of the thermal energy $k_B T$ and thermal fluctuations thus play an important role in most biologically relevant systems. Therefore, the dynamics in these systems cannot be described on a deterministic (macroscopic) level. In this regime, models for thermodynamic machines must incorporate fluctuation effects and thus allow also for backward steps in a directed motion [3, 4].

A simple model system with the mentioned features is a Brownian particle immersed in a fluid which can be described by a (stochastic) Langevin equation. Typically, experiments are performed with colloidal particles of size $d \simeq 1 \mu m$. Such a system can be driven out of equilibrium by an optical trap which acts as a potential on the particle. Moving the focus of such a trap time-dependently leads to a nonequilibrium situation. The seminal work of Sekimoto [5, 6] opened the door for a thermodynamic description of Langevin systems driven far out of equilibrium. Thermodynamic quantities such as work, heat, internal energy, and entropy can even be defined on a single stochastic trajectory [6, 7, 8], yielding the respective ensemble quantities after averaging. Specifically, the work applied to the Brownian particle by a time-dependent external potential during a transition time t can be defined. For macroscopic systems, the second law of thermodynamics constrains the deterministic work to obey $W \geq \Delta F$, where ΔF is the equilibrium free energy difference between initial and final state. For mesoscopic systems, the work is a stochastic quantity with a probability distribution $p(\mathcal{W})$ which may also have a non-zero value for $\mathcal{W} < \Delta F$. Thus, the second law should be formulated for the average of the work $W \equiv \langle \mathcal{W} \rangle \geq \Delta F$ rather than for every possible trajectory of the system.

A decade ago, Jarzynski proposed the remarkable relation [9]

$$e^{-\Delta F/(k_B T)} = \left\langle e^{-\mathcal{W}/(k_B T)} \right\rangle \tag{1.1}$$

which constrains the possible distributions of the work. It is important to note that the Jarzynski relation (1.1) quite generally holds for nonequilibrium transitions between equilibrium states. It has been proven for a variety of different dynamics [10, 11, 12] and it holds for any time-dependent driving described by an external control parameter $\lambda(\tau)$. The Jarzynski relation can be used to infer free energy differences from a set of nonequilibrium trajectories. Recently, several schemes have been proposed to improve such free energy estimates.

For a Gaussian work distribution

$$p(\mathcal{W}) = \frac{1}{2\pi\sigma^2} e^{\frac{(\mathcal{W}-\langle\mathcal{W}\rangle)^2}{2\sigma^2}}, \tag{1.2}$$

see Fig. 1.1, the Jarznyski relation (1.1) directly yields the relation $\langle\mathcal{W}\rangle = \Delta F + \sigma^2/2$ between average work $\langle\mathcal{W}\rangle$ and variance σ^2 which can be interpreted as a fluctuation-dissipation relation. However, a Gaussian distribution is only obtained for simple harmonic systems or for quasistatic driving. This is in agreement with the common understanding that fluctuation-dissipation theorems are only valid in the linear response regime. It has been confirmed experimentally [13] that the Jarzynski relation is valid beyond this regime.

Beyond nonequilibrium transitions between equilibrium states, it is important to understand thermodynamic machines on the mesoscale. In the biological cell, such machines can typically be described by non-equilibrium stationary states (NESS) where probability distributions are stationary but there is constant dissipation due to fluxes through the system. In these systems, the fluctuations of the entropy production are constrained by fluctuation theorems [14, 15] which are closely related to the Jarzynski relation. These relations have been extended to various related theorems [7, 8, 16, 17, 18, 19, 20] for different thermodynamic quantities on a single trajectory. Beyond the overdamped Langevin dynamics suitable to describe a Brownian particle in a potential, model studies have been performed for underdamped Langevin dynamics [21, 22], where inertial effects are taken into account. From a theoretical point of view, it is also interesting to consider Hamiltonian [9, 23, 24] or Schrödinger [12, 25, 26] dynamics with canonical initial conditions.

An important class of models for thermodynamic machines on the mesoscale are Brownian motors [27]. Such motors are either driven by chemical potential differences or a varying temperature (either time-dependent or position-

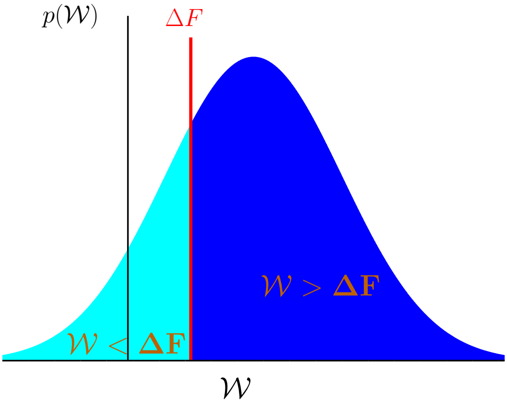

Figure 1.1 Typical (Gaussian) work distribution $p(\mathcal{W})$ which satisfies the Jarzynski relation. While there is a finite probability that the work is smaller than the free energy difference, it is larger than the free energy difference on average.

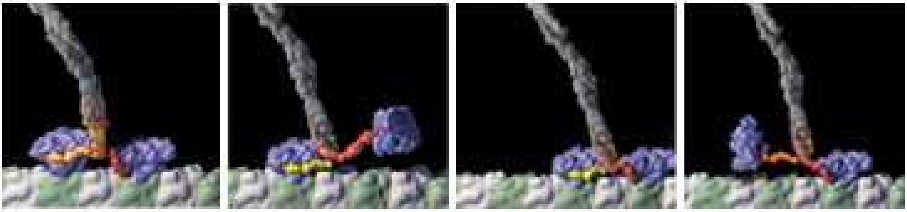

Figure 1.2 Kinesin motor on microtubule track. This motor is driven by ATP hydrolysis and moves processively in descrete 8 nm steps. For sufficiently small loads, the chemical energy input leads to an average movement in forward direction (which is defined by the polarity of the microtubule track). However, there are also backward steps due to thermal fluctuations. Kinesin is essential for intracellular transport.

dependent). While the first class is often used as a model for molecular biomotors such as kinesin, see Fig. 1.2, the second class is of great theoretical importance since it can directly be linked to results for macroscopic heat engines. The stochastic dynamics of such motors is typically modelled either on a continuous state space by Langevin equations or on a discrete state space by master equations. Since biological motors are typically driven far out of equilibrium, linear response thermodynamics is not appropriate to describe these systems. In the last two decades, a variety of aspects of such Brownian motors has been studied, including dynamics [4, 27], stochastic energetics [5, 6, 28, 29], efficiencies [30, 31, 32], and also fluctuation theorems [33, 34].

The main objective of this thesis is the analysis of optimization problems for nonequilibrium processes on the mesoscale. In the context of equilibrium thermodynamics, optimization has always played an important role. For thermodynamic processes, it is a practical purpose rather than a variational theory to choose the parameters to yield an optimal performance. A macroscopic steam engine, *e. g.*, should operate at a maximal possible efficiency and a maximal possible power output. This example already illustrates that there can be competing goals.

Quite generally, a natural optimization principle for nonequilibrium processes is the requirement that a defined result should be achieved with the smallest possible amount of dissipation. For a transition between two given equilibrium states in a given finite time t, this is directly linked to a process schedule which leads to a minimal (mean) work. For Brownian motors, it is also natural to ask for a maximal current within a given range of parameter values. It is quite obvious that these goals cannot be achieved concomittantly.

Processes occuring in the biological cell are often assumed to be intrinsically optimized by the evolutionary pressure for a high "fitness". However, it is unknown for most processes how the different competing goals are weighted. It is therefore interesting to study which optimization principles are able to explain the observed dynamics.

Recently, various optimization aspects of mesoscopic nonequilibrium processes have been discussed. For different discrete models of mesoscopic heat engines, where the potential landscape is characterized by only a few parameters, an optimization for a maximum current or a maximum power output has been performed [35, 36, 37]. Paradoxical Parrondo games [38] which can be interpreted as discrete analogues of Brownian motors [39], have also been optimized [40]. For continuous motor models, where optimization requires variational calculus, only few results exist. The optimization of driving schemes has been studied for time-dependently driven ratchet motors [41, 42]. Potential landscapes have been optimized for the transport across membrane channels [43] and for temperature ratchets [44]. Maximizing the current by using a feedback control strategy has been proposed recently [45, 46].

The present thesis is structured as follows: In the second chapter, we give an overview of the concept of stochastic thermodynamics, introducing relevant quantities for the following chapters.

In the third chapter, we study optimal protocols yielding a minimal mean work for the time-dependent transition from an initial equilibrium state to a final equilibrium state. We discuss different types of dynamics: (i) overdamped Langevin dynamics, (ii) underdamped Langevin dynamics, (iii) Hamiltonian dynamics with canonical initial conditions and (iv) Schrödinger dynamics with canonical initial conditions.

In the fourth chapter, we discuss the optimization of two different types of Brownian motor models with respect to a maximum power output. First, we consider a cyclic Brownian heat engine between two heat baths at different temperatures which can be regared as the mesoscopic analogue of a Carnot engine. We show that the efficiency at maximum power obeys a universal law. Second, we calculate the efficiency at maximum power for two generic models of biological motors.

In the fifth chapter, we optimize a recently introduced model for kinetic proofreading in the translation stage during gene expression. Here, we study the competing goals of a preferably high protein production rate and a preferably low error rate. We show that the experimentally observed rate constants cannot be explained by the optimization with respect to these evolutionary goals.

Last, we give perspectives for future research and discuss open questions. Technical details of the optimization approach for underdamped Langevin dynamics in the case study II are discussed in Appendix A.

2 Stochastic Thermodynamics

Most processes occuring within the biological cell have two common properties: (i) fluctuations are important since typical binding energies are on the order of the thermal energy $k_B T$, (ii) they are driven far out of equilibrium by chemical potential differences whereas the temperature T remains constant. For such situations, new thermodynamic approaches have been developped which will be outlined in the following for two paradigmatic nonequilibrium situations: the motion of a colloidal particle in an externally given, time-dependent potential $V(x, \lambda(\tau))$ and the motion of a colloidal particle in a nonequilibrium steady state created by a time-constant potential $V(x)$ and a constant force f acting on the particle.

Such a time-dependent external potential can be created, *e.g.*, by optical traps [47] and/or external boundaries. The potential is changed time-dependently by an external control parameter $\lambda(\tau)$, *e.g.* the position of the focus of the laser trap. For a sufficiently fast change of the control parameter, the system is driven far out of equilibrium and neither equilibrium thermodynamics nor linear irreversible thermodynamics are apllicable to describe thermodynamic properties of the system. Specifically, we consider a transition with total transition time t, $0 \leq \tau \leq t$, with initial value of the control parameter $\lambda(0) = \lambda_i$ and final value of the control parameter $\lambda(t) = \lambda_f$. We assume that the system initially is in thermal equilibrium with Boltzmann distribution

$$p(x, \tau = 0) = \frac{1}{Z} \exp[-\beta V(x, \lambda_i)] \tag{2.1}$$

where Z is the canonical partition function and $\beta \equiv 1/T$. The motion of the colloidal particle is stochastic due to the interaction with the surrounding fluid. It can be described to good accuracy by the Langevin equation

$$\dot{x} = -\mu \frac{\partial V(x, \lambda)}{\partial x} + \zeta \tag{2.2}$$

where μ is the mobility of the particle and the dot will denote time derivatives througout the thesis. The thermal fluctuations are modelled as Gaussian white noise

$$\left\langle \zeta(\tau) \zeta(\tau') \right\rangle = 2 \mu T \delta(\tau - \tau'). \tag{2.3}$$

Here, we have set Boltzmann's constant $k_B = 1$ by choosing natural units for energies. Unless stated otherwise, we will use this convention throughout this thesis. The time evolution of the probability density function $p(x,\tau)$ to observe the particle at position x at time τ is then governed by the Fokker-Planck equation

$$\partial_\tau p(x,\tau) = \partial_x \left[\mu \frac{\partial V}{\partial x} + \mu T \partial_x \right] p(x,\tau). \tag{2.4}$$

The first law of thermodynamics can consistently be defined [6] by intruducing the work which is applied to the particle by the change of the external potential

$$\mathcal{W}[x(\tau)] \equiv \int_0^t d\tau \frac{\partial V}{\partial \lambda} \dot{\lambda}, \tag{2.5}$$

the difference in internal energy of the particle

$$\Delta\mathcal{E}[x(\tau)] \equiv V(\lambda_f, x(t)) - V(\lambda_i, x(0)) = \int_0^t d\tau \left[\frac{\partial V}{\partial \lambda} \dot{\lambda} + \frac{\partial V}{\partial x} \dot{x} \right] \tag{2.6}$$

and the heat

$$\mathcal{Q}[x(\tau)] \equiv \mathcal{W}[x(\tau)] - \Delta\mathcal{E}[x(\tau)] = -\int_0^t d\tau \frac{\partial V}{\partial x} \dot{x} = \int_0^t d\tau F \dot{x} \tag{2.7}$$

which is transferred via Stokes friction with a force $F \equiv -\partial_x V$ to the heat bath of the surrounding fluid.

These quantities are stochastic in the sense that they depend on the whole trajectory of the particle which is subject to thermal fluctuations. It can be shown [9, 10] that the probability density function $p(\mathcal{W})$ of the stochastic work $\mathcal{W}$ is related to the equilibrium free energy difference between initial and final state by the Jarzynski relation

$$\left\langle e^{-\beta \mathcal{W}} \right\rangle = e^{-\beta \Delta F}$$

where the average $\langle \cdot \rangle$ is defined by $\langle f(\mathcal{W}) \rangle \equiv \int d\mathcal{W} p(\mathcal{W}) f(\mathcal{W})$. The definition of the heat flux into the medium (2.7) allows for the definition of the entropy flux to the heat bath

$$\Delta s_M[x(\tau)] \equiv \mathcal{Q}[x(\tau)]/T. \tag{2.8}$$

The nonequilibrium entropy of the system can be defined as

$$s(\tau) \equiv -\ln p(x(\tau),\tau) \tag{2.9}$$

which yields the conventional Shannon entropy after averaging. The change of the nonequilibrium system entropy during the transition thus is given by

$$\Delta s[x(\tau)] = -\ln p(x(t),t) + \ln p(x(0),0). \tag{2.10}$$

It is now straightforward to define the total entropy production [7]

$$\Delta s_{\text{tot}} \equiv \Delta s_M[x(\tau)] + \Delta s[x(\tau)] \tag{2.11}$$

which can be shown to satisfy the integral fluctuation theorem

$$\left\langle e^{-\Delta s_{\text{tot}}} \right\rangle = 1. \tag{2.12}$$

This immediately implies the second law of thermodynamics

$$\langle \Delta s_{\text{tot}} \rangle \geq 0 \tag{2.13}$$

via the Jensen inequality.

So far, we have considered only transitions between equilibrium states. Within the cell, however, most processes are constantly driven out of equilibrium by persisting constant thermodynamic forces, *e.g.* chemical potential differences. In such a situation, the system typically reaches a nonequilibrium steady state, where probability distributions do not change anymore while the system is permanently in nonequilibrium. As a paradigm, the motion of a colloidal particle in a spatial periodic potential $V(x)$ subject to an additional external force f, which can be realized in experiments by a rapidly rotating optical trap, has been studied extensively [48, 49, 50]. Since the potential is time-independent, the work then is given by the contribution of the external force f

$$\mathcal{W} \equiv \int_0^t d\tau f \dot{x}, \tag{2.14}$$

while the difference in internal energy is given by

$$\Delta\mathcal{E}[x(\tau)] = V(\lambda_f, x(t)) - V(\lambda_i, x(0)) = \int_0^t d\tau \frac{\partial V}{\partial x}\dot{x}. \tag{2.15}$$

The heat then can consistently be defined as

$$\mathcal{Q}[x(\tau)] = \mathcal{W}[x(\tau)] - \Delta\mathcal{E}[x(\tau)] = \int_0^t d\tau \left(f - \frac{\partial V}{\partial x}\right)\dot{x}. \tag{2.16}$$

In such a nonequilibrium steady state, the total entropy production in a given time interval $0 \leq \tau \leq t$ can be defined in complete analogy to the case discussed above. The total entropy production then satisfies also the detailed fluctuation theorem [7]

$$p(-\Delta s_{\text{tot}}) = p(\Delta s_{\text{tot}}) e^{-\Delta s_{\text{tot}}} \tag{2.17}$$

which immediately implies the integral fluctuation theorem (2.13), where $p(\Delta s_{\text{tot}})$ is the probability density function to observe the entropy production Δs_{tot}. For large systems or large times, the entropy production will also typically be large and thus the probability to find a negative entropy production decays exponentially. For macroscopic systems, this probability is negligible and the observed entropy production will always be strictly positive.

3 Optimal protocols

3.1 Introduction

The free energy difference ΔF between two equilibrium states is an important quantity in isothermal statistical mechanics which allows, *e. g.*, for the calculation of occupation probabilities under equilibrium conditions. Moreover, the free energy is also important for the dynamics of biomolecules. In many cases, the effective dynamics in terms of "good" reaction coordinates can be formulated by an overdamped Langevin equation. Assuming a constant mobility μ, the dynamics then is determined only by the free energy landscape.

Strategies to extract ΔF from experiments or computer simulations are traditionally based on either thermodynamic integration or thermodynamic perturbation [51] which use one infinitesimally slow transition or many infinitesimally fast transitions, respectively, between the two equilibrium states. A decade ago, Jarzynski proposed the remarkable relation

$$e^{-\Delta F/T} = \left\langle e^{-\mathcal{W}/T} \right\rangle \tag{3.1}$$

which interpolates between these extreme cases using nonequilibrium work values $\mathcal{W}$ obtained from trajectories of finite time transitions between the equilibrium states at temperature T (with Boltzmann's constant $k_B = 1$) [9, 10]. Although these (necessarily irreversible) finite time transitions occur in nonequilibrium, the equilibrium quantity ΔF can be inferred from a sufficient number of trajectories either from computer simulations [52, 53, 54, 55] or real experiments [56, 57]. The Jarzynski relation is valid for any given driving scheme $\lambda(\tau)$ between the two equilibrium states. It even allows to combine data from different driving schemes in free energy calculations in a straightforward way [58]. A generalization of the Jarzynski relation [8] has recently been used to calculate the difference of the grand canonical potential between two equilibrium states for the adsorption of polyelectrolytes on a charged surface [59].

Beyond the free energy difference between two equilibrium states, one is often interested in the complete free energy "landscape" (also termed potential of mean force) as a function of a given reaction coordinate. A variant of the

Jarzynski relation [18] has been used to extract potentials of mean force both in simulations [60, 61, 62, 63, 64, 65, 66] and in experiments [67] (see also the comment [68] and reply [69]). In order to fully describe the dynamics of the reaction coordinate, the mobility μ, which may be a function of the reaction coordinate, must be known. It has been shown recently [70, 71, 72] that the mobility can easily be extracted from the same nonequilibrium pulling experiments / simulations. In fact, an accurate estimate of the mobility as a function of the reaction coordinate requires much less nonequilibrium trajectories than the accurate estimate of the potential of mean force.

For free energy calculations via "fast growth" techniques using the Jarzynski relation or some variant, the convergence of the involved exponential average causes problems for far out of equilibirium transitions where the mean work W is substantially larger than the free energy difference ΔF [73]. In this regime, the exponential average is dominated by low work values which are very rarely sampled [74]. As a remedy, several path sampling techniques biasing the dynamics for low work have been proposed [75, 76, 77, 78]. Alternatively, the Jarzysnki relation may be interpreted in terms of a bijective map which must not correspond to any realistic dynamics and which can also be optimized [24, 79]. It has even been proposed to optimize free energy estimates by using two distinct protocols for the generation of nonequilibrium trajectories and the calculation of the work [80]. For the reconstruction of free energy landscapes, only few studies have discussed schemes to improve the convergence of these calculations [61, 81].

It is still under debate [82, 83, 84] for which systems "fast growth" techniques are superior to refined "conventional" approaches such as umbrella sampling [85] or flat histogram methods [86]. It is also unclear how the "cost" of obtaining correctly sampled initial values can be taken into account. Though valuable for computer simulations, it is hard to imagine how to bias dynamics in real experiments, where, however, apparatus drift may prevent long measurements necessary for thermodynamic integration [57, 87] and thus render fast growth methods competitive.

Both for thermodynamic integration and "fast growth" methods, efficiency gains can be achieved by optimizing the driving scheme $\lambda(\tau)$. For thermodynamic integration, where the work $\mathcal{W}$ with mean value $W \geq \Delta F$ is taken as an estimator for ΔF, it is quite obvious that a minimal work gives the best result. In this context, studies of optimal driving schemes have either been restricted to the linear response regime [88, 89] or involved only an optimization with respect to a single parameter [90, 91]. In the case of fast growth methods, the statistics for free energy estimates quite generally also improves with smaller mean work [74, 76].

In this chapter, we discuss optimal protocols for four different types of dynamics.

First, we calculate optimal protocols for overdamped Langevin dynamics which is a good description for many biological processes on time scales much larger than the characteristic decay time of the momentum. Most experimental studies on the Jarzynski relation and fluctuation theorems use overdamped Langevin dynamics to describe the motion of a colloidal particle in a potential generated by optical traps [92, 93, 94, 13]. In paradigmatic protein pulling experiments [56, 57], the dynamics can also be described by an overdamped Langevin equation if the pulling direction is a “good” reaction coordinate. As a main result, we find that the optimal protocol for overdamped Langevin dynamics shows jumps at the beginning and end of the finite time transition for two harmonic case studies.

Second, we study underdamped Langevin dynamics which is relevant for most molecular dynamics (MD) simulations of the dynamics of biomolecules. Such simulations typically are on time-scales where inertia plays an important role (see [95] for a review on steered MD). It is an interesting question how the results for the overdamped limit transfer to underdamped dynamics. In particular, it is important to know whether the jumps are a result of having neglected inertia. As a main result, we find that the optimal protocol does not only involve jumps but also delta-type singularities at the beginning and end.

Third, we optimize the driving protocol for purely Hamiltonian dynamics using the equilibrium thermal initial distribution for the particle's position and momentum. While biomolecules are typically described by a Langevin equation where effects of the thermal bath are included in friction and fluctuation terms, the Jarzynski relation has originally been derived in the framework of purely Hamiltonian dynamics with initial canonical equilibrium distribution [9]. This situation corresponds to an experiment where the heat bath of temperature T is decoupled from a small Hamiltonian system at time $\tau = 0$. During a time intevall $\tau \in [0, t]$ a control parameter λ is varied time-dependently. Such dynamics has been used in various generalizations of the Jarzynski relation [96, 23] and for the optimization of the free energy reconstruction from nonequilibrium work data [24, 82, 97]. While this approach is elegant from a theoretical point of view, it is important to note that such a dynamics has quite different properties than a system subject to a permanent heat bath modelled *e. g.* by a Langevin equation. The most important difference concerns the quasistatic work which is achieved for infinitesimally slow transitions $t \to \infty$, independent of the detailed shape of the protocol for the control parameter λ. For a system coupled permanently to a heat bath conserving the canonical distribution for fixed control parameter, this quasistatic work is equivalent to the free energy difference. This property gives rise to the free energy calculation method termed thermodynamic integration where the free energy is approximated by the work for a very slow transition. For purely Hamiltonian dynamics, however, the quasistatic work (which then is called adiabatic work) can exceed the free energy difference [82]. Still, the Jarzynski relation is valid and can be used to estimate free energy differences. It can be shown that under reasonable assumptions (mainly ergodicity), both the work is a monotonically decreasing function of the transition time t for a given protocol shape and the adiabatic work is independent of the shape of the protocol [98].

Last, we calculate optimal protocols for quantum systems with initial thermal equilibrium distribution. There has been considerable interest in deriving fluctuation theorems and analogues of the Jarzynski relation also for systems in the quantum domain [12, 25, 99, 100, 101, 102]. Here, it is more subtle than in the classical case to define thermodynamic quantities such as work on a single trajectory [99, 100, 101]. Apart from recent progresses for open quantum systems [101], most studies [12, 26, 103, 104] consider the case where the energy is measured at beginning and end, defining the work as the difference between final and initial energy. These studies rely on Schrödinger dynamics which has similar properties as Hamiltonian dynamics. In particular, the quasistatic work then is also different from the free energy difference. We show that the adiabatic work can be reached in any given finite time for harmonic potentials. The optimal protocol again is highly degenerate for these systems. We also study a two-level system of a single spin in a time-dependent magnetic field.

3.2 Overdamped Langevin dynamics

3.2.1 The model

Paradigmatically, a Langevin equation describes the driven overdamped motion of a single degree of freedom with coordinate x in a time-dependent one-dimensional potential $V(x, \lambda(\tau))$. As discussed in Chapter 2, the overdamped Langevin equation (2.2)

$$\dot{x} = -\mu \frac{\partial V(x, \lambda)}{\partial x} + \zeta \qquad (3.2)$$

with thermal fluctuations modelled as Gaussian white noise

$$\big\langle \zeta(\tau)\zeta(\tau')\big\rangle = 2\mu T\delta(\tau-\tau'), \tag{3.3}$$

describes, *e. g.*, the motion of a colloidal particle in a potential created by laser traps [92, 93] and/or external boundaries [13].

We consider a situation as described in Chapter 2. Initially, the system is in thermal equilibrium in the potential $V(x,\lambda_i)$. During the time-interval $0\le\tau\le t$, the control parameter $\lambda(\tau)$ is varied from λ_i to the final value λ_f. The time evolution of the probability distribution $p(x,\tau)$ to observe the particle at position x at time τ is governed by the Fokker-Planck equation (2.4)

$$\partial_\tau p(x,\tau) = \partial_x\left[\mu\frac{\partial V}{\partial x}+\mu T\partial_x\right]p(x,\tau). \tag{3.4}$$

The mean work spent in this process

$$W[\lambda(\tau)] = \int_0^t d\tau\dot{\lambda}\left\langle\frac{\partial V}{\partial\lambda}(x(\tau),\lambda(\tau))\right\rangle \tag{3.5}$$

is obtained from the stochastic work (2.5) by averaging over the initial thermal distribution and over the noise history where $\langle\dots\rangle$ denotes this averaging procedure. Since we are interested in processes leading to a minimal mean work, we will omit the averaging brackets and denote the mean work by W in the following. The mean work (3.5) is a functional of the protocol $\lambda(\tau)$ which now is to be minimized. We will first investigate two case studies motivated by previously set up experiments on colloidal particles and then analyze the general case.

3.2.2 Case study I: Moving harmonic potential

As an almost trivial, but still instructive introductory example, we consider a colloidal particle dragged through a viscous fluid by optical tweezers with harmonic potential

$$V(x,\tau) = \frac{k}{2}\left(x-\lambda(\tau)\right)^2, \tag{3.6}$$

see Fig 3.1a, with corresponding Langevin equation

$$\dot{x} = \mu k(\lambda - x) + \zeta. \tag{3.7}$$

The focus of the optical tweezers is moved according to the protocol $\lambda(\tau)$. In previous experiments, such protocols have been used to test the fluctuation theorem [92] and the Hatano-Sasa relation [94]. The optimal protocol $\lambda^*(\tau)$ connecting given boundary values $\lambda_i = 0$ and λ_f in a time t minimizes the mean total work (3.5)

$$W[\lambda(\tau)] = k \int_0^t d\tau \dot{\lambda}(\lambda - u) \tag{3.8}$$

with the mean position of the particle $u(\tau) \equiv \langle x(\tau) \rangle$. The mean work is a non-local functional of the protocol $\lambda(\tau)$, since $u(\tau)$ depends on all previous values of $\lambda(\tau')$, $\tau' < \tau$ via the ordinary differential equation

$$\dot{u} = \mu k(\lambda - u) \tag{3.9}$$

which follows from averaging the Langevin equation. However, by solving (3.9) for λ and $\dot{\lambda}$,

$$\begin{aligned} \lambda &= u + \dot{u}/(\mu k), \\ \dot{\lambda} &= \dot{u} + \ddot{u}/(\mu k), \end{aligned} \tag{3.10}$$

the mean work can be expressed as a time-local functional of the mean particle position $u(\tau)$ as

$$\begin{aligned} W[\lambda(\tau)] &= k \int_0^t d\tau \dot{\lambda}(\lambda - u) = \frac{1}{\mu^2 k} \int_0^t d\tau (\mu k \dot{u} + \ddot{u}) \dot{u} \\ &= \frac{1}{\mu} \int_0^t d\tau \dot{u}^2 + \frac{1}{2\mu^2 k} \left[\dot{u}^2 \right]_0^t . \end{aligned} \tag{3.11}$$

The Euler-Lagrange equation corresponding to (3.11),

$$\ddot{u} = 0, \tag{3.12}$$

is solved by $u(\tau) = m\tau$, where $u(0) = 0$ is enforced by the initial condition. Equation (3.9) then requires the boundary conditions

$$\begin{aligned} \dot{u}(0) &= \mu k \left(\lambda_i - u(0) \right) = 0, \\ \dot{u}(t) &= \mu k \left(\lambda_f - m t \right), \end{aligned} \tag{3.13}$$

which can only be met by discontinuities in $\dot{u}$ at the boundaries which correspond to jumps in λ. Note that these "kinks" do not contribute to the integral

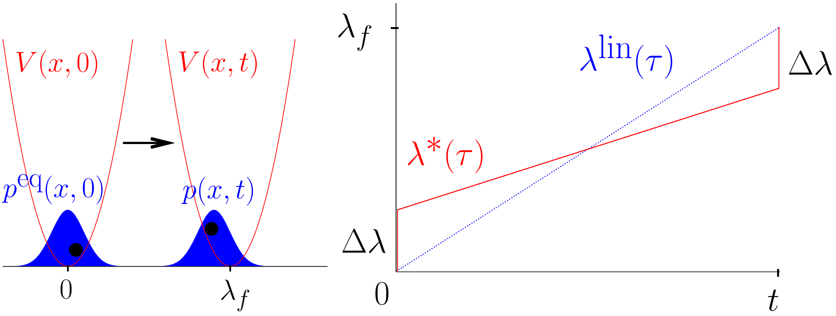

Figure 3.1 Optimal protocol for a moving harmonic potential (Case Study I). (a) Sketch of the considered nonequilibrium transition where the minimum of the potential (which may, *e. g.*, correspond to the focus of a laser trap) is moved according to a protocol $\lambda(\tau)$. Initially, the system is in thermal equilibrium with distribution $p^{\text{eq}}(x)$. (b) Optimal protocol $\lambda^*(\tau)$ with initial and final jumps with amplitude $\Delta\lambda$ compared to the linear protocol $\lambda^{\text{lin}}(\tau)$.

in the second line of (3.11). The yet unknown parameter m follows from minimizing the mean total work

$$W = m^2 \frac{t}{\mu} + \frac{k}{2}(\lambda_f - mt)^2 \tag{3.14}$$

which yields

$$m^* = \lambda_f \frac{\mu k}{\mu k t + 2}, \tag{3.15}$$

where the asterisk will denote optimal from now on. The minimal mean work

$$W^* = k\lambda_f^2 \frac{1}{\mu k t + 2} \tag{3.16}$$

vanishes in the quasi-static limit $t \to \infty$. The optimal protocol then follows from (3.9) as

$$\lambda^*(\tau) = \lambda_f \frac{\mu k \tau + 1}{\mu k t + 2}, \tag{3.17}$$

for $0 < \tau < t$. As a surprising result, this optimal protocol implies two distinct symmetrical jumps of size

$$\Delta\lambda \equiv \lambda(0^+) - \lambda_i = \lambda_f - \lambda(t^-) = \frac{\lambda_f}{\mu k t + 2} \tag{3.18}$$

at the beginning and the end of the process.

The benefit of having jumps in the optimal protocol can be understood intuitively as follows. From the perspective of minimal dissipation, it is obvious that the particle should be dragged at a constant (mean) velocity from the beginning rather than being accelerated during a finite time. This initial jump in the velocity of the particle can only be achieved by a finite initial difference $\lambda(0) - u(0)$, corresponding to a jump in λ at $\tau = 0$. The final jump is harder to grasp intuitively. In fact, it stems from focussing on the minimal work rather than on the minimal (mean) dissipation (or entropy production). If we had searched for the minimal entropy production (as defined in [7]), we would have found an optimal protocol without a final jump. In the present minimization, at the final time t, the particle is still in non-equilibrium with respect to the final potential $V(x, \lambda(t))$. Relaxation to equilibrium leads to further dissipation *after* time t which has, however, already been paid for by the total work since at constant λ no work is exerted anymore. A smaller final particle position $u(t)$ leads to a longer relaxation time which can decrease the total dissipation of the combined process (nonequilibrium transition and relaxation).

A priori, one might have expected a continuous linear protocol

$$\lambda^{\text{lin}}(\tau) = \lambda_f \tau / t \tag{3.19}$$

to yield the lowest work. The mean work for such a linear protocol can be calculated analytically by solving the ordinary differential equation (3.9) with initial condition $u(0) = 0$ which yields

$$u(\tau) = \frac{\lambda_f}{\mu k t}\left(e^{-\mu k \tau} - 1 + \mu k \tau\right). \tag{3.20}$$

The mean work then is given by (3.11)

$$W^{\text{lin}} = k \int_0^t d\tau \dot{\lambda}(\lambda - u) = \left(\frac{\lambda_f}{\mu k t}\right)^2 (e^{-\mu k t} - 1 + \mu k t) > W^*. \tag{3.21}$$

For any $t > 0$, the linear protocol yields a larger mean work than the optimal protocol with a maximal value $W^{\text{lin}}/W^* \simeq 1.14$ at $\mu t \simeq 2.69$, see Fig. 3.2.

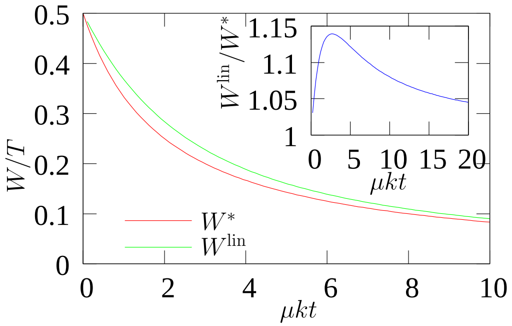

Figure 3.2 Optimal work W^* for a moving harmonic potential (case study I) compared to the work for a linear protocol W^{lin} as a function of the scaled transition time μkt.

In macroscopic finite-time thermodynamics, the occurrence of such jumps has previously been rationalized by pointing out the special nature of this type of variational problem where the highest derivative (here $\ddot{u}$ in (3.11)) occurs linearly [105]. In the present model where fluctuations are irrelevant to the mean work, these jumps have the same formal origin.

3.2.3 Case study II: Harmonic potential with time-dependent stiffness

In this example, fluctuations are crucial. We consider the motion of a colloidal particle in a trap whose strength becomes time-dependent whereas its position remains constant. The corresponding potential reads

$$V(x,\tau) = \frac{\lambda(\tau)}{2}x^2 \tag{3.22}$$

with $\lambda(0) = \lambda_i$ and $\lambda(t) = \lambda_f > \lambda_i$ as boundary conditions. Such a potential with a sudden jump protocol has been investigated experimentally as test of the fluctuation theorem [93]. We first derive the equation of motion for the variance $w(\tau) \equiv \langle x^2(\tau) \rangle$

$$\dot{w} = -2\mu\lambda w + 2\mu T \tag{3.23}$$

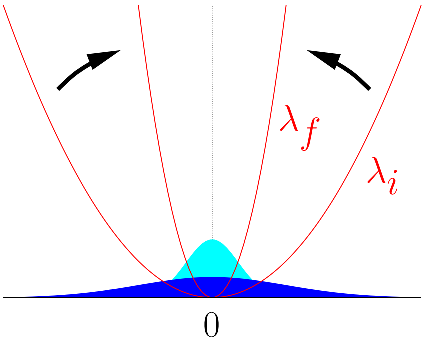

Figure 3.3 Sketch of the considered nonequilibrium transition where the stiffness of the harmonic potential is changed according to a protocol $\lambda(\tau)$. Initially, the system is in thermal equilibrium with distribution $p^{\mathrm{eq}}(x)$.

by multiplying (3.4) with x^2 and integrating over x. By solving (3.23) for λ,

$$\lambda = \frac{2\mu T - \dot{w}}{2\mu w}, \tag{3.24}$$

the mean work (3.5) can again be cast in a local functional of the new variable w and its first derivative

$$\begin{aligned} W[\lambda(\tau)] &= \int_0^t d\tau \dot{\lambda}\frac{w}{2} = [\lambda w/2]_0^t - \int_0^t d\tau \frac{\lambda \dot{w}}{2} \\ &= \frac{1}{2}\left[\lambda w - T\ln w\right]_0^t + \frac{1}{4\mu}\int_0^t d\tau \frac{\dot{w}^2}{w}. \end{aligned} \tag{3.25}$$

The minimization of the work functional then requires solving the Euler-Lagrange equation

$$\dot{w}^2 - 2w\ddot{w} = 0. \tag{3.26}$$

Its general solution

$$w(\tau) = c_1(1 + c_2\tau)^2 \tag{3.27}$$

contains two constants. The thermal initial distribution with $w(0) = T/\lambda_i$ fixes $c_1 = T/\lambda_i$. The second constant c_2 follows from minimizing the total mean work

$$W = T\left[\frac{(c_2t)^2}{\mu\lambda_i t} - \ln\left(1+c_2t\right) + \frac{1}{2}(\lambda_f/\lambda_i)\left(1+c_2t\right)^2 - \frac{1}{2}\right] \tag{3.28}$$

which leads to

$$c_2^* t = \frac{-1-\mu\lambda_f t + \sqrt{1+2\mu\lambda_i t + \mu^2\lambda_f\lambda_i t^2}}{2+\mu\lambda_f t}. \tag{3.29}$$

The optimal protocol derived from (3.24)

$$\lambda^*(\tau) = \frac{\mu\lambda_i - c_2^*(1+c_2^*\tau)}{\mu(1+c_2^*\tau)^2} \tag{3.30}$$

for $0 < \tau < t$ again implies jumps at the beginning and end of the process as shown in Fig. 3.4a. Both the minimal work W^*/T, see Fig. 3.4b, and the scaled optimal protocol $\lambda^*(\tau/t)/\lambda_i$ depend only on two parameters (λ_f/λ_i) and $\lambda_i t$.

For the two limiting cases of an immediate jump, $t \to 0$, and a quasi-static process, $t \to \infty$, respectively, the values of W^* also follow from general principles. For an immediate jump, the minimal work

$$W^{\mathrm{jp}} \equiv \lim_{t\to 0} W^* = \left\langle \frac{(\lambda_f-\lambda_i)x^2}{2} \right\rangle_{\lambda_i} = \frac{1}{2}T((\lambda_f/\lambda_i)-1) \tag{3.31}$$

is equal to the difference in energy evaluated in the thermal initial ensemble. In this limit, the optimal protocol $\lambda^*(\tau)/\lambda_i \approx ((\lambda_f/\lambda_i)+1)/2$ is constant for $0 < \tau < t$ but has discontinuities at $\tau = 0$ and $\tau = t$. In the quasi-static limit, the minimal work

$$W^{\mathrm{qs}} \equiv \lim_{t\to\infty} W^* = \frac{1}{2}T\ln(\lambda_f/\lambda_i) = \Delta F \tag{3.32}$$

is equal to the free energy difference ΔF between the final and the initial state. In this limit, the optimal protocol is continous at $\tau = 0$ and $\tau = t$ and takes the form

$$\lambda^*(\tau/t) \approx \frac{\lambda_i}{\left(1-(\tau/t)+\sqrt{(\lambda_i/\lambda_f)}(\tau/t)\right)^2}. \tag{3.33}$$

For $(\lambda_f/\lambda_i) \gg 1$, the minimal work is of the order of the quasi-static work for any $\mu\lambda_i t^* \gg 2/\ln(\lambda_f/\lambda_i)$ as a simple analysis of eqs. (3.28) and (3.29) shows.

Thus, the larger the change of the control parameter λ, the smaller is the time-interval required to essentially reach the quasi-static work, as quantitatively shown in Fig. 3.4c. The origin of this surprising features lies in the fact that the relaxation time scales like $1/\lambda$. For large λ, the particle can follow a larger change of the control parameter almost quasi-statically. Therefore, the optimal protocol can become quite steep towards the end of the process for large λ_f.

3.2.4 General case

For a general non-harmonic potential, it is not possible to express the mean work as a local functional of just one variable as we have done for the two harmonic cases. Rather, our optimization problem becomes non-local in time since changing the protocol at a time τ affects the mean work increments for all later times $\tau' > \tau$. This fact becomes obvious by expressing the mean work as a path integral average

$$W[\lambda(\tau)] = \int d[x(\tau)]p[x(\tau)] \int_0^t d\tau \dot{\lambda} \frac{\partial V}{\partial \lambda} \tag{3.34}$$

over all possible trajectories $x(\tau)$ with weight

$$p[x(\tau)] = \mathcal{N} p(x,0) \exp\left[- \int_0^t d\tau \left(\frac{(\dot{x} + \mu \partial_x V)^2}{4\mu T} - \mu \frac{\partial_x^2 V}{2} \right) \right], \tag{3.35}$$

where $\mathcal{N}$ is a normalization constant. Minimizing the mean work (3.5) then requires solving the non-local Euler-Lagrange equation

$$\frac{d}{d\tau} \left\langle \frac{\partial V}{\partial \lambda} \right\rangle_{|\tau=\sigma} = \frac{\delta W[\lambda(\tau)]}{\delta \lambda(\sigma)} \tag{3.36}$$

where the right hand side can be expressed by correlation functions as

$$\begin{aligned} \frac{d}{d\tau} \left\langle \frac{\partial V}{\partial \lambda} \right\rangle_{|\tau=\sigma} &= \dot{\lambda} \left\langle \frac{\partial^2 V}{\partial \lambda^2} \right\rangle_{|\tau=\sigma} + \\ \int_\sigma^t d\tau \frac{\dot{\lambda}}{2} &\left\langle \left(\mu \frac{\partial^3 V}{\partial \lambda \partial^2 x} - \frac{(\dot{x} + \mu \partial_x V)}{T} \frac{\partial^2 V}{\partial \lambda \partial x} \right)_{|\tau=\sigma} \cdot \frac{\partial V}{\partial \lambda}_{|x(\tau)} \right\rangle . \end{aligned} \tag{3.37}$$

Note that it suffices to let the integral in (3.37) start at σ since all contributions from times $\tau < \sigma$ vanish due to causality. For harmonic potentials, this integro-differential equation can be solved, confirming the results obtained in the case studies I and II [106]. In general, equation (3.37) solved by the optimal protocol

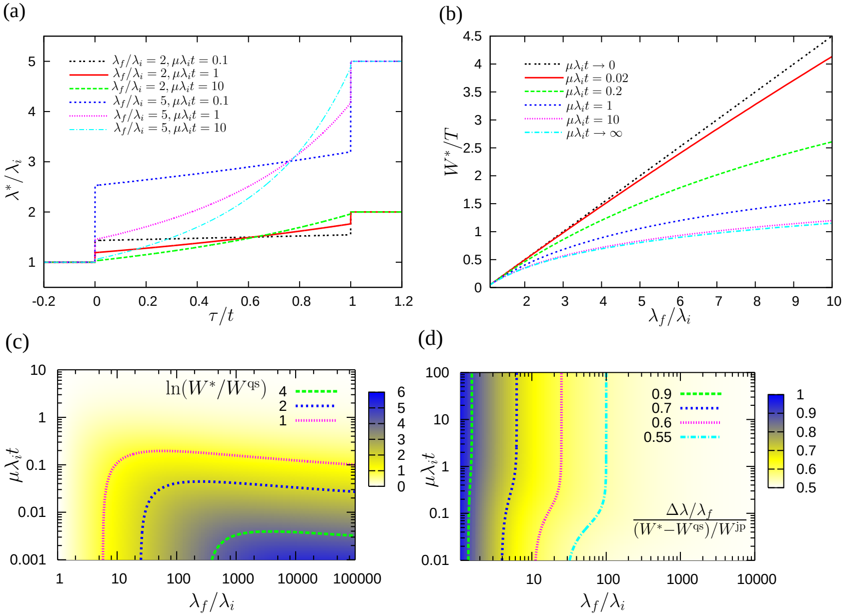

Figure 3.4 Optimization results for a time-dependent strength $\lambda(\tau)$ of a laser trap for different values of (λ_f/λ_i) and $\mu\lambda_i t$ (case study II): (a) Optimal protocols λ^*/λ_i as a function of the scaled time τ/t. (b) Minimal work W^* in units of T. (c) Logarithmic fraction $\ln(W^*/W^{\mathrm{qs}})$ of the optimal work and the quasistatic work. (d) Relative height $\Delta\lambda/\lambda_f$ of the jump of the optimal protocol at $t = 0$ in units of $(W^* - W^{\mathrm{qs}})/W^{\mathrm{jp}}$.

$\lambda^*(\tau)$ looks rather inaccessible. However, exploring a variational ansatz for $\lambda^*(\tau)$ with numerical evaluation of the mean work is a viable approach even for anharmonic potetials [106, 107].

In order to use jumps in the protocol $\lambda(\tau)$ for the efficient extraction of free energy differences from finite-time path sampling via the Jarzynski relation, one needs an estimate for the height of these jumps without knowing the underlying potential. For the moving laser trap (case study I), we get the relation

$$\Delta\lambda/\lambda_f = 2(W^* - W^{\mathrm{qs}})/W^{\mathrm{jp}}. \tag{3.38}$$

For case study II, we find numerically that the relative height of the jump $\Delta\lambda/\lambda_f$ at $t = 0$ is also of the order of $(W^* - W^{\mathrm{qs}})/W^{\mathrm{jp}}$, see Fig 3.4d. If such a relation gave the correct order of magnitude for the optimal jump in general cases, it could become a helpful tool for estimating the optimal jump heights.

3.3 Underdamped Langevin dynamics

We next discuss optimal protocols for underdamped Langevin dynamics

$$m\ddot{x} = -\gamma\dot{x} - V'(x, \lambda) + \eta(\tau), \tag{3.39}$$

of a Brownian particle with mass m in a viscous fluid with friction coefficient γ. The thermal fluctuations are modeled by Gaussian white noise

$$\langle \eta(\tau)\eta(\tau')\rangle = 2T\gamma\delta(\tau - \tau'). \tag{3.40}$$

In contrast to the overdamped Langevin equation, such dynamics does not neglect inertia effects. It has been shown that it is crucial to include the inertial term in an experimental test of the fluctuation theorem for a mesoscopic torsion pendulum immersed in a fluid where x is the angular displacement [21].

We again consider finite time transitions where the control parameter λ is changed time-dependently from the inital value λ_i to the final value λ_f and ask for the optimal protocol $\lambda(\tau)$ leading to a minimal mean work

$$W \equiv \int_0^t d\tau \dot{\lambda} \left\langle \frac{\partial V(x, \lambda)}{\partial \lambda} \right\rangle, \tag{3.41}$$

where the average $\langle \dots \rangle$ is over the intitial thermal distribution and over the noise history. The optimal protocol is calculated for both case studies introduced in Section 3.2.

3.3.1 Case Study I: Moving harmonic potential

Optimal protocol

As in the overdamped case, We first consider a Brownian particle dragged through a viscous fluid by the harmonic potential (3.6)

$$V(x,\tau) = \frac{k}{2}(x - \lambda(\tau))^2, \tag{3.42}$$

where k is the (constant) stiffness of the harmonic potential. Again, the minimum of the potential $\lambda(\tau)$ is changed time-dependently from an initial position $\lambda_i = 0$ to a final position λ_f. Including inertial effects, the Langevin equation reads

$$m\ddot{x} = -\gamma\dot{x} - k(x - \lambda(\tau)) + \eta(\tau), \tag{3.43}$$

The mean work spent in the process of total duration t is given by (3.41) which, in the present case, reduces to

$$W = \int_0^t d\tau k\dot{\lambda}(\lambda - u) = k\int_0^t d\tau \lambda\dot{u} + \frac{k}{2}\lambda_f^2 - k\left[\lambda u\right]_0^t, \tag{3.44}$$

where, for simplicity in the notation, we have defined the mean position of the particle as $u \equiv \langle x \rangle$. This quantity $u(\tau)$ depends on the whole history of $\lambda(\tau)$ and thus, the work W is a non-local functional of the protocol $\lambda(\tau)$. However, in analogy to the overdamped limit, see Chapter 3.2, we can express the work as a local functional of the mean particle position u. Averaging the evolution equation (3.43) yields

$$\lambda = u + \gamma\dot{u}/k + m\ddot{u}/k, \tag{3.45}$$

which inserted in (3.44) leads to

$$W = \left[\frac{m}{2}\dot{u}^2 + \frac{m^2}{2k}\ddot{u}^2 + \frac{m\gamma}{k}\dot{u}\ddot{u} + \frac{\gamma^2}{2k}\dot{u}^2\right]_0^t + \gamma\int_0^t d\tau\dot{u}^2. \tag{3.46}$$

The only term remaining in the integral, $\dot{u}^2$, is identical to the corresponding integrand in the overdamped limit, see equation (3.11), while the boundary terms are different. In complete analogy to the overdamped case, we now proceed in two steps. First, we calculate the optimal shape $u(\tau)$ minimizing only the integral given initial values $u(0^+) = 0$ and $\dot{u}(0^+) = A$. Note that despite the initial equilibrium value $\dot{u}(0) = 0$, we are free to choose $\dot{u}(0^+) = A$

since the necessary “kink” in $u(\tau)$ at $\tau = 0$ does not contribute to the integral. Similarly, at the end of the protocol (at $\tau = t$) there can be another jump in the velocity. In a second step, we adjust the constant A to yield the minimal total work. First, from the Euler-Lagrange equation corresponding to the Lagrangian $\dot{u}^2$ (and subject to the initial conditions just mentioned), we find

$$u(\tau) = A\tau \tag{3.47}$$

for $0 < \tau < t$. In contrast to the overdamped case, we cannot determine all the boundary terms at t from the evolution equation. Thus, $C \equiv \dot{u}(t)$ is another free parameter. With

$$\ddot{u}(t) = [k(\lambda_f - At) - \gamma C]/m, \tag{3.48}$$

we get the total work as a function of the yet unknown constants A and C

$$W(A, C) = \frac{m}{2}C^2 + \frac{k}{2}(\lambda_f - At)^2 + \gamma \int_0^t d\tau A^2. \tag{3.49}$$

We next minimize the work with respect to the remaining parameters A and C. Obviously, the work is minimal for $C^* = 0$. The remaining terms then read

$$W(A) = \frac{k}{2}(\lambda_f - At)^2 + \gamma t A^2, \tag{3.50}$$

which, surprisingly, is exactly the same expression that was found in the overdamped limit. Minimizing this expression with respect to A leads to

$$A^* = \frac{\lambda_f}{2\gamma/k + t} \tag{3.51}$$

which yields the work

$$W^* = k\lambda_f^2 \frac{1}{2 + kt/\gamma}. \tag{3.52}$$

Inserting (3.47) into (3.45), we find the optimal protocol

$$\lambda^*(\tau) = \lambda_f \frac{k\tau/\gamma + 1}{kt/\gamma + 2}, \tag{3.53}$$

for $0 < \tau < t$ implying symmetrical jumps

$$\Delta\lambda \equiv \lambda(0^+) - \lambda_i = \lambda_f - \lambda(t^-) = \lambda_f \frac{1}{kt/\gamma + 2} \tag{3.54}$$

at the beginning and at the end of the process.

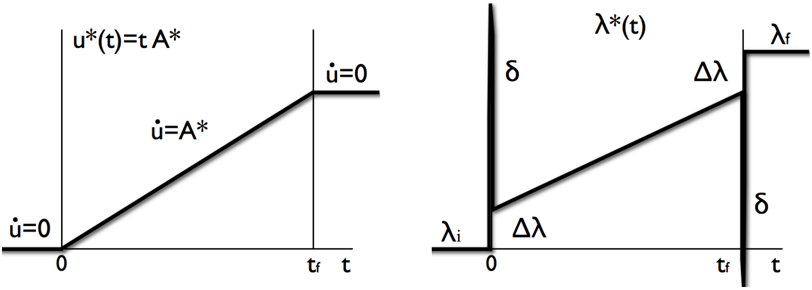

Figure 3.5 Scheme of the optimal mean position $u^*(\tau)$ and protocol $\lambda^*(\tau)$.

Superficially, this optimal protocol looks like the expression in the overdamped case, see Chapter 3.2. There is, however, a subtle difference arising from the presence of inertia terms. The optimal protocol forces the mean velocity to instantly jump at the beginning of the process from its initial equilibrium value $\dot{u}(0) = 0$ to $\dot{u}(0^+) = A^*$. At the end of the protocol, the optimal strategy consists in setting back the mean velocity to zero $\dot{u}(t) \equiv C^* = 0$. Due to the second time derivative in the equation of motion such jumps in the velocity, which require delta functions in the acceleration, imply a delta-type singularity in the protocol. Specifically, in (3.45), the jumps in $\dot{u}$ imply a δ-function for $\ddot{u}$ and hence a δ function in $\lambda(\tau)$. The optimal protocol (3.53) thus becomes

$$\lambda^*(\tau) = \lambda_f \frac{k\tau/\gamma + 1}{kt/\gamma + 2} + \frac{m\lambda_f}{2\gamma + kt} \left[\delta(\tau) - \delta(\tau - t)\right], \tag{3.55}$$

as shown in Fig. 3.5. In the overdamped limit, $m \to 0$, the delta peaks vanish.

Physical origin of singularities in the optimal protocol

The benefit of having jumps in the optimal protocol has already been rationalized in the previous section. There, we have argued that it is obvious that the particle should be dragged at a constant (mean) velocity from the beginning rather than being accelerated during a finite time. In the present underdamped regime, such a velocity jump corresponds to a jump in the (mean) particle momentum which can only be achieved by a delta peak in the force, corresponding to a delta peak in the protocol.

The final delta peak corresponds to setting the final velocity to zero. This decreases the kinetic energy of the particle and thus is beneficial for a small work. It also explains the surprising fact that, according to (3.52), we do not have to pay any extra cost for having inertia. During the initial singularity, the exerted work is stored in the (mean) kinetic energy of the particle. This contribution is fully recovered during the final singularity where the kinetic energy of the particle is set back to the equilibrium value.

Comparison to a linear protocol

As in the overdamped case, we compare the optimal work to the work obtained for the continuous linear protocol

$$\lambda^{\mathrm{lin}}(\tau) \equiv \lambda_f \tau / t. \tag{3.56}$$

In the overdamped limit, the work for a linear protocol was at most 14% larger than for the optimal protocol. We now check how much smaller the value of the optimal work W^* is compared to a linear protocol if we include inertia. First, we rescale the system in order to compactly write the relevant combination of parameters. With the rescaled mass $\tilde{m} \equiv mk/\gamma^2$, the energy scale $e \equiv k\lambda_f^2$ and a rescaled time $\tilde{t} \equiv tk/\gamma$, the work can be written as $W = e\tilde{W}(\tilde{t}, \tilde{m})$, with the optimal work $W^* = e/\left(2+\tilde{t}\right)$.

Solving the second order differential equation of motion (3.45) using the linear protocol $\lambda^{\mathrm{lin}}(\tau)$, we find the ratio:

$$\frac{W^{\mathrm{lin}}}{W^*} = \begin{cases} \frac{2+\tilde{t}}{\tilde{t}^2}\left(\theta_0 + \tilde{t} - e^{-\frac{\tilde{t}}{2\tilde{m}}}\left[\theta_0 \cosh\left(\nu\tilde{t}\right) + \theta_1 \sinh(\nu\tilde{t})\right]\right) & \tilde{m} < \frac{1}{4} \\ \frac{2+\tilde{t}}{\tilde{t}^2}\left(\theta_0 + \tilde{t} - e^{-\frac{\tilde{t}}{2\tilde{m}}}\left[\theta_0 \cos\left(\nu\tilde{t}\right) + \theta_1 \sin(\nu\tilde{t})\right]\right) & \tilde{m} > \frac{1}{4} \end{cases} \tag{3.57}$$

with

$$\nu = \frac{\sqrt{|4\tilde{m} - 1|}}{2\tilde{m}} \tag{3.58}$$

and

$$\theta_0 = \tilde{m} - 1, \quad \theta_1 = \frac{3\tilde{m} - 1}{2\tilde{m}\nu}. \tag{3.59}$$

In Fig. 3.6, we plot the ratio W^{lin}/W^* as a function of rescaled time $\tilde{t}$ and mass $\tilde{m}$. This result shows that the optimal protocol significantly reduces the work spent in the process compared to a linear protocol.

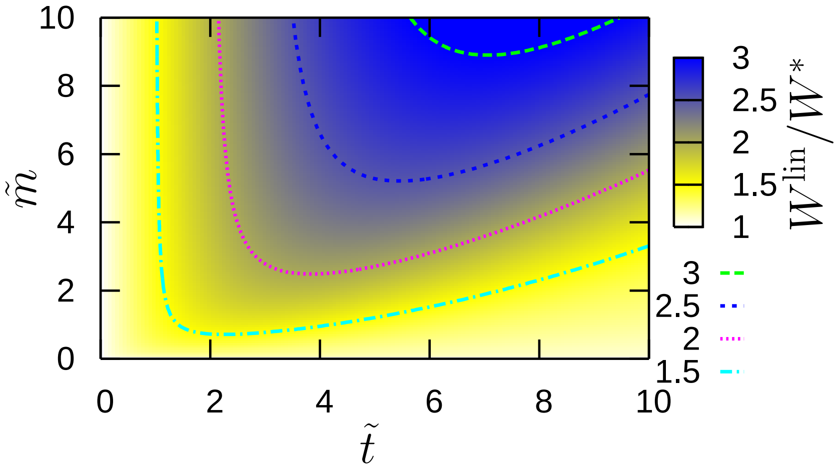

Figure 3.6 Ratio between mean work W^{lin} spent using the continuous linear protocol $\lambda^{\text{lin}}(\tau)$ and optimal work W^* as a function of the dimensionless parameters $\tilde{m} \equiv mk/\gamma^2$ and $\tilde{t} \equiv tk/\gamma$.

3.3.2 Case Study II: Harmonic potential with time-dependent stiffness

In the first case study, only the averaged quantity $u = \langle x \rangle$ appeared in the work and thus the same result could have been obtained from a deterministic damped dynamics. In analogy to the overdamped case, we next examine a second case study where fluctuations are important. We consider a Brownian particle of mass m in a harmonic potential with time-dependent stiffness $\lambda(\tau)$ which is driven from an initial value $\lambda(0) = \lambda_i$ to a final value $\lambda(t) = \lambda_f$ in a finite time t. The time-dependent potential

$$V(x,\tau) = \frac{\lambda(\tau)}{2} x^2, \tag{3.60}$$

leads to the underdamped Langevin equations

$$\begin{aligned} \dot{x} &= p/m \\ \dot{p} &= -\gamma p/m - \lambda(\tau) x + \eta(\tau), \end{aligned} \tag{3.61}$$

where p is the momentum of the particle and the noise $\eta(\tau)$ has the same properties introduced in the first case study. Again our main goal is to find the protocol for which the corresponding total (mean) work (3.41)

$$W = \int_0^t d\tau \dot{\lambda} \frac{\langle x^2 \rangle}{2} \tag{3.62}$$

is minimal. Note that the mean squared position

$$w \equiv \langle x^2 \rangle \tag{3.63}$$

of the particle is non-trivially coupled to the mean squared momentum

$$z \equiv \langle p^2 \rangle \tag{3.64}$$

and to the position-momentum correlation

$$y \equiv \langle xp \rangle. \tag{3.65}$$

Their time evolution is governed by the set of coupled differential equations

$$\begin{aligned} \dot{w} &= 2y/m, & (3.66)\\ \dot{z} &= -2\lambda y - 2\gamma z/m + 2\gamma T, & (3.67)\\ \dot{y} &= z/m - \lambda w - \gamma y/m. & (3.68) \end{aligned}$$

Unlike both the moving trap (with and without inertia) and the stiffening trap in the overdamped limit, the present case is much more involved since one cannot eliminate the protocol and write the work as a function of one variable only. We thus express the work as a time-local functional of $x(\tau)$ and $z(\tau)$. Solving Eqs. (3.66) and (3.68) for λ yields

$$\lambda = \frac{1}{w}[z/m - \gamma \dot{w}/2 - m\ddot{w}/2] \tag{3.69}$$

which, inserted in (3.62) and after partial integration, leads to

$$W = \left[\frac{\lambda w}{2} + \frac{m\dot{w}^2}{8w} \right]_0^t + \frac{1}{2} \int_0^t d\tau \mathcal{L} \tag{3.70}$$

with the “Lagrangian”

$$\mathcal{L} = \frac{\gamma \dot{w}^2}{2w} - \frac{z\dot{w}}{mw} + \frac{m\dot{w}^3}{4w^2}. \tag{3.71}$$

We proceed in two steps analogously to the moving trap. We first minimize the integral in (3.70) for given initial conditions and then optimize with respect to remaining free parameters. The integrand $\mathcal{L}$ depends on w (and $\dot{w}$) but also on z. The variables w and z are not independent. Eliminating λ and y from the equations of motion (3.66), (3.67), and (3.68), we find the physical constraint

$$\mathcal{G} \equiv z\dot{w} - m\gamma\dot{w}^2/2 - m^2\dot{w}\ddot{w}/2 - 2\gamma T w + 2\gamma w z/m + w\dot{z} = 0. \tag{3.72}$$

A detailed analysis of the solution of this optimization problem using Euler-Lagrange equations is given in Appendix A.

The results for both the rescaled optimal protocol $\lambda^*(\tau/t)/\lambda_i$ and the optimal work W^*/T depend on the dimensionless quantities

$$\tilde{t} \equiv t\lambda_i/\gamma, \quad \tilde{\lambda} \equiv \lambda_f/\lambda_i, \quad \tilde{m} \equiv \lambda_i m/\gamma^2. \tag{3.73}$$

An extensive analysis of the optimal protocol as a function of all three parameters is out of scope. Since the overdamped limit ($\tilde{m} \to 0$) has been discussed previously, we focus on the behaviour as a function of $\tilde{m}$ for given $\tilde{\lambda} = 2$, $\tilde{t} = 1$. Given these parameters, the optimization problem can be solved numerically and the corresponding total work W can be calculated. In Fig. 3.7a, we plot the value of the minimal work W^* (obtained from the optimal protocol) as a function of the rescaled dimensionless mass $\tilde{m}$ and compare it to other benchmark protocols. All work values are bounded from below by the free energy difference $\Delta F = (\ln 2/2)\, T \simeq 0.35T$. Quite generally, work values are also bounded from above by the work for an immediate jump $W^{\mathrm{jp}} \equiv \lim_{t\to 0} W^* = T/2$. We study (i) a linear protocol, (ii) a protocol leading to a parabolic mean-squared position

$$w(\tau) = \frac{T}{\lambda_i}(1 + c\tau)^2 \tag{3.74}$$

with optimized parameter c and optimized final delta peak, and (iii) a protocol leading to

$$w(\tau) = 1 + a\tau^3\left(1 - e^{-1/\left[0.01 + (5\tau/t)^2\right]}\right) + b\tau^5 + c\tau^7 + d\tau^9 \tag{3.75}$$

without any discontinuities (except for a final jump) but with free parameters a, b, c, d. The work arising from protocol (i) lies significantly above the optimal protocol. Protocol (ii) implies (optimized) jumps and delta peaks at the beginning and end. The work for protocol (ii) and the optimal work almost coincide. The inset shows that the optimal work is in fact slightly smaller than

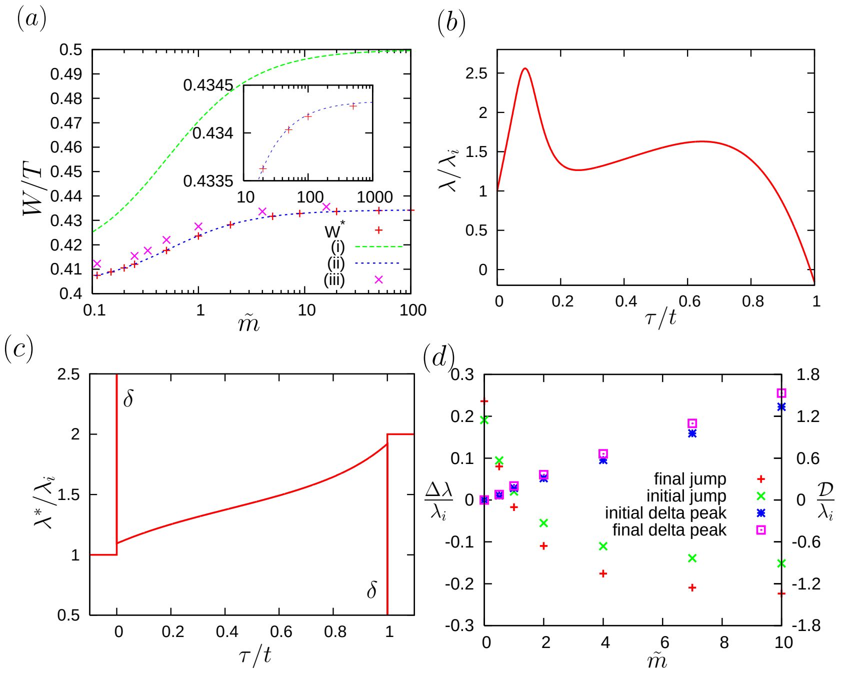

Figure 3.7 Optimization results for case study II for $\tilde{t} = 1$ and $\tilde{\lambda} = 2$. (a) Mean work W^* in units of T as a function of the rescaled mass $\tilde{m}$ compared to (i) a linear protocol, (ii) a protocol leading to $w(t)$ given by (3.74), and (iii) a continuous (except for a final jump) protocol leading to $w(\tau)$ given by (3.75) with adjusted parameters to yield a minimal work (see main text for details). (b) Protocol (iii) with optimized parameters for $\tilde{m} = 1$. (c) Optimal protocol $\lambda^*(\tau)$ for $\tilde{m} = 0.5$. (d) Jump heights $\Delta\lambda$ and amplitudes $\mathcal{D}$ of delta peaks (in rescaled time τ/t) for the optimal protocol as a function of the rescaled mass $\tilde{m}$.

the work obtained for the protocol (ii). The difference to the numerically obtained exact solution W^* decreases for decreasing $\tilde{m}$ which is consistent with the analytical finding that protocol (ii) is optimal in the overdamped limit. The fact that protocol (ii) which involves optimized singularities but not the optimized shape is so close to the optimal work highlights the importance of jumps for the optimal protocol. Protocol (iii) has no delta peaks and no initial jump but mimics these features approximately since the parameters a, b, c, d have been optimized, see Fig. 3.7b. These trial protocols show that jumps and delta peak-like singularities can decrease the total work and confirms that our numerical solution of the Euler-Lagrange equations is the solution of the optimization problem.

Finally, the explicit shape of the optimal protocol $\lambda^*(\tau)$ can be reconstructed numerically from (3.69), see Fig. 3.7c. It displays initially a delta peak upwards accompanied with a jump $\Delta\lambda$ and, finally, a delta peak downwards together with another jump $\Delta\lambda'$. Such discontinuities in the protocol are a consequence of the discontinuities in z, $\dot{w}$ and $\ddot{w}$. The first singularity is "needed" to suddenly increase $\langle p^2 \rangle$ from its equilibrium value and also to change the derivative of $\langle x^2 \rangle$, which is proportional to the correlation $\langle xp \rangle$. Note that both size and direction of the jumps strongly depend on the rescaled mass $\tilde{m}$ as shown in Fig. 3.7d. For small $\tilde{m}$, the protocol jumps upwards (as also observed in the overdamped regime, see Chapter 3.2) while for large $\tilde{m}$, the protocol jumps downwards.

3.3.3 Discussion

We have calculated optimal protocols yielding the minimal mean work for underdamped Langevin dynamics in two different harmonic model potentials. Surprisingly, these optimal protocols involve jumps and delta peaks at the initial and final times $t_i = 0$ and t_f. While we have shown that the singularities in the optimal protocol appear for harmonic potential, there is no reason to believe that this feature generically vanishes for anharmonic potentials. In fact, in the overdamped limit, a recent study has shown that initial and final jumps are also present in a simple anharmonic potential [106]. At first sight, such singularities seem to be unphysical since neither jumps nor delta peaks can be implemented in real experiments. Still our theoretical result is an important insight because it implies that there exists no optimal continuous protocol. Every such protocol could be improved by even steeper gradients mimicking the jumps and delta peaks at the beginning and end. If there was an experimental constraint on the allowed maximum rate of change in λ, $|\dot{\lambda}| < r$, the minimal work would still be achieved by a protocol which looks roughly like the optimal one, with the jumps and delta peaks replaced by their best approximation consistent with $|\dot{\lambda}| < r$ (*e. g.* steep straight lines instead of jumps). Thus, it should be possible to exploit our results for real experiments.

Our results may also be used in steered MD simulations. Even though we here have calculated optimal protocols for underdamped Langevin dynamics, there is no reason to believe that other thermostats frequently used in MD simulations would yield qualitatively different results for the optimal protocol. We have neglected memory effects by assuming white noise. While there are systems for which the underdamped Langevin equation is an appropriate physical description [21], it might still be interesting to see how our results are altered when considering memory effects.

3.4 Hamiltonian dynamics

In this section, we will study minimum work protocols for Hamiltonian dynamics. We again consider the two harmonic case studies of a moving harmonic potential and a harmonic potential with time-dependent stiffness. Additionally, we discuss an anharmonic quartic potential.

3.4.1 Case Study I: Moving harmonic potential

We consider a particle of mass m subject to a moving harmonic potential

$$V(x,\tau) = \frac{k}{2}(x-\lambda(\tau))^2, \tag{3.76}$$

where k is the (constant) stiffness of the potential. The minimum of the potential $\lambda(\tau)$ is changed time-dependently from an initial position $\lambda_i = 0$ to a final position λ_f. The Hamiltonian dynamics of position and momentum of the particle at time τ then is governed by the equations of motion

$$\begin{aligned} \dot{x} &= p/m, \\ \dot{p} &= -V'(x,\tau) = k(\lambda(\tau) - x) \end{aligned} \tag{3.77}$$

where the prime denotes the derivative with respect to x. The particle initially is in thermal equilibrium with probability density

$$\rho(x_0,p_0) = \mathcal{N} \exp[-\beta V(x_0,0)] \exp[-\beta p_0^2/(2m)] \tag{3.78}$$

for the initial position x_0 and the initial momentum p_0 with normalization constant $\mathcal{N}$.

Since there is no heat transfer during the (purely Hamiltonian) transition, the work is given by the change of internal energy. Averaging over all initial conditions yields the mean work

$$\begin{aligned} W &= \left[\frac{\langle p^2\rangle}{2m} + \langle V\rangle\right]_0^t \\ &= \left[\frac{\langle p^2\rangle}{2m} + \frac{k}{2}\left(\langle x^2\rangle - 2\lambda\langle x\rangle + \lambda^2\right)\right]_0^t \end{aligned} \tag{3.79}$$

where $\langle\cdot\rangle$ denotes the average over the initial distribution of position and momentum (3.78). It can easily be shown that the variances $\langle x^2\rangle - \langle x\rangle^2$ and $\langle p^2\rangle - \langle p\rangle^2$ are time independent for any protocol $\lambda(\tau)$. Thus, the work (3.79) can be written as

$$\begin{aligned} W &= \left[\frac{\langle p\rangle^2}{2m} + \frac{k}{2}\left(\langle x\rangle^2 - 2\lambda\langle x\rangle + \lambda^2\right)\right]_0^t \\ &= \left[\frac{\langle p\rangle^2}{2m} + \frac{k}{2}\left(\langle x\rangle - \lambda\right)^2\right]_0^t \end{aligned} \tag{3.80}$$

which becomes zero, *i.e.*, minimal for

$$\begin{aligned} \langle p(t)\rangle &= 0, \\ \langle x(t)\rangle &= \lambda_f. \end{aligned} \tag{3.81}$$

The evolution equations for these mean values are given by

$$\begin{aligned} \frac{\mathrm{d}}{\mathrm{d}\tau}\langle x\rangle &= \langle p\rangle/m, \\ \frac{\mathrm{d}}{\mathrm{d}\tau}\langle p\rangle &= -k(\langle x\rangle - \lambda) \end{aligned} \tag{3.82}$$

with initial values $\langle x(0)\rangle = 0$ and $\langle p(0)\rangle = 0$. With the freedom to choose the continuous function $\lambda(\tau)$ which corresponds to an infinite number of free parameters, it is quite obvious that the two final conditions can easily be met. In fact, the optimal protocol is highly degenerate.

For a specific choice, taking, *e. g.*, a third order polynomial

$$\lambda(\tau) = a(\tau/t) + b(\tau/t)^2 + (\lambda_f - a - b)(\tau/t)^3 \tag{3.83}$$

with two free parameters a, b suffices to meet the optimality conditions. The solution of the evolution equations (3.82) can be solved analytically and, inserted into (3.81), leads to

$$
\begin{aligned}
a &= \frac{12\lambda_f \sin(\omega t/2) - 6\omega t \lambda_f \cos(\omega t/2)}{(12 - \omega^2 t^2)\sin(\omega t/2) - 6\omega t \cos(\omega t/2)},\\
b &= \frac{-3\omega^2 t^2 \lambda_f \sin(\omega t/2)}{(12 - \omega^2 t^2)\sin(\omega t/2) - 6\omega t \cos(\omega t/2)}
\end{aligned}
\tag{3.84}
$$

with $\omega \equiv \sqrt{k/m}$. For short transitions times $t \ll 1$, the coefficients diverge as $a \sim 1/t^2$ and $b \sim -1/t^2$.

As a quite different choice, both conditions can also be met by a linear protocol with delta singularities at the boundaries, in analogy to the underdamped stochastic dynamics case, see Sect. 3.3. Indeed, it can easily be verified that the protocol

$$
\lambda^*(\tau) = \lambda_f \frac{\tau}{t} + \frac{m\lambda_f}{kt}\left[\delta(\tau) - \delta(\tau - t)\right] \tag{3.85}
$$

fulfills the conditions (3.81). This expression could also have been obtained as the limit of the underdamped optimal protocol for $\gamma \to 0$.

Thus, for any given total transition time t the minimal mean work is given by

$$
W^* = 0. \tag{3.86}
$$

For infinitely long transition times, quite generally, the work is given by the adiabatic work. For the studied model system, we have $W^{\mathrm{ad}} = 0$. As shown above, this lower bound on the work can even be achieved for arbitrarily short transition time. This surprising result shows that purely Hamiltonian dynamics can beat Langevin evolution where short transition times $t \to 0$ yield the work for an instantaneous jump $W^{\mathrm{jp}} = k\lambda_f^2/2$.

3.4.2 Case Study II: Harmonic potential with time-dependent stiffness

As in the previous sections, we next consider the time-dependent potential

$$
V(x,\tau) = \frac{\lambda(\tau)}{2} x^2, \tag{3.87}
$$

where the stiffness $\lambda(\tau)$ is changed from an initial value $\lambda(0) = \lambda_i$ to a final value $\lambda(t) = \lambda_f$ in a finite time t. The work exerted on the system during the finite time transition is given by the change in internal energy

$$W = \left[\frac{\langle p^2 \rangle}{2m} + \langle V \rangle \right]_0^t = \left[\frac{\langle p^2 \rangle}{2m} + \frac{\lambda}{2} \left\langle x^2 \right\rangle \right]_0^t . \tag{3.88}$$

The dynamics (3.77) leads to coupled evolution equations for the mean squared position $w \equiv \langle x^2 \rangle$ and the mean squared momentum $z \equiv \langle p^2 \rangle$

$$\dot{z} = -m\lambda\dot{w}, \tag{3.89}$$

$$\ddot{w} = \frac{2z}{m^2} - \frac{2}{m}\lambda w. \tag{3.90}$$

Multiplication of (3.90) with a factor $\dot{w}$ and insertion of (3.89) leads to the relation

$$\ddot{w}\dot{w} = \frac{2}{m^2} \left(z\dot{w} + w\dot{z} \right) \tag{3.91}$$

which, using the equilibrium initial conditions $w(0) = T/\lambda_i$, $\dot{w}(0) = 0$, and $z(0) = mT$ can be integrated to yield

$$zw = \frac{m^2}{4}\dot{w}^2 + \frac{mT^2}{\lambda_i}. \tag{3.92}$$

Minimization of the mean work

$$W = \left[\frac{z}{2m} + \frac{\lambda w}{2} \right]_0^t = \frac{z(t)}{2m} + \frac{\lambda_f w(t)}{2} - T \tag{3.93}$$

then requires $w(t)$ and $z(t)$ to be minimal. Since their product is contrained by (3.92), it is optimal to choose $\dot{w}(t) = 0$ which is equivalent to the final condition

$$z^*(t) = \frac{mT^2}{\lambda_i w(t)}. \tag{3.94}$$

The (mean) total work thus becomes

$$W = \frac{1}{2} \left[\lambda_f w(t) + \frac{T^2}{w(t)\lambda_i} - 2T \right]. \tag{3.95}$$

Optimizing this expression with respect to $w(t)$ leads to

$$w^*(t) = \frac{T}{\sqrt{\lambda_i \lambda_f}} \tag{3.96}$$

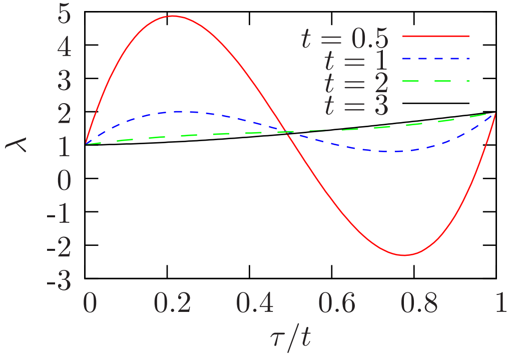

Figure 3.8 Optimal third order polynomial protocols $\lambda_p^*(\tau/t)$ for case study II with $m = 1, T = 1, k = 1, \lambda_i = 1, \lambda_f = 2$ for different transition times t. For short transition times, the optimal protocol shows a pronounced positive peak in the first part of the transition and a pronounced negative peak in the second part of the process, thereby regaining the invested work.

which yields the optimal work

$$W^* = T\left(\sqrt{\frac{\lambda_f}{\lambda_i}} - 1\right). \tag{3.97}$$

Similar to the first case study, the optimal protocol is highly degenerate. For a third order polynomial, the equations of motion cannot be solved analytically. However, as expected, the two parameters can be chosen such that the boundary conditions (3.94) and (3.96) are fulfilled. Optimal third order polynomial protocols $\lambda_p^*(\tau/t)$ are shown in Fig. 3.8 for different transition times t. A short transition time requires pronounced peaks with increasing height for decreasing transition times. These peaks serve to accelerate the Brownian particle in the first part of the transition and to deccelerate the particle in the second part of the transition.

Another convenient choice is a linear protocol with superimposed delta peak singularities at beginning and end. The initial singularity allows for setting the initial mean squared momentum instantaneously to a value $z(0+) \neq z(0) = mT$ which can be tuned to meet the boundary condition on $w(t) = w^*(t)$. The second delta singularity at the final time t allows for setting $\dot{w}(t) = 0$.

Note that, similar to the first case study, the minimal work (3.97) does not depend on the transition time t. Naively, in the limit $t \to 0$, one would expect the result obtained for an instantaneous jump of the protocol $W^{\mathrm{jp}} = (\lambda_f - \lambda_i)/2$ which is substantially larger than the optimal work. However, the possibility to use a protocol with increasing absolute values of λ (and thus increasing forces) for decreasing transition times t leads to the singular limit at $t \to 0$. For any fixed shape of the protocol $\lambda(\tau/t)$, the work approaches W^{jp} with $t \to 0$.

3.4.3 Quartic anharmonic potential

In both harmonic case studies, the optimal work W^* is given by the adiabatic work W^{ad}, independent of the total transition time t. The optimal protocols $\lambda^*(\tau)$ are highly degenerate. It is interesting to see whether these (unexpected) features persist for anharmonic potentials where the optimality conditions cannot be cast into only two conditions for the moments of the probability distribution. However, it is computationally quite difficult to determine optimal protocols in the anharmonic case. For a case study, we use the quartic potential

$$V(x, \lambda) = \frac{1}{4}\lambda x^4 \tag{3.98}$$

with $T = 1$, $\lambda_i = 1$, and $\lambda_f = 2$ together with a Fourier ansatz for the optimal protocol

$$\lambda^*(\tau) = 1 + \frac{\tau}{t} + a_0 \sin(\pi\tau/t) + \sum_{k=1}^{n} a_k \sin(2k\pi\tau/t) \tag{3.99}$$

where we omit higher odd frequencies because their symmetry is not suitable to produce the peak structure found in the two harmonic cases. We next optimize the parameters a_k for a minimal mean work which we calculate as the average of work values from 25000 randomly sampled initial values for x_0 and p_0. For the minimization, we use a standard Mathematica algorithm. Note that the optimal work values obtained in this numerical procedure are upper bounds for the true optimal work since we have used a finite number of parameters.

The adiabatic work can be calculated using the microcanonical distribution for given energy E and given λ. The change of internal energy then is given by

$$\frac{dE}{d\lambda} = \left\langle \frac{\partial V}{\partial \lambda} \right\rangle_{\mathrm{micro}} \equiv \frac{1}{Z} \int dx \frac{1}{\sqrt{2m\,(E - V(x,\lambda))}} \frac{\partial V(x,\lambda)}{\partial \lambda} \tag{3.100}$$

with the microcanonical partition function

$$Z \equiv \int dx \frac{1}{\sqrt{2m\,(E - V(x,\lambda))}}. \tag{3.101}$$

The evolution equation (3.100) is an ordinary differential equation for $E(\lambda)$. For the potential $V(x,\lambda) = \lambda x^4/4$, we obtain

$$\frac{dE}{d\lambda} = \frac{E}{3\lambda} \tag{3.102}$$

which has the solution $E = E_0\lambda^{1/3}$ with initial energy E_0. Averaging over initial conditions x_0, p_0 according to the appropriate initial Boltzmann distribution (3.78) then yields

$$W^{\mathrm{ad}} = 3\frac{(\sqrt[3]{2} - 1)\Gamma(5/4)}{\Gamma(1/4)} \simeq 0.1949. \tag{3.103}$$

In Fig. 3.9a, we compare optimal work values with the adiabatic work. It is hard to decide from the numerics whether this adiabatic work can be reached in a finite time. Clearly, even for very fast transitions compared to the characteristic oscillation time $t_{\mathrm{char}} \simeq 3$, the optimal work is well below the work for a linear protocol which has the limit $W^{\mathrm{jp}} = 0.25$ for $t \to 0$. The optimal protocol again shows pronounced peaks for short transition times t, see Fig. 3.9b. Since we use an ansatz with a finite number of parameters, it is impossible to decide whether the optimal protocol is degenerate.

3.5 Quantum Systems

In this section, we investigate optimal protocols for quantum system. Fortunately, for harmonic systems which are comparable to the first two case studies from the previous sections, work distributions $p(\mathcal{W})$ have recently been calculated for Schrödinger dynamics [103, 104]. By using their results, it is easy to derive optimal protocols since in both cases, the work distributions (and therefore also the mean work) depend on a single “rapidity” parameter which vanishes for quasistatic transitions. In the last subsection, we study the two level system of a single spin in a time-dependent magnetic field. If we impose that the absolute value of the magnetic field stays fixed, the adiabatic work can only be reached in a finite (non-zero) time t_c.

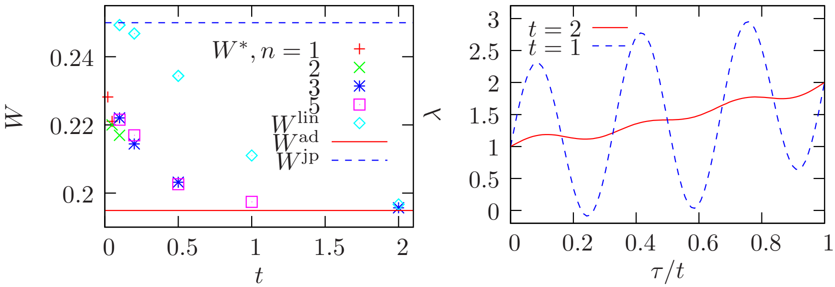

Figure 3.9 (a) Optimal work from the Fourier ansatz (3.99) as a function of the transition time t for different number of Fourier modes n compared to the work W^{lin} obtained for the linear protocol $\lambda^{\text{lin}} \equiv 1 + \tau/t$ and the adiabatic work $W^{\text{ad}} \simeq 0.1949$. (b) Optimal protocols as obtained from the Fourier ansatz (3.99) with $n = 3$ for different transition times t.

3.5.1 Case Study I: Moving harmonic potential

We consider the quantum analogue of a moving harmonic potential

$$V(x,\tau) = \frac{m\omega^2}{2}(x - \lambda(\tau))^2 \tag{3.104}$$

with Hamiltonian

$$H = \hbar\omega \left[a^\dagger a - \sqrt{\frac{m\omega}{2\hbar}} \lambda(\tau) \left(a + a^\dagger \right) \right] + \frac{m\omega^2}{2} \lambda(\tau)^2 \tag{3.105}$$

with creation and annihilation operators

$$\begin{aligned} a^\dagger &= \sqrt{\frac{m\omega}{2\hbar}} \left(x - i\frac{p}{m\omega} \right), \\ a &= \sqrt{\frac{m\omega}{2\hbar}} \left(x + i\frac{p}{m\omega} \right), \end{aligned} \tag{3.106}$$

Planck constant $\hbar$, frequency ω and a time-dependent minimum of the harmonic potential $\lambda(\tau)$ which is changed from an initial value $\lambda(0) = 0$ to a final value $\lambda(t) = \lambda_f$ during a given finite time t. It has been shown [104, 108] that the work distribution $p(\mathcal{W})$ for an initially thermalized ensemble depends only on the absolute value $|z|$ of a “rapidity” parameter

$$z \equiv \sqrt{\frac{m\omega}{2\hbar}} \int_0^t d\tau \dot{\lambda}(\tau) e^{i\omega\tau} \tag{3.107}$$

which vanishes for adiabatic transitions with $t \to \infty$. However, even for transitions in a finite time t, there exist appropriate protocols $\lambda(\tau)$ which lead to a vanishing “rapidity parameter” z and thus to a vanishing mean work $W^* = W^{\mathrm{ad}} = 0$. For a specific choice, it suffices to consider the simple trigonometric protocol

$$\lambda_n^*(\tau) = \lambda_f \left[\frac{\tau}{t} + \frac{\left(4\pi^2 n^2 - t^2\omega^2\right) \sin\left(\frac{2n\pi\tau}{t}\right)}{2n\pi t^2 \omega^2} \right] \tag{3.108}$$

which can be easily shown to yield $z = 0$ for any integer n. Thus, the adiabatic work can also be achieved in an arbitrarily short transition time. Again, the optimal protocol is highly degenerate. This degeneracy arises because the continuous protocol $\lambda(\tau)$ with an infinite number of parameters has to satisfy only two boundary conditions $\lambda(0) = 0$, $\lambda(t) = \lambda_f$ and the adiabaticity condition $z = 0$.

3.5.2 Case Study II: Harmonic potential with time-dependent frequency

A similar argument can be applied to the quantum analogue of the harmonic potential with time-dependent stiffness $m\lambda(\tau)$ with Hamiltonian

$$H = \frac{p^2}{2m} + \frac{m}{2}\lambda(\tau) x^2. \tag{3.109}$$

The control parameter λ is changed time-dependently from an initial value $\lambda(0) = \lambda_i$ to a final value $\lambda(t) = \lambda_f$ during a finite transition time t, which corresponds to a time-dependent oscillator frequency $\omega(\tau) \equiv \sqrt{\lambda(\tau)}$. It has been shown [103] that the work distribution and therefore also the mean work only depends on a single parameter

$$\begin{aligned} Q = \frac{1}{2\sqrt{\lambda_i \lambda_f}} & \left[\lambda_i \left(\lambda_f X(t)^2 + \dot{X}(t)^2 \right) \right. \\ & \left. + \left(\lambda_f Y(t)^2 + \dot{Y}(t)^2 \right) \right] - 1 \end{aligned} \tag{3.110}$$

where $X(t)$ and $Y(t)$ are solutions for the classical harmonic oscillator equation

$$\ddot{X}(\tau) + \lambda(\tau) X(\tau) = 0 \tag{3.111}$$

with initial conditions

$$X(0) = 0\ , \quad \dot{X}(0) = 1\ , \quad Y(0) = 1\ , \quad \dot{Y}(0) = 0. \tag{3.112}$$

The dynamics of $X(\tau)$ and $Y(\tau)$ is constrained by their time evolution with common protocol $\lambda(\tau)$ which yields the relation

$$\ddot{X}Y = \ddot{Y}X. \tag{3.113}$$

Addition of the term $\dot{X}\dot{Y}$ on both sides and subsequent integration leads to

$$\dot{X}Y = X\dot{Y} + 1 \tag{3.114}$$

where the integration constant is determined by the initial conditions (3.112). Using standard techniques, we perform a minimization of Q under the constraint (3.114) with respect to $X(t)$, $\dot{X}(t)$, $Y(t)$, and $\dot{Y}(t)$. The optimality conditions then are given by

$$\begin{aligned} X^*(t) &= \frac{1}{\sqrt{\lambda_i \lambda_f}} \sqrt{\sqrt{\lambda_i \lambda_f} - \lambda_f Y^*(t)^2} \\ \dot{X}^*(t) &= \sqrt{\frac{\lambda_f}{\lambda_i}} Y^*(t) \end{aligned} \tag{3.115}$$

where $Y^*(t)$ can be chosen arbitrarily. The minimal value of the parameter Q then is $Q^* = 0$ and the optimal work is given by the adiabatic work which can be calculated [103] as

$$W^* = W^{\text{ad}} = \frac{1}{2}\hbar(\omega_f - \omega_i) \coth(\beta \hbar \omega_i / 2) \tag{3.116}$$

where $\omega_f \equiv \sqrt{\lambda_f}$ and $\omega_i \equiv \sqrt{\lambda_i}$. Again, only a finite number of optimality conditions have to be fulfilled while the continuous protocol $\lambda(\tau)$ corresponds to an infinite number of parameters. The optimal protocol $\lambda^*(\tau)$ thus is highly degenerate and the adiabatic work can be reached in any given (arbitrarily short) transition time.

3.5.3 Two-level system

We next study a simple two level system consisting of a single spin in a time-dependently rotating magnetic field $\mathbf{B}(\tau) = B\mathbf{e}(\tau)$ where $\mathbf{e}(\tau)$ is a unit vector which is to be changed from an initial value $\mathbf{e}(0) = \hat{\boldsymbol{e}}_z$ to a final value $\mathbf{e}(t) = -\hat{\boldsymbol{e}}_z$ in a given finite transition time t, keeping the absolute value of the magnetic field B fixed. Here $\hat{\boldsymbol{e}}_i$ denotes the unit vector in i-direction, $i \in \{x, y, z\}$. The Hamiltonian of the system is given by

$$H = -\hbar\gamma\mathbf{B}\boldsymbol{\sigma}/2 \tag{3.117}$$

with Pauli matrices $\boldsymbol{\sigma}$ and gyromagnetic ratio γ. In the basis of eigenvectors of σ_z, the initial canonical density matrix is given by

$$\rho(0) = \frac{1}{Z}\left(e^{\beta\hbar\gamma B/2}\,|+\rangle\,\langle+| \quad + \quad e^{-\beta\hbar\gamma B/2}\,|-\rangle\,\langle-|\right), \tag{3.118}$$

where $|+\rangle$ is eigenvector of σ_z with eigenvalue $+1$, $|-\rangle$ is eigenvector of σ_z with eigenvalue -1 and Z is the canonical partition function. The work in such a finite time transition then is given by

$$W = \langle E\rangle_t - \langle E\rangle_0 = \mathrm{tr}\{H(t)\rho(t)\} - \mathrm{tr}\{H(0)\rho(0)\} \tag{3.119}$$

where the time evolution of the density matrix $\rho(\tau)$ is given by the Liouville-von-Neumann equation

$$\partial_\tau \rho(\tau) = \frac{i}{\hbar}\left[\rho(\tau), H(\tau)\right]. \tag{3.120}$$

Quite generally, due to the adiabatic theorem in quantum mechanics, the occupation probabilities of the states do not change for quasistatic driving. The density matrix at the end of an adiabatic transition is therefore given by

$$\rho_1 \equiv \frac{1}{Z}\left(e^{-\beta\hbar\gamma B/2}\,|+\rangle\,\langle+| \quad + \quad e^{\beta\hbar\gamma B/2}\,|-\rangle\,\langle-|\right). \tag{3.121}$$

Thus, initial and final energy are equal $\mathrm{tr}\{H(0)\rho(0)\} = \mathrm{tr}\{H(t_c)\rho(t_c)\}$ and the adiabatic work is zero $W^{\mathrm{ad}} = 0$.

We next try to identify optimal protocols for such a transition. Generally, any pure spin state corresponds to a Bloch vector of unit length. Applying a magnetic field $\mathbf{B}$ leads to a precession of the Bloch vector around the axis of the magnetic field with angular frequency $\omega_L \equiv \gamma B$. Therefore, after an appropriate time $t_c = \pi/\omega_L$, the direction of a Bloch vector perpendicular to the magnetic field is reversed. During the adiabatic evolution from initial state

ρ_0 to the final state ρ_1, the initial Bloch vectors in $\hat{\boldsymbol{e}}_z$ and $-\hat{\boldsymbol{e}}_z$ directions are also reversed. In order to reach the adiabatic work in a total transition time $t = t_c$, it therefore suffices to choose the protocol

$$\mathbf{e}^*(\tau) = \begin{cases} \hat{\boldsymbol{e}}_z & \text{for } \tau = 0 \\ \hat{\boldsymbol{e}}_x & \text{for } 0 < \tau < t_c \\ -\hat{\boldsymbol{e}}_z & \text{for } \tau = t_c \end{cases} \tag{3.122}$$

which corresponds to an initial jump to a (constant) magnetic field perpendicular to the z-direction, *i.e.* $\mathbf{B} = B\hat{\boldsymbol{e}}_x$, and a final jump to the magnetic field $\mathbf{B} = -B\hat{\boldsymbol{e}}_z$. At the end of the transition, the density matrix is given by

$$\rho(t_c) = \rho_1 \tag{3.123}$$

and the mean work thus is equal to the adiabatic work $W^* = W^{\text{ad}} = 0$. The adiabatic work thus can be reached in the finite time t_c. In order to reach the adiabatic work for any larger transition time $t > t_c$, it suffices to choose the protocol $\mathbf{e}^*(\tau)$ for times $t \leq t_c$, keeping the magnetic field $\mathbf{B}(\tau > t_c) = -B\hat{\boldsymbol{e}}_z$ unchanged for all times $\tau > t_c$. For transition times $t < t_c$, the adiabatic work cannot be reached since there is no possibility to obtain the density matrix ρ_1 from the given dynamics in a time $t < t_c$.

However, if we had not constrained the magnetic field to have a given absolute value B but allowed for any value of the magnetic field during the transition, we would have found that the adiabatic work can be reached in any transition time t. This is obvious because the spin precession frequency is proportional to B and thus any precession frequency can be achieved in such a setup. For a given transition time t, the magnetic field then can be tuned to yield a precession frequency $\omega_L = \pi/t$ which leads to $W^* = 0$.

More generally, if one allows any form of the Hamiltonian, it is obvious that a work value arbitrarily close to the adiabatic work can be reached in any given (short) time t for the following reason. Assume that the work W_1 can be reached in a slow transition with dynamics $\Psi_1(\tau)$ for the time-dependent Hamiltonian $H_1(\tau)$ with $t_1 \gg t$. The Hamiltonian $H(\tau) \equiv H_1(t_1 \cdot \tau/t) \cdot t_1/t$ then leads to an equivalent dynamics $\Psi(\tau) = \Psi_1(t_1 \cdot \tau/t)$ and therefore to an equivalent final mean internal energy at time t. Thus, the work W_1 (which is arbitrarily close to W^{ad} for long times t_1) can already be reached in the (arbitrarily short) time t. Note, however, that this argument is no longer true if one allows only for any form of the potential $V(x, \tau)$ since the kinetic energy (and thus the dependence on the momentum p) in the Hamiltonian $H(\tau)$ is given and thus cannot be rescaled in this manner.

For most practical purposes, the range of the control parameter will be limited by the experimental conditions. For quantum systems, refined strategies for the optimal control of the time evolution of wave functions under such constraints have been developpped [109, 110, 111, 112]. These techniques may be generalized in order to specify minimum work protocols for quantum nonequilibrium transitions in complex systems with additional constraints on the possible values of the control parameter $\lambda(\tau)$.

3.6 Benefits for free energy reconstruction

We will next discuss the benefits for free energy calculations from the consideration of optimal protocols. The Jarzynski relation

$$e^{-\Delta F/T} = \left\langle e^{-\mathcal{W}/T} \right\rangle \tag{3.124}$$

allows for the calculation of a free energy difference ΔF from the average $\left\langle e^{-\mathcal{W}/T} \right\rangle$ over non-equilibrium work values. Consequently, from a finite set of N non-equilibrium trajectories, the free energy ΔF can be estimated as

$$\Delta F^{\text{est}} \equiv -T \ln \left[\sum_{i=1}^{N} \exp(-\beta \mathcal{W}_i)/N \right] . \tag{3.125}$$

First, we will describe how to define the error of a free energy estimate (3.125) from the Jarzynski reconstruction. We assume that N nonequilibrium trajectories (either from simulations or experiments) are used. Since the dynamics is stochastic and therefore also the work values, the estimate for the free energy difference will also have a stochastic contribution. Additionally, the free energy estimate is biased because of the nonlinear averaging procedure [73]. We thus have two different types of errors: (i) a systematic bias characterized by the error of the mean value

$$B = \left\langle \Delta F^{\text{est}} \right\rangle - \Delta F \tag{3.126}$$

and (ii) statistical errors characterized by the standard deviation of the distribution

$$\sigma = \sqrt{\mathrm{Var}(\Delta \mathrm{F}^{\text{est}})} = \sqrt{\left\langle (\Delta F^{\text{est}})^2 \right\rangle - \left\langle \Delta F^{\text{est}} \right\rangle^2}. \tag{3.127}$$

The mean squared error (MSE) then is the sum of both contributions:

$$\text{MSE} \equiv \left\langle \left(\Delta F^{\text{est}} - \Delta F \right)^2 \right\rangle = B^2 + \sigma^2. \tag{3.128}$$

In order to give a quantitative measure of the error, one defines the root mean squared error

$$\mathrm{RMSE} \equiv \sqrt{\mathrm{MSE}} = \sqrt{B^2 + \sigma^2}. \tag{3.129}$$

Both the bias and the statistical error will decrease with an increasing number of trajectories. On the other hand, faster trajectories which are computationally cheaper lead to larger dissipation and therefore to an increased bias.

The optimal protocol for a minimal mean work is not strictly equivalent to a protocol leading to an optimized free energy estimate. However, it has been found that the latter shares the same features (jumps at the boundaries) for overdamped Langevin dynamics [107]. We expect that this result holds also for underdamped Langevin dynamics. As we will show in the following, the optimal protocol leads to improved estimates of the free energy difference for an underdamped Brownian particle for both our case studies of harmonic potentials. For an anharmonic double-well potential, we show that approximated delta-peaks at beginning and end of the process lead to an improved estimate for the free energy difference.

3.6.1 Harmonic potentials

For Langevin dynamics (both overdamped and underdamped), the work distribution for the moving harmonic potential (case study I) is Gaussian [113, 22]. For a Gaussian work distribution, it has been shown that the error in the estimate of the free energy difference decreases with decreasing mean work [73]. In the harmonic potential with time-dependent stiffness (case study II), the work distribution is no longer Gaussian. For underdamped Langevin dynamics, the error in the estimate of the free energy difference is indeed lower for the optimal protocol compared to a linear protocol, see Fig. 3.10. We expect a similar behaviour also for overdamped dynamics. For thermodynamic integration, it is obvious that a minimum mean work leads to the best estimate of the free energy difference. We thus conjecture that appropriate singularities at the boundaries generically improve free energy calculations from either fast growth methods or thermodynamic integration.

3.6.2 Anharmonic potentials

It is computationally very difficult to obtain optimal protocols for anharmonic potentials. The dynamics then is no longer governed by only a few parameters and an optimization in analogy to harmonic potentials is not feasible. However,

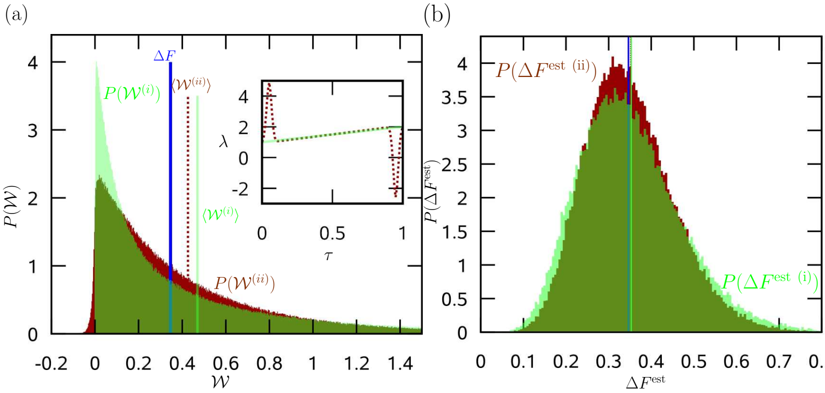

Figure 3.10 Comparison of free energy estimates for underdamped Langevin dynamics in a harmonic potential with time-dependent stiffness (case study II) for a linear protocol and a continous approximation to the optimal protocol for $\tilde{t} = 1, \tilde{m} = 1, \tilde{\lambda} = 2$. The data were obtained from Langevin simulation of 10^6 trajectories for each protocol with $\gamma = 1, m = 1, T = 1, \lambda_i = 1$. (a) Distribution $P(\mathcal{W})$ of work values $\mathcal{W}$ for the two protocols shown in the inset: (i) the linear protocol $\lambda(\tau) = 1 + \tau$ and (ii) the linear protocol with additional continuously approximated delta singularities. The columns show the free energy difference $\Delta F \simeq 0.3466$ and the mean work values $\left\langle \mathcal{W}^{(i)} \right\rangle \simeq 0.4700(\pm 0.0006)$, $\left\langle \mathcal{W}^{(ii)} \right\rangle \simeq 0.4270(\pm 0.0005)$ which both are consistent with a direct evaluation based on (3.62). (b) Histogram of 10^5 Jarzynski estimates for the free energy difference ΔF^{est} obtained from $N = 10$ single trajectory work values $\mathcal{W}_i$ each. The columns show the free energy difference and the mean value of the estimates obtained from the two protocols. Since the bias ($B^{(i)} = 0.0066(\pm 0.0004)$, $B^{(ii)} = 0.0052(\pm 0.0003)$) can be neglected for both protocols, the RMSE is dominated by the statistical error ($\sigma^{(i)} = 0.119$, $\sigma^{(ii)} = 0.104$) which is smaller for protocol (ii).

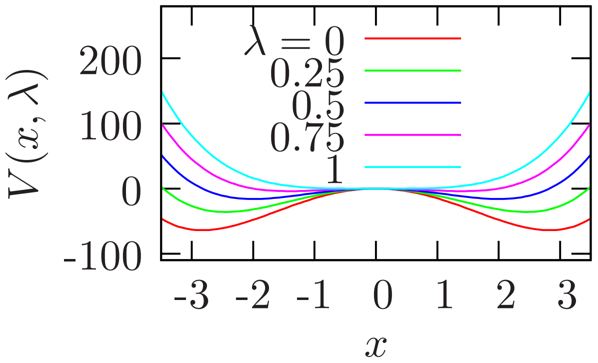

Figure 3.11 Sun potential (3.130) for different values of the control parameter between $\lambda_i = 0$ and $\lambda_f = 1$. For increasing values of the control parameter λ, the double well minimas move together and become shallower until they merge to form a quartic potential at $\lambda_f = 1$.

we want to demonstrate in the following that the general features observed for the optimal protocol (jumps and delta-peaks) can help to construct protocols which lead to an improved estimate of the free energy. As a test case, we use the Sun potential [97]

$$V(x,\tau) = T\left(x^4 + 16x^2(1-\lambda(\tau))\right) \tag{3.130}$$

with dimensionless position x. We consider initial value of the control parameter $\lambda_i = 0$ and final value of the control parameter $\lambda_f = 1$, see Fig. 3.11. Instead of searching for the optimal shape of the protocol, we show that singularities at beginning and end which will be approximated by Gaussians superimposed on an otherwise linear protocol generally improve free energy estimates. More specifically, we use the protocol

$$\begin{aligned}\lambda(\tau) \quad &= \quad v\left[\left(1+(a+b)e^{-4}+(a+b)e^{-4(1-d)^2/d^2}\right)\tau + ae^{-4(\tau-d)^2/d^2}\right.\\ &\qquad \left. -be^{-4(\tau-1+d)^2/d^2} - ae^{-4} + be^{-4(1-d)^2/d^2}\right]. \end{aligned} \tag{3.131}$$

with velocity $v \equiv 1/t$. We use underdamped Langevin dynamics as described in Sect. 3.3 with $m = 1$, $\gamma = 1$, and $T = 1$. The free parameters a, b, d

tune heigth and position of the peaks. A crude parameter search shows that $a = 0.19$, $b = 0.21$, $d = 0.15$ are appropriate values for the considered velocity $v = 1$. We next discuss the effect on free energy difference estimates which will also depend on the number of available trajectories. In Tab. 3.1, we compare free energy estimates obtained from the protocol (3.131) with free energy estimates from a linear protocol $\lambda^{\text{lin}}(\tau) \equiv \tau/t = v\tau$ for different numbers N of trajectories. As expected, the estimates become better for an increasing number of trajectories. In contrast to the results for the harmonic potential with time-dependent stiffness shown in Fig. 3.10, the RMSE here is dominated by the biased mean value of the estimate while the statistical error is small. For only one trajectory, $N = 1$, the Jarzynski estimate is equivalent to thermodynamic integration, where the measured work $\mathcal{W}$ is taken as an estimate for the free energy difference. Also in this case, the protocol with singularities leads to a significantly improved free energy estimate compared to a linear protocol. However, while the mean work is lower for the protocol with singularities, the standard deviation of the work is larger. For increasing number of trajectories N, the ratio $\text{RMSE}^{(i)}/\text{RMSE}^{(ii)}$ of the RMSE of the protocol with singularities $\text{RMSE}^{(i)}$ and the linear protocol $\text{RMSE}^{(ii)}$ decreases, *i.e*, the advantage of the optimal protocol becomes larger. For $N = 1000$, the RMSE can be reduced by more than 40% by using approximated singularities in the protocol. In Fig. 3.12, histograms of the work distribution $p(\mathcal{W})$ and the probability distribution function of free energy estimates for $N = 1000$ for both the linear protocol and the protocol (3.131) are shown. Even though the work distribution $p(\mathcal{W})$ is broader for the protocol with approximated peaks (3.131), this protocol yields a better free energy estimate than the linear protocol. This can be understood by considering the tail of the distributions for low work values. While the linear protocol has a slightly asymmetric work distribution $p(\mathcal{W})$, the work distribution $p(\mathcal{W})$ for the protocol (3.131) is almost Gaussian. The histograms for the estimates of the free energy difference in Fig. 3.12b also illustrate that the RMSE for this double-well potential (3.130) is dominated by the bias rather than the statistical error.

3.6.3 Sampling of initial conditions

In discussions on the efficiency of free energy calculations using the Jarzynski relation as compared to “classical” alternatives such as thermodynamic integration or umbrella sampling, the computational cost of sampling the necessary number of independent equilibrium initial configurations is often neglected. It is obvious that this computational cost increases with the number of trajectories

N	$\Delta F^{\mathrm{est(i)}}$	$B^{(i)}$	$\sigma^{(i)}$	RMSE$^{(i)}$
1	70.103	7.163	3.424	7.939
10	66.702	3.761	1.861	4.196
100	65.225	2.284	1.181	2.571
1000	64.518	1.577	0.811	1.773

N	$\Delta F^{\mathrm{est(ii)}}$	$B^{(ii)}$	$\sigma^{(ii)}$	RMSE$^{(ii)}$
1	70.708	7.77	2.909	8.294
10	67.929	4.988	1.713	5.274
100	66.587	3.646	1.191	3.836
1000	65.825	2.885	0.869	3.013

Table 3.1 Contributions to the root mean squared error (RMSE) in the free energy estimate from the Jarzynski relation for the Sun potential (3.130) for different number of trajectories N. Shown are numerical values obtained from Langevin simulation of $1.5 \cdot 10^6$ trajectories with $\gamma = 1, m = 1, T = 1, \lambda_i = 1$ for the protocol with approximated singularities (3.131) (left) and the linear protocol (right). The total error is smaller for the protocol with approximated singularites with increasing advantage for an increasing number of trajectories N.

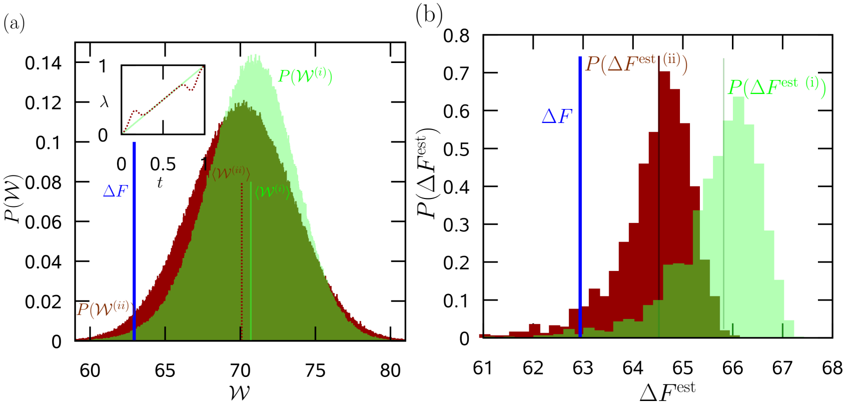

Figure 3.12 Comparison of free energy estimates for the anharmonic potential (3.130) for a linear protocol and a linear protocol with additional continuously approximated delta singularities (3.131). The data were obtained from Langevin simulation of $1.5 \cdot 10^6$ trajectories for each protocol with $t = 1$, $\gamma = 1$, $m = 1$, $T = 1$, and $\lambda_i = 1$. (a) Distribution $P(\mathcal{W})$ of work values $\mathcal{W}$ for the two protocols shown in the inset: (i) the linear protocol $\lambda(\tau) = \tau$ and (ii) the linear protocol with additional continuously approximated delta singularities (3.131). The columns show the free energy difference $\Delta F \simeq 62.941$ and the mean work values $\left\langle \mathcal{W}^{(i)} \right\rangle \simeq 64.518(\pm 0.004)$, $\left\langle \mathcal{W}^{(ii)} \right\rangle \simeq 65.825(\pm 0.003)$. (b) Histogram of $1.5 \cdot 10^3$ Jarzynski estimates for the free energy difference obtained from $N = 1000$ single trajectory work values $\mathcal{W}_i$ each. The columns show the free energy difference and the mean value of the estimates obtained from the two protocols. The RMSE is dominated by the bias ($B^{(i)} = 1.577(\pm 0.004)$, $B^{(ii)} = 2.884(\pm 0.0003)$) which is smaller for protocol (ii).

used in the calculations since for each trajectory, an independent initial configuration is needed. For thermodynamic integration, where only one (very long) trajectory is considered, this effect is negligible. However, for thermodynamic pertubation or its refined version, umbrella sampling, where "trajectories" are instantaneous jumps and no dynamics is needed at all, equilibrium sampling is the most important cost factor. For the Jarzynski method using finite-time transitions, computational cost is shared among the sampling of initial configurations and the calculation of dynamic trajectories. It is thus interesting whether the computational cost of thermodynamic perturbation (or umbrella sampling) can be improved by using finite-time trajectories rather than instantaneous jumps. For a case study, we consider the quartic potential

$$V(x,\tau) = \frac{\lambda(\tau)}{4} x^4 \tag{3.132}$$

with initial value $\lambda_i = 1$ and final value $\lambda_f = 2$ of the control parameter $\lambda(\tau)$. For underdamped Langevin-dynamics with $m = 1$, $\gamma = 1$, we have calculated free energy estimates for different initial sampling times. If initial sampling is too short, no proper equilibrium configuration is reached and the free energy estimate will be biased. On the other hand, if sampling is too long, fewer trajectories can be calculated with given computational cost and the free energy estimate will also be biased. In Fig. 3.13, root mean squared errors (RMSE) for different times t_r used for initial equilibration are compared. While slow transitions yield better estimates for very short and very long equilibration, there is a interval of times t_r where faster transitions yield lower errors. In any realistic free energy calculation, however, optimal times t_r are not known and in order to avoid incalculable biases, one would rather use long times t_r. In this situation and for the considered potential, it seems to be advantageous to use few long trajectories rather than many short trajectories. In contrast, if one had considered only the computational cost for the dynamics, many short trajectories would have yielded a better estimate. It is thus crucial to include the computational cost of equilibration when comparing different methods for the calculation of free energy differences.

3.6.4 Discussion

We have shown that, in principle, optimal protocols can greatly improve free energy calculations via the Jarzynski relation. For determining the optimal protocol for an unknown potential, we envisage an adaptive procedure in which trial protocols (including estimated singularities) are successively improved in

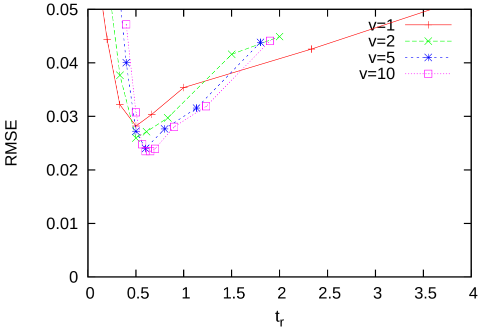

Figure 3.13 Root mean squared error (RMSE) of Jarzynski free energy estimates from underdamped Langevin simulations of a Brownian particle in the potential (3.132) as a function of the time t_r used for the initial equilibration of the particle. The number of trajectories used in the free energy calculation is adjusted such that the overall computational cost of equilibration and generation of dynamic trajectories is equivalent for each data point.

an iterative fashion guided by the monitored work values. It might also prove beneficial to use the optimal moving trap protocol (case study I) rather than a linear protocol in simulations of (protein) pulling experiments.

4 Optimization of Brownian motors

4.1 Introduction

According to Carnot, the second law leads to a maximal efficiency $\eta_{\mathrm{C}} \equiv 1 - T_{\mathrm{c}}/T_{\mathrm{h}}$ for heat engines working between two heat baths at temperatures $T_{\mathrm{h}} > T_{\mathrm{c}}$. However, this efficiency can only be achieved in the quasistatic limit, where transitions occur infinitesimally slowly and hence the power output vanishes. For real heat engines, it is more meaningful to calculate the efficiency at the maximal power output of the machine. This concept is illustrated in Fig. 4.1. The Curzon-Ahlborn efficiency at maximum power $\eta_{\mathrm{CA}} \equiv 1 - \sqrt{T_{\mathrm{c}}/T_{\mathrm{h}}}$ was originally derived for a Carnot-engine in the endoreversible regime, i. e. with finite thermal resistance coupling to the thermal reservoirs [114]. This behaviour is even recovered if path optimization techniques are used to maximize the work output with respect to the driving scheme, see [115] and references therein. Recent extensions [116, 117] of this apparent universal law to an infinitesimal series of coupled heat engines operating in a linear response regime (i.e. between heat baths with small temperature difference) have again risen the question whether the Curzon-Ahlborn result is quite generally a bound on the efficiency of heat engines working at maximum power output.

In contrast to the macroscopic heat engines considered in conventional endoreversible thermodynamics, thermal fluctuations play a crucial role in most biologically relevant systems and dynamics cannot be described on a deterministic (macroscopic) level. In this regime, models for thermodynamic machines must incorporate fluctuation effects. A paradigmatic model for such a heat engine is a thermal ratchet where transport is induced by an spatially asymmetric potential in a temperature profile [118, 119, 120]. For such models, several studies on the efficiency at maximum power have been performed [35, 121, 36, 122, 37]. In the quantum domain, the efficiency at maximum power has been studied for a quantum dot [123] and a maser model [124]. Very recently, it has been shown that the Curzon-Ahlborn efficiency is universal up to second order in the scaled temperature difference $(T_{\mathrm{h}} - T_{\mathrm{c}})/T_{\mathrm{h}}$ if a symmetry relation between the two heat baths is fulfilled [124].

While heat engines on the mesoscale are interesting from a theoretical point

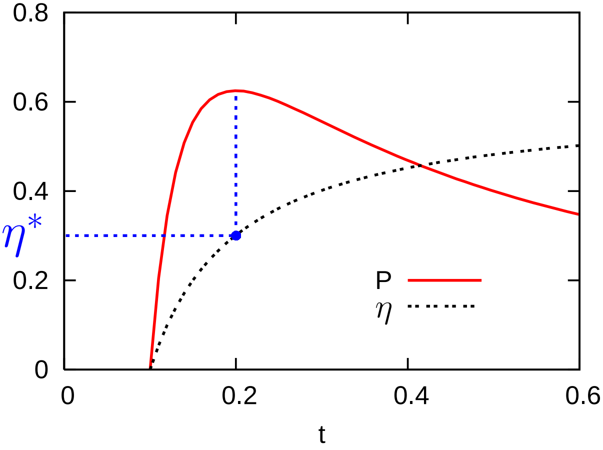

Figure 4.1 The concept of the efficiency at maximum power. First, the power output of the considered machine is optimized with respect to some parameter, *e. g.* the cycle time for a cyclic heat engine. In a second step the efficiency is calculated at this operational point of maximum power.

of view, most biological motors are driven by chemical potential differences. For these motors, one could expect that evolution has tuned their parameters such that they operate in an optimal way. It is quite natural to analyze such motors in the framework of finite-time thermodynamics, calculating their efficiency at maximum power.

4.2 Cyclic Brownian heat engine

Most models for microscopic heat engines focus on thermal ratchets where transport along a spatially varying time-independent potential is driven by a periodic spatial temperature profile [118, 119, 120, 125]. Even if the recent generation of temperature gradients on small length scales [126, 127, 128] is a step towards the experimental realization of such ratchet heat engines, the achievable currents are very small [44]. Moreover, a macroscopic limit of such heat engines does not lead to heat engines of the Carnot type. In order to overcome these difficulties, we introduce a simple model system of a stochastic heat engine whose degrees of freedom are subject to a time-dependent potential with time-dependent coupling to and decoupling from the two heat baths. This model is somewhat distinct from the thermal ratchets which are driven by spatial temperature differences. Ratchet heat engines with a time-dependent but spatially constant temperature have been studied in [129, 130, 131].

Brownian heat engines have been investigated with a model system using a spatial temperature profile and a ratchet potential [118, 119, 120]. This thermal ratchet model has also been extended to a Brownian particle in the underdamped regime [125]. Efficiencies of such ratchet heat engines [5, 132, 121, 122] and related Brownian heat engines [133] have been calculated. Recent studies on the efficiency at maximum power, however, have either been restricted to the linear response regime [122] or use a questionable definition of work (which allows for the efficiency to exceed the Carnot bound) [121]. For a ratchet heat engine on a discrete state space, a violation of the Curzon-Ahlborn bound has been found [35, 37].

We first describe the general setup of a stochastic heat engine consisting of two adiabatic and two isothermal steps. We then illustrate this setup by a simple one-dimensinal example and show that our model exhibits a universal dependence of work and heat on the cycling time. This leads to a universal form of the efficiency at maximum power. We first neglect the effect of kinetic energy in our overdamped description and discuss its role (cf. [31]) at the end.

4.2.1 The model

We consider a thermodynamic machine with internal degrees of freedom $\mathbf{x}$ and an external time-dependent potential $V(\mathbf{x}, \tau)$. On a microscopic scale, it is crucial to include thermal fluctuations in the description and thus to consider the probability density $p(\mathbf{x}, \tau)$ to find the system in state $\mathbf{x}$ at time τ. In the overdamped limit, the time evolution of $p(\mathbf{x}, \tau)$ is governed by the Fokker-Planck equation

$$\partial_\tau p(\mathbf{x}, \tau) = -\nabla \cdot \mathbf{j} = -\nabla \cdot \mu \left[-(\nabla V) - T\nabla\right] p(\mathbf{x}, \tau) \tag{4.1}$$

which is the generalization of (2.4) to the multidimensional case. The mobility then is replaced by a mobility matrix μ. Similar to a macroscopic Carnot engine, we consider the machine cycle to consist of two isothermal and two adiabatic transitions.

Isothermal steps .– The potential $V(\mathbf{x}, \tau)$ is varied during a time-interval $t_i \leq \tau \leq t_f$ at a given constant temperature T. The mean work W spent in this process (or extracted for $W < 0$)

$$\begin{aligned} W &= \int_{t_i}^{t_f} d\tau \int dx \; p(\mathbf{x}, \tau) \frac{\partial V}{\partial \tau} \\ &= W_{\text{irr}} - T\Delta S + \Delta E \end{aligned} \tag{4.2}$$

becomes a functional of the time dependent potential $V(\mathbf{x}, \tau)$. In (4.2), we have introduced the (mean) irreversible work

$$W_{\text{irr}} \equiv \int_{t_i}^{t_f} d\tau \int dx \; \frac{\mathbf{j}(\mathbf{x}, \tau)\mu^{-1}\mathbf{j}(\mathbf{x}, \tau)}{p(\mathbf{x}, \tau)}, \tag{4.3}$$

the (mean) internal energy

$$E(\tau) \equiv \int dx \; p(\mathbf{x}, \tau) V(\mathbf{x}, \tau), \tag{4.4}$$

and the system entropy

$$S(\tau) \equiv -\int dx \; p(\mathbf{x}, \tau) \ln(p(\mathbf{x}, \tau)), \tag{4.5}$$

see also Chapter 2.

Adiabatic steps .– Adiabatic steps are somewhat more difficult to conceive realistically (just as for macroscopic heat engines). Here, they are idealized as sudden jumps of the potential while uncoupling from one heat bath and coupling to the other heat bath occurs instantaneously and thus without heat exchange. Note that, within our overdamped description, we first neglect kinetic energies. Considering the kinetic energy of the degrees of freedom would lead to an additional heat flux in these steps because of the relaxation of the momentum due to the temperature change. This issue is discussed in detail at the end of this section. Since there is no time for relaxation, the distribution $p(\mathbf{x},\tau)$ and thus the system entropy S does not change during these steps and hence these transitions are also isentropic. The mean work applied in such a transition occuring at time τ is given by

$$W = \Delta E = \int dx\; p(\mathbf{x},\tau)\,[V(\mathbf{x},\tau+0) - V(\mathbf{x},\tau-0)]\,. \tag{4.6}$$

Cyclic process.– We construct a cyclic process by performing subsequently the following four steps, see Fig. 4.2.

(1) Isothermal transition at temperature T_h during time interval $0 < \tau < t_1$. The potential $V(\mathbf{x},\tau)$ is changed time-dependently and work is extracted $(W < 0)$.

(2) Adiabatic transition (instantaneously) from temperature T_h to temperature T_c at time $\tau = t_1$. The distribution $p_b(\mathbf{x}) \equiv p(\mathbf{x},\tau = t_1)$ does not change during this step.

(3) Isothermal transition at temperature T_c during time interval $t_1 < \tau < t_1 + t_3$. The potential $V(\mathbf{x},\tau)$ is changed time-dependently (with $W > 0$).

(4) Adiabatic transition from temperature T_c to temperature T_h at time $\tau = t_1 + t_3$. The distribution $p_a(\mathbf{x}) \equiv p(\mathbf{x},\tau = t_1 + t_3)$ does not change during this step.

For a cyclic process, periodicity in time requires $p(\mathbf{x}, t_1 + t_3) = p(\mathbf{x}, 0)$ thus imposing a constraint on the admissible time-dependence of $V(\mathbf{x},\tau)$. Moreover, a cyclic process implies $\sum_{i=1}^4 \Delta E^{(i)} = \sum_{i=1}^4 \Delta S^{(i)} = 0$. Since the system entropy S does not change during the adiabatic steps, $\Delta S^{(2)} = \Delta S^{(4)} = 0$, we even have $\Delta S^{(1)} = -\Delta S^{(3)} \equiv \Delta S$. The total work then is given by

$$\begin{aligned} W &= \sum_{i=1}^{4} W^{(i)} = \sum_{i=1}^{4} W_\mathrm{irr}^{(i)} - \sum_{i=1}^{4} T_i \Delta S^{(i)} + \sum_{i=1}^{4} \Delta E^{(i)} \\ &= W_\mathrm{irr}^{(1)} + W_\mathrm{irr}^{(3)} - (T_\mathrm{h} - T_\mathrm{c})\Delta S. \end{aligned} \tag{4.7}$$

The heat uptake during one complete cycle from the hotter heat bath at temperature T_h is

$$-Q^{(1)} \equiv -W^{(1)} + \Delta E^{(1)} = T_\mathrm{h}\Delta S - W_\mathrm{irr}^{(1)}\,. \tag{4.8}$$

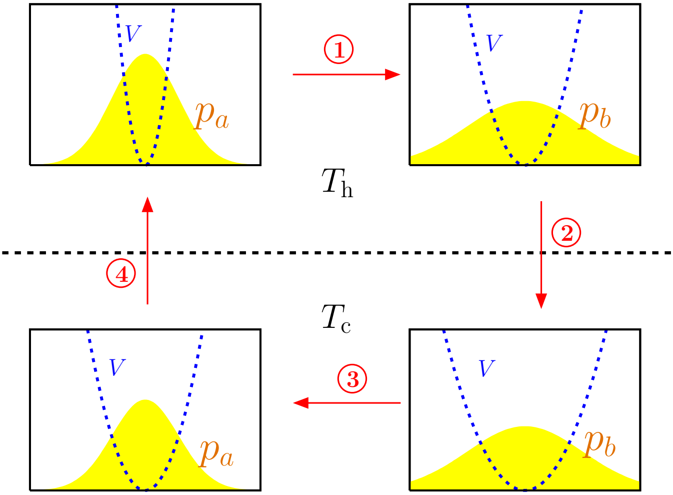

Figure 4.2 Scheme for a cyclic process of a stochastic heat engine operating between heat baths at temperature T_h and T_c. The dotted curve shows a one-dimensional potential $V(x,\tau)$ and the filled curve the boundary values $p_a(x)$, $p_b(x)$ of the corresponding distribution $p(x,\tau)$. Steps 1 and 3 are isothermal whereas steps 2 and 4 are adiabatic.

4.2.2 Example

In order to illustrate this general concept of a stochastic heat engine, we consider the motion of a colloidal particle in a harmonic potential with time-dependent stiffness. The corresponding potential is given by (3.22)

$$V(x,\tau) = \frac{\lambda(\tau)}{2} x^2. \tag{4.9}$$

The probability distribution $p(x,\tau)$ remains Gaussian for all times τ if it is so initially. The equation of motion for the variance $w(\tau) \equiv \langle x^2(\tau) \rangle$ is given by (3.23)

$$\dot{w} = -2\mu\lambda w + 2\mu T. \tag{4.10}$$

For any initial Gaussian distribution $p(x,0)$, the internal energy of the system is given as

$$E(\tau) = \int dx \; p(x,\tau) V(x) = w(\tau)\lambda(\tau)/2. \tag{4.11}$$

For a constant temperature T, the mean work (4.2) can be cast into a local functional of w, see (3.25),

$$\begin{aligned} W[\lambda(\tau)] &= \int_{t_i}^{t_f} d\tau \dot{\lambda} \frac{w}{2} = W_{\text{irr}} - T\Delta S + \Delta E \qquad (4.12) \\ &= \frac{1}{4\mu} \int_{t_i}^{t_f} d\tau \frac{\dot{w}^2}{w} - \frac{1}{2} T \left[\ln w\right]_{t_i}^{t_f} + \frac{1}{2} \left[\lambda w\right]_{t_i}^{t_f} . \end{aligned}$$

We now have to choose a protocol $\lambda(\tau)$ for the isothermal transitions. The variance w of the particle position depends on this protocol via (4.10). As a consequence, the mean work (4.12) will also depend on this protocol. We next identify protocols $\lambda_1^*(\tau)$ and $\lambda_3^*(\tau)$ yielding a maximal (mean) work output which corresponds to a minimal (mean) work. Rather than imposing boundary conditions on the control parameter λ, we impose boundary values of the particle position variances $w_a \equiv w(0) = w(t_1 + t_3)$ and $w_b \equiv w(t_1)$ for a given finite cycle time $t_{\text{tot}} \equiv t_1 + t_3$. While it might seem more natural to impose a range of (experimentally) possible λ values, such an approach can lead to unphysical optimal processes which are driven infinitely fast with infinitesimally small changes in the variance $w(\tau)$. With slight modification of the results from Chapter 3.2 due to the different boundary conditions, we get the optimal protocols for the variances

$$w_1^*(\tau) = w_a \left(1 + (\sqrt{w_b/w_a} - 1)\tau/t_1\right)^2 \tag{4.13}$$

$$w_3^*(\tau) = w_b \left(1 + (\sqrt{w_a/w_b} - 1)(\tau - t_1)/t_3\right)^2 . \tag{4.14}$$

The optimal protocols $\lambda_i^*(\tau)$ for the strength of the trap can then be calculated from (4.10). The resulting quantities are shown in Fig. 4.3.

For this cyclic process, we get the total work output

$$\begin{aligned} -W &= \frac{1}{2}(T_\mathrm{h} - T_\mathrm{c}) \ln \frac{w_b}{w_a} - \frac{1}{\mu}\left(\frac{1}{t_1} + \frac{1}{t_3}\right)(\sqrt{w_b} - \sqrt{w_a})^2 \\ &\equiv (T_\mathrm{h} - T_\mathrm{c})\Delta S - \left(\frac{1}{t_1} + \frac{1}{t_3}\right) A_\mathrm{irr}, \end{aligned} \tag{4.15}$$

with the irreversible “action” A_irr. The work only depends on the “reduced time”

$$t_r \equiv 1/(1/t_1 + 1/t_3) = t_1 t_3/(t_1 + t_3). \tag{4.16}$$

The heat uptake during one complete cycle from the hotter heat bath at temperature T_h is given as

$$-Q^{(1)} = T_\mathrm{h}\Delta S - W_\mathrm{irr}^{(1)} = T_\mathrm{h}\Delta S - \frac{A_\mathrm{irr}}{t_1} \tag{4.17}$$

yielding the efficiency

$$\eta \equiv \frac{-W}{-Q^{(1)}} = \frac{(T_\mathrm{h} - T_\mathrm{c})\Delta S - A_\mathrm{irr}/t_r}{T_h \Delta S - A_\mathrm{irr}/t_1} \tag{4.18}$$

For $t_1, t_3 \to \infty$, we recover the Carnot efficiency $\eta_\mathrm{C} \equiv 1 - T_\mathrm{c}/T_\mathrm{h}$. This shows that the sudden adiabatic steps do not spoil the reversibility.

We immediately recognize from (4.15) that there exists a “stall time”

$$t_r^\mathrm{st} \equiv \frac{A_\mathrm{irr}}{(T_\mathrm{h} - T_\mathrm{c})\Delta S} = \frac{2\left(\sqrt{w_b} - \sqrt{w_a}\right)^2}{\mu (T_\mathrm{h} - T_\mathrm{c}) \ln\left(w_b/w_a\right)} \tag{4.19}$$

where the heat engine does not perform work anymore. Rather, at smaller times $t_r < t_r^\mathrm{st}$, it consumes work.

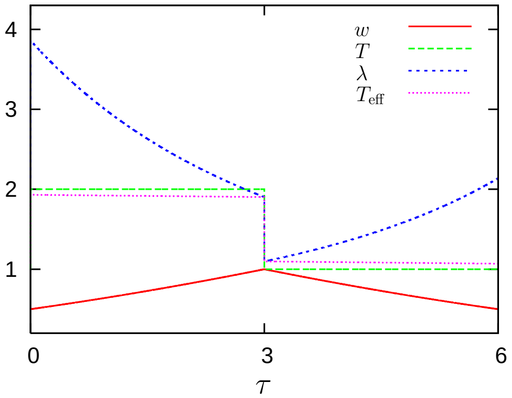

Figure 4.3 Stochastic heat engine in a harmonic potential: Time dependence of the variance of the particle position w, the temperature T, the trap strength λ and the effective temperature T_{eff} (4.34) for one cycle with $t_1 = t_3 = 3$, $w_a = 0.5$, $w_b = 1$, $T_h = 2$, $T_c = 1$, and $\mu = 1$, starting with step 1.

We next explore how fast the heat engine must be driven to yield a maximal power output. The power $P = -W/(t_1 + t_3)$ has a maximum for

$$t_1^* = t_3^* = \frac{4A_{\text{irr}}}{(T_{\text{h}} - T_{\text{c}})\Delta S} \tag{4.20}$$

which yields a reduced optimal time

$$t_r^* = \frac{1}{2} t_1^* = 2t_r^{\text{st}}. \tag{4.21}$$

A similar relation between the stall force and the force at maximum power has been obtained in [116] within a linear response treatment. The total work output at maximum power

$$-W^* = \frac{1}{2}(T_{\text{h}} - T_{\text{c}})\Delta S \tag{4.22}$$

and the corresponding heat uptake

$$-Q^{*(1)} = \frac{1}{4}\Delta S(3T_{\text{h}} + T_{\text{c}}) \tag{4.23}$$

then yield the efficiency at maximum power

$$\eta^* = \frac{2(T_\mathrm{h} - T_\mathrm{c})}{3T_\mathrm{h} + T_\mathrm{c}} = \frac{\eta_\mathrm{C}}{2 - \eta_\mathrm{C}/2}. \tag{4.24}$$

This result is independent of the imposed boundary values w_a and w_b, suggesting a certain degree of universality confirmed below. For large temperature differences, $T_\mathrm{h} - T_\mathrm{c} \gg T_\mathrm{c}$, the efficiency has the limit $\eta^* \to 2/3$. An expansion for small relative temperature differences, $\mathcal{T} \equiv (T_\mathrm{h} - T_\mathrm{c})/T_\mathrm{c} \ll 1$,

$$\eta^* = \frac{2\mathcal{T}}{3\mathcal{T} + 4} = \frac{\mathcal{T}}{2} - \frac{3\mathcal{T}^2}{8} + \frac{9\mathcal{T}^3}{32} + \mathcal{O}\left(\mathcal{T}^4\right) \tag{4.25}$$

shows that the deviation from the Curzon-Ahlborn efficiency

$$\eta_\mathrm{CA} = 1 - \sqrt{T_\mathrm{c}/T_\mathrm{h}} = \frac{\mathcal{T}}{2} - \frac{3\mathcal{T}^2}{8} + \frac{10\mathcal{T}^3}{32} + \mathcal{O}\left(\mathcal{T}^4\right) \tag{4.26}$$

occurs at the third order in the relative temperature difference $\mathcal{T}$. The validity of the Curzon-Ahlborn efficiency in a linear response regime has been shown quite generally in [116]. We recover this result even including the second order in the relative temperature difference, which goes beyond linear response. For larger deviations from equilibrium, however, the efficiency at maximum power in this example is smaller than the Curzon-Ahlborn bound.

4.2.3 General Case

We now relax the restriction to one degree of freedom in a harmonic potential and go back to the general case where we also impose two boundary distributions: $p_a(\mathbf{x})$ at $\tau = 0$ (and at $\tau = t_1 + t_3$) and $p_b(\mathbf{x})$ at $\tau = t_1$ for the two isothermal transitions. As seen from (4.7), minimizing the total mean work W (leading to a maximal work output) subject to such boundary conditions, which leave the ΔS term invariant, is equivalent to the minimization of the irreversible work (4.3) for both isothermal transitions. Using a normalized time $\hat{\tau} \equiv (\tau - t_i)/(t_f - t_i)$ and thus a time-dependent distribution $\mathcal{P}(\mathbf{x}, \hat{\tau})$, it follows from (4.1) that the current can be expressed as $\mathbf{j} = \mathcal{J}(\mathbf{x}, \hat{\tau})/(t_f - t_i)$. The irreversible work (4.3) can then be written as

$$W_\mathrm{irr} \equiv \frac{1}{(t_f - t_i)} \int_0^1 d\hat{\tau} \int dx\, \frac{\mathcal{J}(\mathbf{x}, \hat{\tau}) \mu^{-1} \mathcal{J}(\mathbf{x}, \hat{\tau})}{\mathcal{P}(\mathbf{x}, \hat{\tau})}. \tag{4.27}$$

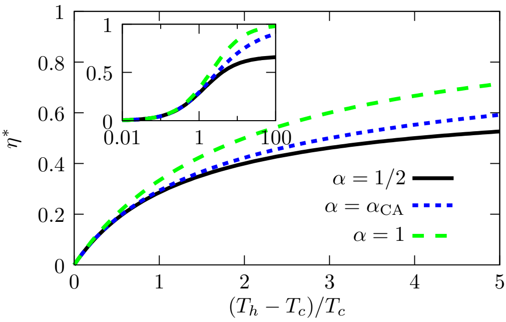

Figure 4.4 Efficiency η^* at maximum power as a function of $(T_{\rm h} - T_{\rm c})/T_{\rm c}$ for $\alpha = 1/2$, $\alpha_{\rm CA}$, and 1, corresponding to the temperature independent mobility of the example, the Curzon-Ahlborn efficiency, and the upper bound of (4.32), respectively. The inset shows the same data in a log-plot.

Minimizing the irreversible work $W_{\rm irr}$ thus is equivalent to minimizing the integral in (4.27) which only depends on $\mathcal{P}(\mathbf{x}, \hat{\tau})$ and $\mathcal{J}(\mathbf{x}, \hat{\tau})$. The time evolution $\partial_\tau p = -\nabla \cdot \mathbf{j}$ expressed in the time-normalized quantities imposes the constraint $\partial_{\hat{\tau}} \mathcal{P} = -\nabla \cdot \mathcal{J}$. Minimizing the integral in (4.27) subject to this constraint leads to the optimal distribution $\mathcal{P}^*(\mathbf{x}, \hat{\tau})$ which does not depend on the total transition time. Since this optimization has to be done for each of the isothermal transitions separately, we get optimal distributions $\mathcal{P}_1^*(\mathbf{x}, \tau/t_1)$ and $\mathcal{P}_3^*(\mathbf{x}, (\tau - t_1)/t_3)$ for the two isothermal transitions which both are independent of the total transition times t_j, $j = 1, 3$.

The optimization with respect to maximal work output is tractable analytically only if we restrict to harmonic potentials $V(\mathbf{x}, \tau)$, as shown above in the example. Otherwise, the resulting Euler-Lagrange equations are non-linear partial differential equations and even the numerical solution seems to be a difficult task. For a derivation of our central result, however, we do not need an explicit solution. It suffices to observe that (4.27) implies a remarkable universal feature for the optimal driving scheme: The (mean) irreversible work in the isothermal transitions scales exactly with the inverse transition time

$$W_{\rm irr}^{(j)} = A_{\rm irr}^{(j)}/t_j, \tag{4.28}$$

where $A_{\rm irr}^{(j)}$ is independent of the transition times $t_j (j = 1, 3)$ and becomes a functional only of $p_a(\mathbf{x})$, $p_b(\mathbf{x})$, and the mobility matrix μ. As a direct consequence, the work output during a complete cycle is given by

$$-W = (T_\mathrm{h} - T_\mathrm{c})\Delta S - \frac{A_\mathrm{irr}^{(1)}}{t_1} - \frac{A_\mathrm{irr}^{(3)}}{t_3}, \tag{4.29}$$

The heat flux from the hotter bath T_h is

$$-Q^{(1)} = T_\mathrm{h}\Delta S - \frac{A_\mathrm{irr}^{(1)}}{t_1}. \tag{4.30}$$

For negative $\Delta S < 0$ and transition times larger than the "stall time" $t > t^\mathrm{st}$, where the engine does not perform work anymore, the setup performs as a heat engine with efficiency

$$\eta \equiv \frac{-W}{-Q^{(1)}} \tag{4.31}$$

approaching the Carnot efficiency $\eta_\mathrm{C} \equiv 1 - T_\mathrm{c}/T_\mathrm{h}$ for infinite cycle time $t \to \infty$. Maximization of $P \equiv -W/(t_1 + t_3)$ with respect to the transition times t_1, t_3 leads to a universal expression for the efficiency at maximum power of

$$\eta^*(\alpha) = \frac{\eta_\mathrm{C}}{2 - \alpha\eta_\mathrm{C}} \tag{4.32}$$

where

$$\alpha \equiv 1/\left(1 + \sqrt{A_\mathrm{irr}^{(3)}/A_\mathrm{irr}^{(1)}}\right). \tag{4.33}$$

This expression for the efficiency at maximal power is our main result. In the linear response limit, $T_\mathrm{h} - T_\mathrm{c} \ll T_\mathrm{c}$, we recover $\eta^* \to \eta_\mathrm{C}/2$, consistent with the analysis in [116]. Beyond linear response, one needs the irreversible action $A_\mathrm{irr}^{(i)}$ which, in principle, can be calculated for any specific system by solving the optimization problem. In general, due to the temperature dependence of the mobility μ, the irreversible action $A_\mathrm{irr}^{(i)}$ is temperature dependent. An explicit statement becomes possible for an isotropic mobility matrix μ in (4.1). In this case, α depends only on the temperature dependence of μ via $A_\mathrm{irr}^{(3)}/A_\mathrm{irr}^{(1)} = \mu(T_\mathrm{h})/\mu(T_\mathrm{c})$. For a temperature independent mobility, i. e. $\alpha = 1/2$, we recover the result (4.24) from the example above which thus holds also in higher dimensions. Only for $\mu \sim 1/T$, corresponding to $\alpha = \alpha_\mathrm{CA} \equiv 1/(1 + \sqrt{T_\mathrm{c}/T_\mathrm{h}})$, we recover the Curzon-Ahlborn efficiency $\eta^* = 1 - \sqrt{T_\mathrm{c}/T_\mathrm{h}}$. These efficiencies at maximum power are shown in Fig. 4.4. From a theoretical perspective, it is important to note that for $1 > \alpha > \alpha_{\mathrm{CA}}$, the result (4.32) exceeds the Curzon-Ahlborn bound. While in the present setup this can be achieved only if the mobility μ decreases faster than $\sim 1/T$ with temperature, $\alpha = 1$ can be reached in discrete ratchet heat engines [35].

As outlined in the introduction, the Curzon-Ahlborn efficiency is a rather universal bound on the efficiency at maximum power for a wide class of model heat engines. Why does the efficiency at maximum power derived here also under quite general conditions differ significantly from the Curzon-Ahlborn result?

A first hint is given by analyzing our example in analogy to an endoreversible Curzon-Ahlborn machine. For the latter, a linear Fourier law for the heat flow is assumed. However, for systems driven strongly out of equilibrium, non-linearities can occur. In order to analyze our model heat engine in this framework, we first have to assign an "effective" temperature to the working medium (the Brownian particle). Since in this harmonic potential the distribution remains equilibrium-like (Gaussian) even out of equilibrium, we can assign an effective temperature

$$T_{\mathrm{eff}}(\tau) \equiv w(\tau)\lambda(\tau) \tag{4.34}$$

to the system. If we (instantaneously) coupled a heat bath at this temperature T_{eff} to our system and kept the current trap strength λ constant, we would recover an equilibrium situation. We now express the heat exchange of the system in terms of this effective temperature

$$\begin{aligned} dQ &= dW - dE = \frac{1}{2} w d\lambda - \frac{1}{2} d(w\lambda) = -\frac{1}{2}\lambda dw \\ &= -\frac{1}{2}\lambda \dot{w} d\tau = -\mu\lambda(T - \lambda w) d\tau \\ &= -\mu\lambda(\tau)(T - T_{\mathrm{eff}}) d\tau \end{aligned} \tag{4.35}$$

and recover a linear Fourier law for the heat flow. However, the thermal conductivity $\mu\lambda(\tau)$ becomes time-dependent in contrast to the assumptions of the endoreversible Curzon-Ahlborn engine.

Secondly, the derivation of an apparent universal Curzon-Ahlborn bound in Refs. [116, 117] by using a cascade construction of N machines working in the linear response regime comes at the price of an infinitesimally small power output in the (implicitly assumed) limit $N \to \infty$. For the setup in [116], it can easily been shown that for a mechanical heat engine in the linear response regime, the maximal power output scales as $P \sim (\Delta T)^2$ where $\Delta T \equiv T_{\mathrm{h}} - T_{\mathrm{c}}$.

The coupling of N such machines with equal temperature differences $\Delta T = (T_\mathrm{h} - T_\mathrm{c})/N$ thus leads to a total maximal power output of $P^* \sim 1/N$.

4.2.4 Role of kinetic energy

So far, we have neglected the kinetic energy of the degrees of freedom. However, even in the overdamped limit, coupling to and decoupling from the heat baths leads to a heat flux due to the kinetic energy of the particle [31]. This additional heat flux $Q_\mathrm{kin} = (T_\mathrm{h} - T_\mathrm{c})/2$ per degree of freedom can easily be considered, leading to a general decrease of efficiencies. For large changes of the potential $V(\mathbf{x}, \tau)$ during the cycle, however, this contribution is small and can be neglected. In general, a given amount of heat leakage Q^leak per cycle (e. g., due to the kinetic energy) leads to an additional term in (4.30)

$$-Q^{(1)} = T_\mathrm{h}\Delta S + Q^\mathrm{leak} - \frac{A_\mathrm{irr}^{(1)}}{t_1}. \tag{4.36}$$

For $Q^\mathrm{leak} > 0$, Carnot efficiency cannot be reached anymore and for $t_1 \to \infty$, $t_3 \to \infty$, we get the quasistatic efficiency

$$\eta_\mathrm{qs} \equiv (T_\mathrm{h} - T_\mathrm{c})\Delta S/(T_\mathrm{h}\Delta S + Q^\mathrm{leak}). \tag{4.37}$$

A straightforward calculation shows that the result (4.32) then is generalized to

$$\eta^*(r) = \frac{\eta_\mathrm{qs}}{2 - \alpha\eta_\mathrm{qs}} \tag{4.38}$$

where η_C now is replaced by the quasistatic efficiency η_qs.

4.3 Molecular motor at maximum power

Molecular motors are essential for directed transport within the cell [134]. They typically operate under nonequilibrium conditions due to the unbalanced chemical potentials of molecules like ATP or ADP involved in the chemical reactions accompanying the motor steps. In contrast to macroscopic engines, fluctuation effects are important thus allowing for backward steps even in directed motion. The stochastic dynamics of these motors under an applied load force can be probed experimentally by single molecule assays (see, e. g., for kinesin [135], myosin [136, 137, 138] or ATPase [139, 140]). Generically, such biomotors are modelled either in terms of continuous "flashing ratchets"

[141, 3, 4, 27] or by a (chemical) master equation on a discrete state space [142, 143, 144, 145, 33, 146, 34].

In contrast to heat engines, biomotors are driven by chemical potential differences. The efficiency of such motors is bounded by $\eta_{\max} = 1$ [30]. This bound can only be reached in an equilibrium situation corresponding to a vanishing power output of the motor. In analogy with heat engines, we here propose to investigate such motors under the condition of maximum power output.

We start with a simple model system for a chemically driven biomotor [142] and show that the qualitative results also apply to a more realistic motor model involving a second cycle. In this second model, a futile cycle leads to ATP consumption even at the stall force. Mechanical and chemical cycles are no longer tightly coupled. In both cases, the efficiency at maximum power crucially depends on the position of the transition state or, equivalently, on the load distribution factor. In fact, a transition state near the initial position is most favorable with respect to a maximal motor power output. For the efficiency at maximum power, we obtain two counter-intuitive results : (i) it increases when the transition state position is changed in such a way that the power output rises and (ii) it can increase when the system is driven further out of equilibrium by a larger chemical potential difference.

4.3.1 Model I

We first consider a linear molecular motor with equivalent discrete states (sites) X_n $(n = 0, \pm 1, \pm 2, \dots)$ with distance l between the sites and next-neighbour transitions between these states subject to a force F in backward direction, see Fig 4.5. Forward reactions are assumed to be driven by ATP molecules with chemical potential μ_{ATP} and backward transitions by ADP and P molecules with chemical potentials μ_{ADP} and μ_{P}, respectively,

$$\mathrm{ATP} + X_n \underset{w^-}{\overset{w^+}{\rightleftharpoons}} X_{n+1} + \mathrm{ADP} + \mathrm{P}. \tag{4.39}$$

If the dilution of all involved species is high, we can assume mass action law kinetics for the rate constants. Additionally, we assume the usual force dependence of rate constants [142] such that the transition rates for forward and backward steps are given by

$$\begin{aligned} w^+ &= c_{\mathrm{ATP}} k^+ e^{-\beta\delta F l} && (4.40) \\ w^- &= c_{\mathrm{ADP}} c_{\mathrm{P}} k^- e^{\beta(1-\delta)F l}, && (4.41) \end{aligned}$$

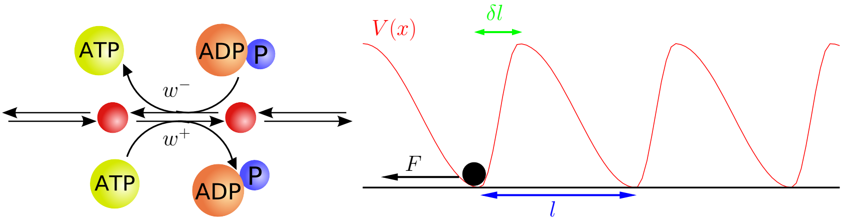

Figure 4.5 Simple linear model (Model I) of a molecular motor with step size l. (a) Scheme of the involved chemical reactions. A forward step involves hydrolysis of ATP into ADP and P. (b) Scheme of the free energy landscape $V(x)$ of the molecular motor. The transition state position δ determines the force dependence of the transition rates.

respectively. Here, c_i are the (dimensionless) concentrations of i molecules ($i = \{\mathrm{ATP}, \mathrm{ADP}, \mathrm{P}\}$) and $\beta \equiv 1/(k_B T)$. Note that we explicitly use Boltzmann's constant k_{B} during this section since we want to compare our results to experimental data. The bare reaction rates k^+, k^- are concentration independent. The load distribution factor $0 \leq \delta \leq 1$ characterizes the location of the transition state, see Fig. 4.5. It can vary between the extreme cases $\delta = 0$ (sometimes characterized as a "power stroke" [147]) and $\delta = 1$, where forward or backward rate constants, respectively, no longer depend on the force. The chemical potential of the involved molecules is

$$\mu_i = \mu_i^0 + k_B T \ln c_i, \tag{4.42}$$

with a reference value μ_i^0. Thermodynamic consistency requires

$$w^+/w^- = e^{(\Delta\mu - Fl)/(k_B T)}, \tag{4.43}$$

where $\Delta\mu \equiv \mu_{\mathrm{ATP}} - \mu_{\mathrm{ADP}} - \mu_{\mathrm{P}}$. The (mean) velocity of the motor can then be calculated as

$$v = l(w^+ - w^-) = k^- c_{\mathrm{ADP}} c_{\mathrm{P}} l \left[e^{\beta(\Delta\mu - \delta F l)} - e^{\beta(1-\delta)Fl} \right]. \tag{4.44}$$

Thermodynamic quantities for each single transition can now be defined [33, 8, 148] on the basis of the transition rates. The chemical work applied during one forward step is just the chemical potential difference $W_{\mathrm{chem}} = \Delta\mu$. The mechanical work delivered by the molecular motor during a single forward

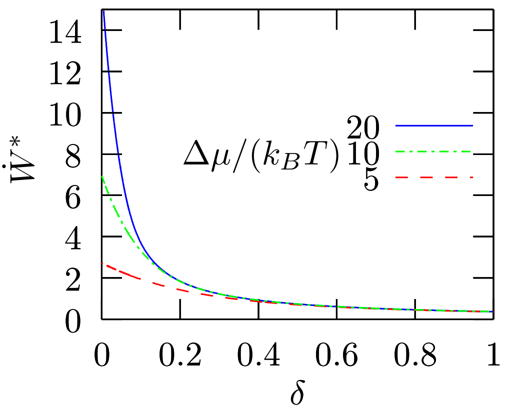

Figure 4.6 Maximum power $\dot{W}^*$ in units of $k^- c_{\rm ADP} c_{\rm P} k_{\rm B} T \exp(\beta\Delta\mu)$ as a function of the position of the transition state δ.

step against the applied force F is given by $W = Fl$. Since all states are equal, the internal energy does not change, $\Delta E = 0$, and thus the difference $Q \equiv W_{\rm chem} - W$ is dissipated as heat in the thermal environment. The efficiency η of this chemical motor is given by the ratio of mechanical work and chemical work applied by the chemical potential difference [30] as

$$\eta = \frac{W}{W_{\rm chem}} = \frac{Fl}{\Delta\mu}. \tag{4.45}$$

With the force velocity relationship (4.44), the power output follows as

$$\dot{W} \equiv Fv = k^- c_{\rm ADP} c_{\rm P} l F \left[e^{\beta(\Delta\mu - \delta F l)} - e^{\beta(1-\delta)Fl} \right]. \tag{4.46}$$

The power $\dot{W}$ is zero for $F \to 0$. When the force approaches the stall force $F \to F^{\rm st} \equiv \Delta\mu/l$, where the velocity vanishes, the power output also becomes infinitesimally small. Thus, there is an optimal force F^*, where the power output is maximal for a given chemical potential difference $\Delta\mu$. This optimal force is given by $d\dot{W}/dF = 0$ which leads to the implicit relation

$$e^{\beta\Delta\mu} = e^{\beta l F^*} \frac{1 + (1-\delta)\beta l F^*}{1 - \delta\beta l F^*}. \tag{4.47}$$

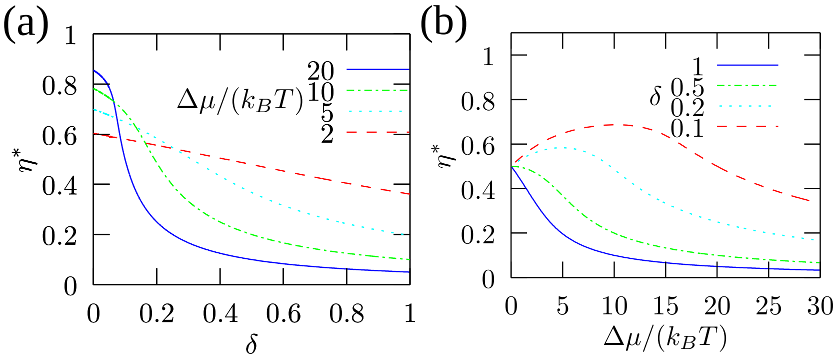

Figure 4.7 Efficiency at maximum power η^* as a function of (a) the position of the transition state δ and (b) the chemical potential difference $\Delta\mu$ for Model I.

For given $\beta\Delta\mu$, the scaled optimal force $\beta l F^*$ depends only on the parameter δ. The optimal power $\dot{W}^*$ is shown in Fig. 4.6 as a function of the transition state position δ. Numerical results for the efficiency at maximum power η^* are shown in Fig. 4.7. Note that the latter results are quite universal since no kinetic parameters enter these graphs. Both, power output and efficiency increase with decreasing δ and thus, a transition state near the initial position ($\delta = 0$) is most favorable. Previously, it has been speculated [147] that such a mechanism, where forward rates are almost independent of the force, is realized in molecular motors in order to reach a large motor velocity (corresponding to a high power output). Beyond corroborating this idea, we find as a new result that small δ also leads to a higher motor efficiency at maximum power. This is somewhat counter-intuitive since an increase in power usually leads to a decrease in efficiency.

In the limit of small chemical potential differences (where the motor works in a linear response regime near equilibrium), efficiencies at maximum power can be obtained analytically. In this limit, the stall force also becomes small and thus the exponentials in (4.44) can be expanded and truncated after the first order in $\Delta\mu$ and F leading to the approximate force-velocity relation

$$v \approx k^- c_{\mathrm{ADP}} c_{\mathrm{P}} \beta l (\Delta\mu - Fl). \tag{4.48}$$

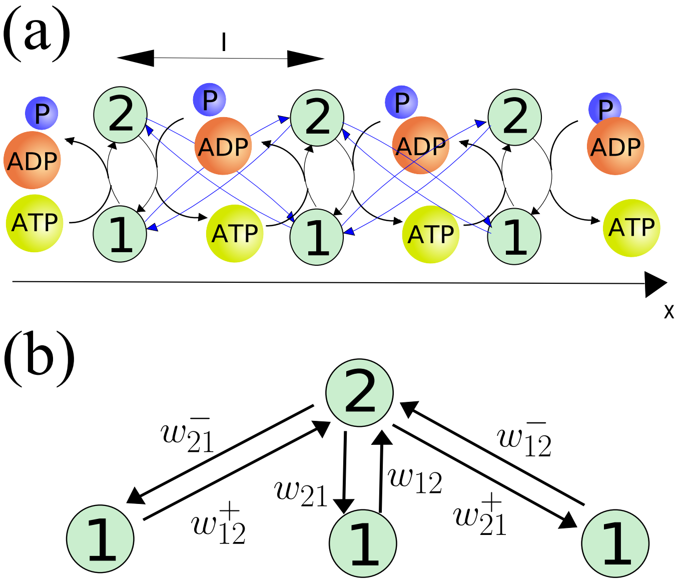

Figure 4.8 Two-cycle model for a molecular motor (Model II). (a) Scheme of the reaction pathways. (b) Definition of rate constants.

In analogy to the linear response result for heat engines [116], the efficiency at maximum power universally becomes $\eta^* = 1/2$. Beyond linear response, as a somewhat surprising result, the efficiency at maximum power increases for increasing chemical potential differences for positions of the transition state $\delta < 1/2$, compare Fig. 4.7b. Usually, dissipative cost increases when the system is driven further out of equilibrium.

4.3.2 Model II

In order to check the generality of the results obtained for the (simple) Model I, we now calculate the efficiency at maximum power for a more involved motor model. Recent experiments focussing on the backsteps of kinesin [135] indicate that a realistic motor model should comprise at least one additional cycle [135, 146, 34] leading to non-zero dissipation even at stall force. Such a mechanism with additional motor cycles presumably also applies to myosin motors which have a similar molecular structure [149]. In order to capture the main experimental finding of ATP-driven backsteps from Ref. [135], we propose a minimal model as shown in Fig. 4.8. This model is very similar to recent kinesin models [135, 146, 34] and thus captures experimental findings qualitatively. Binding and hydrolyzing ATP leads to the unbinding of one motor head. The elastic energy then leads to a biased diffusive search for the next binding site. For high load forces, the probability of a backstep increases. Note that such backsteps involve ATP consumption and thus decrease the coupling ratio between chemical and mechanical motor cycles. The force dependence is modelled as

$$\begin{aligned} w_{21}^{+} &= k_{21}^{+} e^{-\beta\delta_1 lF} \ , \ w_{12}^{+} = k_{12}^{+} e^{-\beta(1-\delta_2)lF} \\ w_{21}^{-} &= k_{21}^{-} e^{\beta\delta_2 lF} \ , \ w_{12}^{-} = k_{12}^{-} e^{\beta(1-\delta_1)lF} \end{aligned} \tag{4.49}$$

with the transition state located at $\delta_{1,2}$ for forward and backward steps, respectively. Thermodynamic consistency requires $k_{21}^{+}/k_{12}^{-} = \exp(\beta\Delta E)$, $k_{21}^{-}/k_{12}^{+} = \exp(\beta\Delta E)$, and $w_{12}/w_{21} = \exp[\beta(\Delta\mu - \Delta E)]$ where ΔE is the potential energy difference between state 1 and state 2. Given all rate constants, the steady state can be calculated as

$$p_1^s = \frac{w_{21} + w_{21}^{+} + w_{21}^{-}}{w_{21} + w_{21}^{+} + w_{21}^{-} + w_{12} + w_{12}^{+} + w_{12}^{-}}, \tag{4.50}$$

$$p_2^s = \frac{w_{12} + w_{12}^{+} + w_{12}^{-}}{w_{21} + w_{21}^{+} + w_{21}^{-} + w_{12} + w_{12}^{+} + w_{12}^{-}} \tag{4.51}$$

with motor velocity

$$v = l\left[p_1^s(w_{12}^{+} - w_{12}^{-}) + p_2^s(w_{21}^{+} - w_{21}^{-})\right]. \tag{4.52}$$

The power output of the motor is $\dot{W} = Fv$. Chemical work is applied to the motor only in the (vertical) transitions involving ATP and ADP + P. In such a step, chemical energy of amount $\Delta\mu$ is transferred to the system and thus the chemical work per unit time is

$$\dot{W}_{\text{chem}} = \Delta\mu(p_1^s w_{12} - p_2^s w_{21}). \tag{4.53}$$

The motor efficiency $\eta \equiv \dot{W}/\dot{W}_{\text{chem}}$ can then be calculated for a given set of rate constants and a given force.

We again ask for the optimal force leading to a maximal power output. We recover the qualitative results of Model I for the maximum power (data not

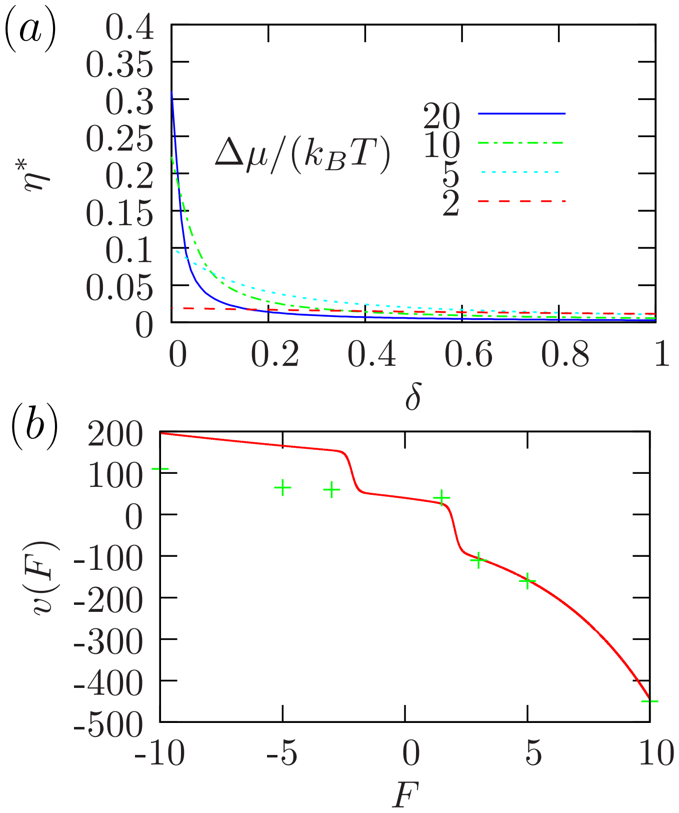

Figure 4.9 Efficiency at maximum power for Model II. (a) Efficiency at maximum power as a function of the transition state position $\delta \equiv \delta_1 = \delta_2$ with $w_{21} = 0.275/s, k_{21}^- = 0.7/s, k_{21}^+ = 1.8/s, \Delta E = 10k_BT$. (b) Relation between force [in pN] and velocity [in nm/s] for $\delta_1 = 0.004, \delta_2 = 0.024, w_{21} = 0.275/s, k_{21}^- = 0.7/s, k_{21}^+ = 1.8/s, \Delta E = 10k_BT, \Delta\mu = 20k_BT, l = 9(k_BT)/pN \simeq 36nm$ compared to corresponding data from myosin experiments [138]. For these parameters, the optimal force is $F^* \simeq 1.5pN$ and the efficiency at maximum power becomes $\eta^* \simeq 0.18$.

shown) and the efficiency at maximum power, see Fig. 4.9a, also in this (more realistic) model of a molecular motor. Specifically, the largest efficiency can be achieved for both transition states near the initial position ($\delta \equiv \delta_1 = \delta_2 = 0$). For small δ, the efficiency first increases with increasing chemical potential difference $\Delta\mu$ until it reaches a maximum. The advantage of a transition state near the initial position with respect to high power output and high efficiency thus seems to be a quite general characteristics for molecular motors. Note that efficiencies are generally lower due to the ATP-driven backward steps leading to additional dissipation in such models with additional cycles.

4.3.3 Discussion

We have first investigated a simple genuine model of a molecular motor under the condition of maximum power output. As our main result, we find that a transition state near the initial position yields both the largest power output and the largest efficiency at maximum power. Qualitatively, this behaviour is also recovered in a more realistic model involving a second motor cycle. The advantage of a small load distribution factor δ with respect to large power output and high efficiency at maximum power thus seems to be quite generic. So far, we have assumed $0 \leq \delta \leq 1$. Recently, it has been proposed to use $\delta < 0$ to interpret non-monotonous force velocity relations [150]. For negative $\delta < 0$, the efficiency at maximum power is even larger than for $\delta = 0$ in both our model systems.

For both models, the efficiency at maximum power can increase when the system is driven further out of equilibrium by a higher chemical potential difference. This result should be distinguished from previous work predicting a maximal efficiency for non-zero chemical potential differences [30, 34]. In our first model, the efficiency decreases monotonically as a function of the chemical potential difference for a given load F.

For kinesin motors, it is difficult to find clear evidence for a putative design principle of a transition state near the initial position. While previous studies have found small $\delta \lesssim 0.1$ for the main motor step [144], a transition state in the range $\delta \simeq 0.3...0.65$ has been extracted recently [146]. For myosin motors, small δ has been reported for the main motor step ($\delta < 0.1$ [137], [145]) , which is also supported by our model II as detailed in the following.

In Fig. 4.9b, the force velocity relation of our model with appropriate rate constants is compared to a recent myosin experiment [138]. For forces $F > 0$, the experimental data, including a step at $F \simeq \Delta\mu/l$, is captured by our simple model. For negative forces, our model shows a second step at $F \simeq -\Delta\mu/l$ which is not present in the experimetal data. Both steps in the theoretical model are explained by the fact that for large forces $|F| \gg \Delta\mu/l$, vertical (ATP driven) transitions are slow compared to the horizontal (force dependent) transitions and the motor is basically pulled by the load. The step at negative forces could be eliminated by introducing a force dependent energy difference $\Delta E(F)$ which corresponds to an additional force dependence of the vertical transitions. However, instead of introducing new parameters, we keep the simple model II and extract from the crude fit shown in Fig. 4.9b transition state positions $\delta_1 = 0.004$, $\delta_2 = 0.024$. These values mainly determine the behaviour of the molecular motor at large loads $|F| \gg \Delta\mu/l$. With these parameters, we find an efficiency at maximum power of $\eta^* \simeq 0.18$ which, given the strong decay of η^* with increasing δ, is quite close to the optimal value $\eta^* \simeq 0.31$ for $\delta_1 = \delta_2 = 0$, see Fig. 4.9a.

We do not claim that our simple model can explain all aspects of myosin motility. Rather, we have chosen model II in order to probe the robustness of our main results concerning the efficiency at maximum power. In order to construct a comprehensive model of myosin, more experimental data seem to be necessary.

5 Optimization of kinetic proofreading in translation

5.1 Introduction

In the biological cell, most processes involve complex proteins which are composed of 20 different aminoacids. These proteins are assembled from the genetic code stored in the form of DNA. This process is called gene expression and occurs in two main steps, see also Ref. [151] and Fig. 5.1. First, a sequence of the DNA is transcribed by an enzyme called RNA-polymerase (RNAP) into messager RNA (mRNA). Both RNA and DNA are chain molecules which are composed of 4 different nucleotides or nucleotide pairs, respectively. Second, the information on the mRNA is translated by a protein complex called ribosome into a protein. Here, aminoacids which are bound to a so called transfer RNA (tRNA) corresponding to the mRNA template are recognized by the ribosome. Each set of 3 nucleotides (which is called codon) codes for a specific aminoacid which is incorporated into the protein. Some aminoacids are coded for by more than one codon. There are also special stop codons which indicate that the protein is complete and thus lead to to the termination of the translational process. In both stages, several regulatory mechanisms are involved and some proteins even serve to regulate the expression of other proteins.

In order to perform its tasks properly, the gene expression machinery must operate (i) at a very low error rate, (ii) at a large rate of protein assembly, and (iii) in a highly cotrolled manner. The error of gene expression can be decomposed in three main contributions: transcriptional errors (incorporation of a wrong nucleotide into the mRNA), errors in the production of complexes of transfer RNA (tRNA) and corresponding aminoacid (aminoacylated tRNAs or aa-tRNAs), and errors during translation (incorporation of a wrong aminoacid into the protein). Since translation is the least accurate of these processes, see Ref. [152], it dominates the overall error of gene expression. It is therefore crucial for the cell to optimize the translation process for a low error rate.

Most biological recognition is performed by a simple key and lock principle. For the translation process, this implies that the ternary complex of the

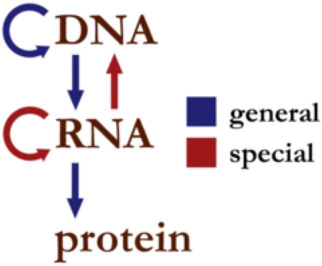

Figure 5.1 Central dogma of molecular biology. The expression of the genetic code into proteins occurs in two subsequent steps. First, a sequence of the genetic information on the DNA is transcribed by an enzyme called RNA-polymerase (RNAP) into RNA. Second, the information on the RNA is translated by a complex protein called ribosome into a protein.

aminoacylated tRNA, an elongation factor (EF-Tu), and the ATP-analogue GTP has a higher binding affinity to the right (also called cognate) codon than to a wrong codon, see Fig. 5.2. Wrong codons are subclassified into near-cognate (with only one wrong nucleotide) and non-cognate (with more than one wrong nucleotide). It has been found that the error rate in the translation stage of gene expression is well below the value expected from thermodynamic binding affinities. A nonequilibrium enzyme reaction scheme with an additional proofreading step has been proposed by Hopfield [153] and independently by Ninio [154] in order to explain the high accuracy in translation.

It has been found in experiments that the translation accuracy is not at its maximum in living species [155]. This is surprising because translation seems to be the least accurate step in protein synthesis (compared to transcription and aminoacylation of tRNA). Therefore, it is tempting to speculate about competing evolutionary goals. For exponentially growing bacterial systems, maximal growth rate has been proposed as a prevailing evolutionary goal [156, 157]. In a recent experimental study, translation speed has been mentioned as a possible reason why accuracy is not at its maximum [158]. It has been found in simulations that the clustering of ribosomes into polysomes leads to faster protein synthesis [159].

Another important issue concerns energy dissipation due to kinetic proofreading. It has been shown recently [160] that error rate and energy dissipation

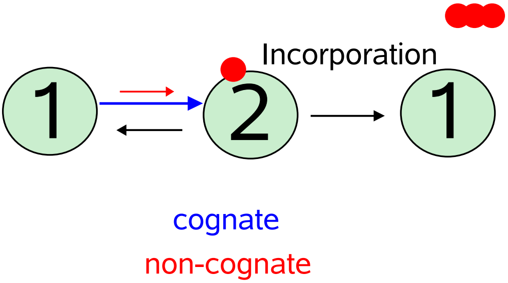

Figure 5.2 Simple key and lock scheme for recognition of the correct aminoacid during the translation process. In a first step from state 1 to state 2, the aminoacid (which is complexed with tRNA and other molecules) binds to the ribosome. The binding affinity is larger for an aminoacid which matches the codon on the mRNA (cognate codon), resulting in a binding rate which is by a factor d larger for a cognate codon than for a non-cognate codon. In a second step from state 2 to state 1, the aminoacid is incorporated into the protein, leaving an "empty" ribosome with shifted mRNA template ready to bind the next aminoacid.

are directly linked in DNA replication. It is known that the theoretical accuracy limit in kinetic proofreading schemes can only be achieved by infinite energy dissipation [161]. The first formulation of the energy cost in kinetic proofreading [162] only counted consumed moles of ATP, neglecting concentration dependent chemical potentials. The minimization of entropy production (and thus energy dissipation) was first discussed by Ehrenberg and Blomberg [161] with the result that an infinite number of checking steps with equal contribution should be used to achieve a given accuracy at minimal energy dissipation. However, most experiments [163, 158] give evidence for just a single checking step.

Summarizing, there are (at least) three competing goals for the cell to achieve during translation. A low error rate should be reached at a preferably high rate of amino acid incorporation. In addition, the necessary energy dissipation should be as low as possible. In this chapter, we address the question, how these competing goals have been weighted by evolution to give the measured rate constants as an optimal choice. This analysis is based on recent experiments, where rate constants of translation steps in *e-coli* have been measured [163, 158].

5.2 The model

For a simple key and lock scheme as shown in Fig. 5.2, the minimal error rate E is determined by the difference in binding affinities for cognate and non-cognate codons. This difference in binding affinities determines the ratio d of binding rates for cognate and near-cognate codons, respectively. More generally, one can assume that the maximal ratio of cognate and non-cognate rate constants for any reaction step is given by the discrimination rate d. The minimal error rate in any near-equilibrium network then is given by $E = 1/d$ [161]. In a branched network in a nonequilibrium steady state, lower error rates can be achieved by additional "proofreading" steps. A crude translation scheme similar to the model originally introduced by Hopfield [153] is shown in Fig. 5.3a. In such a setup, initial binding and proofreading step each contribute a discrimination rate d and the minimal error rate is given by $E = 1/d^2$ [153, 161]. While it has been shown that the error rate can be further reduced by more than one proofreading step, most experiments indicate a single proofreading step during the incorporation of a aminoacid into the protein. However, the observed premature termination of the protein synthesis upon incorporation of a wrong aminoacid [164] can be interpreted as a second proofreading stage, decreasing the error rate even below the rate of independent incorporation of aminoacids.

In Refs. [163, 158], rate constants for a kinetic proofreading scheme of the *tRNA* selection step during translation have been measured at two different buffer conditions leading to a low and a high accuracy regime, respectively. The resulting reaction scheme is more complicated than the simple proofreading scheme since intermediate steps occur, see Fig. 5.3b, and comprises the following (reversible) reactions

$$\begin{aligned}
X_1 \underset{k_{21}}{\overset{k_{12}}{\rightleftharpoons}} X_2 \underset{k_{32}}{\overset{k_{23}}{\rightleftharpoons}} X_3 &\qquad \text{initial binding and codon recognition} \\
X_3 \underset{k_{43}}{\overset{k_{34}}{\rightleftharpoons}} X_4 &\qquad \text{GTPase activation and hydrolysis} \\
X_4 \underset{k_{54}}{\overset{k_{45}}{\rightleftharpoons}} X_5 &\qquad \mathrm{EF-Tu}\ \text{conf. change} \\
X_5 \underset{k_{65}}{\overset{k_{56}}{\rightleftharpoons}} X_6 &\qquad \text{incorporation} \\
X_6 \underset{k_{16}}{\overset{k_{61}}{\rightleftharpoons}} X_1 &\qquad \mathrm{EF-Tu}\ \text{dissociation} \\
X_5 \underset{k_{15}}{\overset{k_{51}}{\rightleftharpoons}} X_1 &\qquad \text{rejection.}
\end{aligned} \tag{5.1}$$

A detailed description of each of these steps is given in the caption of Fig. 5.3b. We denote the intrinsic rate constants for a transition from state i to state j by k_{ij} for cognate codons and by $\tilde{k}_{ij}$ for near-cognate codons. The measured reaction rates for cognate and near-cognate codons are shown in Tab. 5.1. In the high accuracy regime, backward rates could be measured only for the $X_1 \rightleftharpoons X_2 \rightleftharpoons X_3$ reaction steps.

Within this model, the incorporation rate of correct proteins per ribosome can be calculated using standard techniques as

$$k_{\mathrm{inc}} = \frac{\tilde{p}_1^{\mathrm{s}}}{\tilde{p}_1^{\mathrm{s}} + p_1^{\mathrm{s}} - p_1^{\mathrm{s}}\tilde{p}_1^{\mathrm{s}}} (p_5^{\mathrm{s}} k_{56} - p_6^{\mathrm{s}} k_{65}) \tag{5.2}$$

where p_i^{s} is the steady state probability of state X_i when only the cognate network (5.1) is considered and $\tilde{p}_i^{\mathrm{s}}$ is the corresponding steady state probability of state X_i for the near-cognate network. Here, we have used the fact that both networks for cognate and near-cognate tRNA are connected only through one single state X_1 which corresponds to the "empty" ribosome. The prefactor $\tilde{p}_1^{\mathrm{s}}\tilde{p}_1^{\mathrm{s}} + p_1^{\mathrm{s}} - p_1^{\mathrm{s}}\tilde{p}_1^{\mathrm{s}}$ scales the steady state probabilities p_5^{s} and p_6^{s} of the cognate

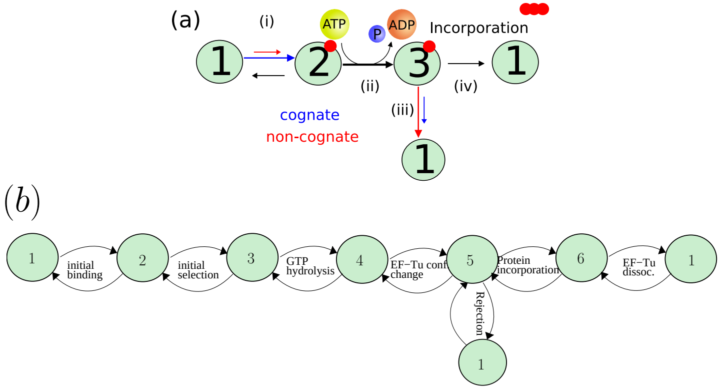

Figure 5.3 (a) Hopfield model of kinetic proofreading with three states 1, 2 and 3 and the basic steps: (i) The initial selection step (1 → 2) discriminates cognate codons from non-cognate ones. State 2 has a higher affinity for the ternary complex (consisting of elongation factor Tu (EF-Tu), aa-tRNA, and GTP) with a cognate $tRNA$ codon. This leads to a larger forward rate for cognate codons. (ii) The hydrolysis of GTP (2 → 3) is the driving mechanism of the proofreading scheme which keeps the reaction network out of equilibrium. The chemical work delivered by hydrolyzation of GTP assures that the forward reaction rate is much larger than the corresponding backward rate. (iii) The rejection step (3 → 1) discriminates between cognate and near-cognate codons and provides a second “proofreading” stage to prevent incorporation of a wrong aminoacids. The rate constant for this step is larger for near-cognate codons. (iv) Protein incorporation. From the ribosome perspective, rejection and protein incorporation yield the same final state (“empty” ribosome, state 1). Selection is achieved in two seperated steps (Initial selection and Rejection) whith different rate constants for cognate and near-cognate codons. (b) Experimentally determined model of proofreading in translation with six states from [158], see also Table 5.1. In a first initial binding step (1 → 2), aa-tRNA binds non-specifically. In the initial selection step (2 → 3), discrimination between cognate and non- or near-cognate codons is achieved by different backward rate constants. The GTP-hydrolysis step (3 → 4) has the same purpose as step (ii) in the simple model (a) but also discriminates between cognate and other codons. After an intermediate conformational change step (4 → 5), proofreading discriminates again between cognate and other condons. Here, both rejection (5 → 1) and protein incorporation (5 → 6) have different rate constants for cognate and other codons. In a last step (6 → 1), the elongation factor Ef-Tu is released.

reaction step		**cognate**	**near-cognate**
initial binding	[e]k_{12}	[a]$140(\mu M s)^{-1}$	[a]$140(\mu M s)^{-1}$
	k_{21}	[a]$85s^{-1}$	[a]$85s^{-1}$
codon recognition	k_{23}	[a]$190s^{-1}$	[a]$190s^{-1}$
	k_{32}	**[a]**$\mathbf{0.23}s^{-1}$	**[a]**$\mathbf{80}s^{-1}$
GTPase activation and hydrolysis	k_{34}	[a]$\mathbf{260}s^{-1}$	[a]$\mathbf{0.4}s^{-1}$
EF-Tu conformational change	k_{45}	[b]$50s^{-1}$	[b]$50s^{-1}$
peptide bond formation	k_{56}	[a]$7s^{-1}$	[c,f]$1s^{-1}$
EF-Tu dissociation	k_{61}	[b]$3s^{-1}$	[b]$3s^{-1}$
rejection	k_{51}	[d]$0.05s^{-1}$	[c,f]$15.7s^{-1}$

Table 5.1 Rate constants used for simulation. [a] : High accuracy measurement compiled from Ref. [158] . [b] : Low accuracy measurement compiled from Ref. [163] . [c] : Plausible values which are consistent with Ref. [158] . [d] : Rate constant reported to be $< 0.3s^{-1}$ in Ref [158] . [e] : Rate constants k_{12} were measured per concentration of ternary complex. We assume for our analysis a ternary complex concetration of $c_T = 0.05\mu M$. [f] : According to [158], the rate constants $\tilde{k}_{56}$ and $\tilde{k}_{51}$ are connected by the measured value of $\tilde{k}_{56}/(\tilde{k}_{56} + \tilde{k}_{51}) \simeq 0.06$.

network to give the corresponding steady state probabilities for the combined cognate and near-cognate network, see Sect. 5.3.4 for details. The error rate then is given by the ratio of near-cognate and cognate incorporation current (per ribosome)

$$E = \frac{(\tilde{p}_5^{\mathrm{s}} \tilde{k}_{56} - \tilde{p}_6^{\mathrm{s}} \tilde{k}_{65})/\tilde{p}_1^{\mathrm{s}}}{(p_5^{\mathrm{s}} k_{56} - p_6^{\mathrm{s}} k_{65})/p_1^{\mathrm{s}}}. \tag{5.3}$$

If all rate constants were known, the steady state probabilities p_i^{s} and $\tilde{p}_i^{\mathrm{s}}$ could be calculated from the rate constants using the Hill method [165, 166]. However, some of the rate constants could not be determined under high accuracy conditions [158] and thus the crucial quantities error rate and incorporation rate cannot be calculated without additional assumptions. We therefore will assume plausible values for the unknown rate constants, see. Tab. 5.1, using to some extent the results from the low accuracy regime [163]. Inserting the rate constants from Tab. 5.1 and assuming zero backward rates, the error rate becomes $E \simeq 0.00096$ which is consistent with the approximative calculation in [158]. However, the error rate which was measured independently was $E^{\mathrm{ex}} \simeq 0.0022$ and thus about twice as large as theoretically expected [158]. We therefore first explore how the error rate depends on the choice of the unknown backward rate constants.

5.2.1 Dependence of the error rate on the backward rate constants

We consider three different strategies to fix the unknown backward rate constants:

Case I.– Since the unknown backward rates are presumably very small, one could neglect them as a first trial. This results in an error rate of $E \simeq 0.00096$, as mentioned above.

Case II.– If backward rates are not to be neglected, one can choose a given ratio $r_{ij} = k_{ji}/k_{ij} = \tilde{k}_{ji}/\tilde{k}_{ij}$ of the unknown backward rate k_{ji} and its corresponding forward rate k_{ij} for each reaction step (equal ratio for both cognate and near-cognate network). This implies that selection is accomplished by the height of the barrier and not by free energy differences between the states. Since nothing is known about the backward rate constants, we employ a Monte Carlo procedure and choose the ratios r_{ij} mentioned above randomly from a wide range of possible (small) values between $2^{-7} \simeq 0.01$ and $2^{-20} \simeq 10^{-6}$.

With all rate constants given, the error rate then can be calculated using (5.3). Unexpectedly, though the chosen backward rates are quite small, the error rate varies in a wide range, mainly dependent on the ratio r_{15}, see Fig.

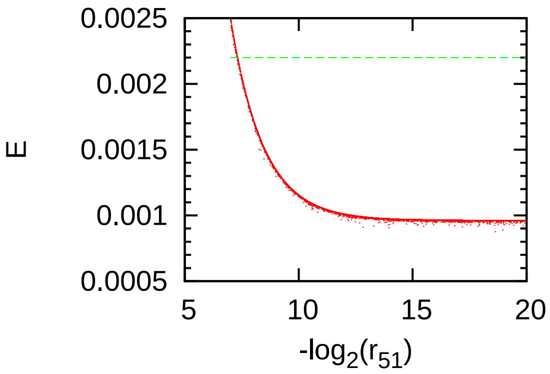

Figure 5.4 Error rate for different values of the logarithm of the rate ratio r_{51} for Case II. The error rate only weakly depends on the other rate ratios r_{ij}. The dashed line shows the experimentally measured error rate E^{ex}.

5.4. The deviation of the calculated error rate from the measured one in [158] could thus possibly be explained by the neglected backward rate k_{15}.

Case III. – Alternatively, one can choose a given ratio r_{ij} of unknown backward rates and their corresponding forward rates only for the cognate network. For the near-cognate network, backward rates are chosen as in the cognate network. This implies that selection is mainly accomplished by free energy differences. The ratios r_{ij} are chosen randomly as explained for Case II. In this regime, the (random) backward rates hardly show an effect on the error rate $E \simeq 0.00096$, see Fig. 5.5a.

Summary. – The deviation of the calculated error rate from the measured one in [158] can possibly be explained by the neglected backward rate k_{15}. Since the error rate depends on this backward rate constant only in Case II, this would imply that selection in the rejection step is mainly accomplished by barrier effects and not by free energy differences.

5.3 Optimization results

5.3.1 Maximization of Incorporation rate at given error rate

We now test the hypothesis that high accuracy is sacrificed *in vivo* for the fast incorporation of aminoacids into the protein. We keep all rate constants but k_{34} and k_{56} fixed at the values given in Tab. 5.1. We then vary the rate constants k_{34} and k_{56}, which are crucial for proofreading. We keep the ratios $k_{34}/\tilde{k}_{34}$ and $k_{56}/\tilde{k}_{56}$ fixed to the measured values, which corresponds to a fixed discrimination ratio. A mere minimization of the error rate would lead to $k_{34} \rightarrow 0$ and $k_{56} \rightarrow 0$. A high incorporation rate is achieved by high values of k_{34}, k_{56}.

We thus explore how the rates k_{34} and k_{56} must be chosen to yield a maximal incorporation rate at a given error rate. We therefore solve (5.3) for k_{56} with the error rate on the left hand side of (5.3) given by the value calculated from the rate constants in Tab. 5.1. After insertion of the result into (5.2), the incorporation rate depends only on the hydrolysis rate constant k_{34}. Maximization yields the optimal rate constant k_{34}^{opt}. We again consider the three strategies for the choice of the backward rate constants.

Case I.– Neglecting backward rates results in an optimal rate constant $k_{34}^{\mathrm{opt}} \simeq 40/s$ which is almost an order of magnitude below the measured rate constant $k_{34} = 260/s$. Thus, contrary to the conjecture in [158], within this case, the measured rate constants cannot be explained by the goal of achieving a large protein incorporation rate.

Case II.– We employ the Monte Carlo procedure for the backward rate ratios r_{ij} as explained above. In Fig. 5.5b, the protein incorporation rate as a function of the rate constant k_{34} is shown for backward rates chosen to give a high or low error rate, respectively. Although the backward rates are chosen quite small, the optimal rate constant k_{34}^{opt} depends on the ratios r_{ij} (mainly on the ratio r_{51}). However, the optimal rate constant does not exceed $k_{34}^{\mathrm{opt}} \simeq 70/s$ for error rates consistent with the experiment. Optimal rate constant and error rate are correlated as shown in Fig. 5.5a.

Case III.– The ratios r_{ij} are chosen randomly as explained above. In this regime, the (random) backward rates show no effect on the optimal rate constant $k_{34}^{\mathrm{opt}} \simeq 40/s$, see Fig. 5.5(a).

Summary.– Contrary to the conjecture in [158], the large value of the measured rate constant $k_{34} \simeq 260/s$ which leads to an error rate well above its theoretical minimum cannot be explained by the goal of a large incorporation rate. Rather, the largest incorporation rate would be reached at significantly smaller values of the rate constant k_{34}.

5.3.2 Role of dissipation

The (intrinsic) mean entropy production in the proofreading reaction networks for cognate (5.1) and near-cognate codons can be extracted from the rate constants as [7, 8]

$$\frac{d}{dt}s_{\mathrm{tot}} = \frac{\tilde{p}_1^{\mathrm{s}}}{\tilde{p}_1^{\mathrm{s}} + p_1^{\mathrm{s}} - p_1^{\mathrm{s}}\tilde{p}_1^{\mathrm{s}}} \sum_{i,j} p_i^{\mathrm{s}} k_{ij} \ln \frac{k_{ij}}{k_{ji}} \tag{5.4}$$

and

$$\frac{d}{dt}\tilde{s}_{\mathrm{tot}} = \frac{p_1^{\mathrm{s}}}{\tilde{p}_1^{\mathrm{s}} + p_1^{\mathrm{s}} - p_1^{\mathrm{s}}\tilde{p}_1^{\mathrm{s}}} \sum_{i,j} \tilde{p}_i^{\mathrm{s}} \tilde{k}_{ij} \ln \frac{\tilde{k}_{ij}}{\tilde{k}_{ji}}. \tag{5.5}$$

If we vary k_{34} and k_{56} again, the total entropy production is almost proportional to the incorporation rate. The entropy production per incorporated aminoacid then is roughly constant and the goal of a minimum dissipation does not yield a reasonable optimization scheme.

5.3.3 Robustness of the results

In order to test the robustness of the results obtained above, we have also randomly varied some of the forward rates in a reasonable range around the measured values keeping however the ratio between cognate and near-cognate rate constants fixed. Specifically, we have varied the measured rate constants k_{23}, k_{32} by 30% and the estimated rate constants $k_{45}, k_{51}, \tilde{k}_{56}$ by a factor of $(2^{-3}....2^{3})$ around the values of Table 5.1). Moreover, the assumed concentration of the ternary complex was varied in a wide range $c_T = (0.005\ldots0.5)$. It is believed that the initial binding step is rate limiting *in vivo*, thus the concentration of ternary complex c_T should be small.

There are parameter values (very low concentration of ternary complex) with a maximal incorporation rate k_{inc} at an optimal rate constant k_{34}^{opt} near the measured rate constant $k_{34} \simeq 260$, see Fig. 5.6a. However, for such rate constants, the achievable incorporation rate k_{inc} is almost independent of the prescribed error rate. Within this regime, a slight decrease (in some cases even an increase) in incorporation rate can lead to a distinctly lower error rate. In order to quantify this effect, we have calculated the incorporation rate yielding an error rate of $E/2$ and compared it to the incorporation rate at an error

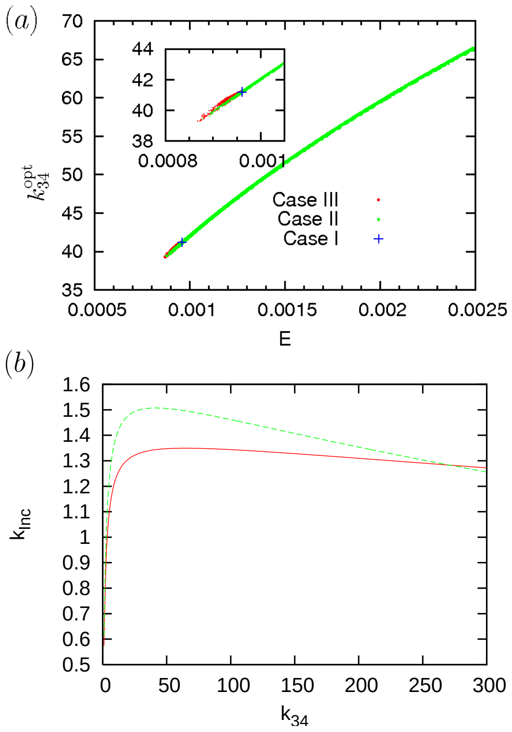

Figure 5.5 (a) : Scatter plot of the error rate E and the optimal rate constant k_{34}^{opt} for 15000 independent runs with random ratios r_{ij} for each of the Cases II and III with fixed forward rate constants as given in Tab. 5.1. For Case II, the error rate E and the optimal rate constant k_{34}^{opt} are strongly correlated and vary in a wide range. For Case III, the deviation of both E and k_{34}^{opt} from their respective values for zero backward rates (Case I) is small. The inset shows a magnification of the scatter plot around the point obtained for zero backward rates (Case I). (b) Protein incorporation rate as a function of the GTP hydrolysis rate constant k_{34} for Case II for a fixed error rate E given by the value calculated from the rate constants from Tab. 5.1. Here, the backward rate constants are chosen to yield either a high ($E \simeq 0.0023$, solid line) or low ($E \simeq 0.00096$, dashed line) error rate. The maximum protein incorporation rate is reached for $k_{34}^{\text{opt}} \simeq 64.5/s$ and $k_{34}^{\text{opt}} \simeq 41.2/s$, respectively.

rate E (both for $k_{34} = k_{34}^{\mathrm{opt}}$), where E is the error rate calculated from the rate constants in Table 5.1. In particular for a low concentration of ternary complex, the ratio of incorporation rate at error rate E and incorporation rate at error rate $E/2$ is close to 1, see Fig. 5.6b. A slightly higher incorporation rate at the expense of a doubled error rate, however, does not seem to be favorable for the cell.

The analysis for Case I and Case III yields qualitatively similar results. We thus can conclude that the high rate constant k_{34} cannot be explained by the goal of a large protein incorporation rate.

5.3.4 Effect of allowing for more than one non-cognate codon

Protein incorporation rate is lowered by non-cognate tRNA binding to the ribosome. In Ref. [158], it was speculated that this might explain why accuracy is not at its maximum. We analyse the effect of non-cognate species on the optimization described above. The networks of different codons are connected by one single state X_1 which is the state of the "empty" ribosome. If we want to take into account the effect of more competing codon species, we first have to calculate the steady state of the whole network consisting of sub-networks corresponding to the different codon-species. We consider a network which consists of n subnetworks connected only by one single state X_1. If the stationary states of the subnetworks are known, the steady state of the entire network can be calculated as

$$p^{\mathrm{s}}_{\mathrm{tot}}(1) = 1/\left(\sum_i \frac{1}{p^{\mathrm{s}}_{(i)}(1)} - 1\right) \tag{5.6}$$

$$p^{\mathrm{s}}_{\mathrm{tot}}(k) = \frac{p^{\mathrm{s}}_{\mathrm{tot}}(1)}{p^{\mathrm{s}}_{(i)}(1)} p^{\mathrm{s}}_{(i)}(k) \tag{5.7}$$

where $p^{\mathrm{s}}_{(i)}(1)$ is the stationary probability of state X_1 in the subnetwork i and $p^{\mathrm{s}}_{\mathrm{tot}}(1)$ is the stationary probability of state X_1 of the entire network.

We assume that the error rate through incorporation of non-cognate codons is negligible. However, the incorporation rate is lowered since initial binding of non-cognate codons can block the ribosome. Still, as we have tested using the measured values of non-cognate rate constants [167], this does not affect the optimal rate constants significantly.

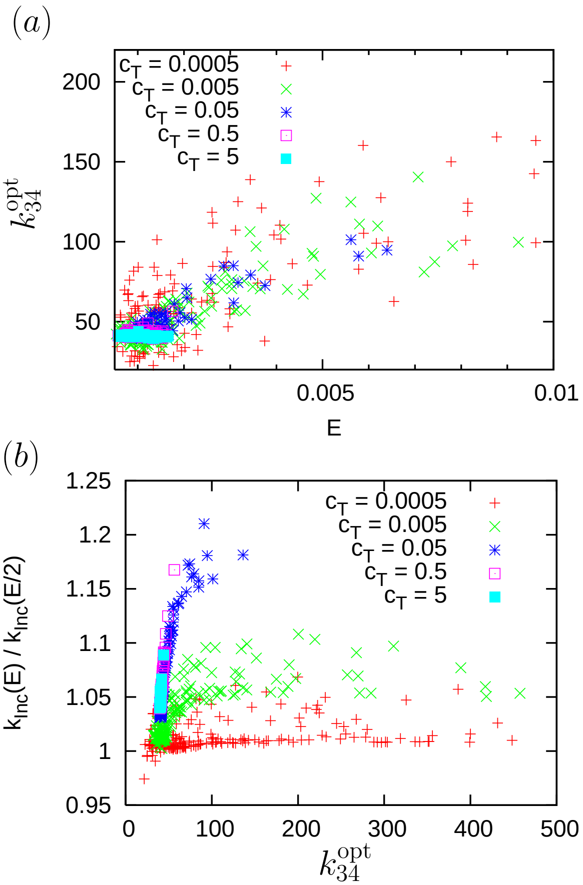

Figure 5.6 (a) Scatter plot of error rate and optimal rate constant k_{34}^{opt} for 200 different random choices of reaction rate constants obtained via a scheme as described in Sect. 5.3.3 for different values of ternary complex concentrations c_T. (b) Scatter plot of the optimal rate constant k_{34}^{opt} and the ratio of incorporation rates with given error rates of E and $E/2$, respectively. The data was obtained from 200 runs as in (a).

5.4 Discussion

Using a kinetic proofreading model for translation in *e-coli* based on experimentally determined rate constants, we have shown that neglecting backward rate constants as is often done in biochemistry can affect the calculated error rate in kinetic proofreading significantly.

Second, we have tested the conjecture that the measured high hydrolyzation rate constant is due to a selectional bias for high protein incorporation rate. This would imply that translational fidelity is sacrificed for translation speed. We find that for a wide parameter range consistent with experiments, the translational machinery does not act at its optimum concerning error rate and translation speed.

There are three possible explanations for this apparent "non-optimality": (i) structural constraints of involved molecules and complexes may have prevented optimal rate constants. (ii) Competing evolutionary goals not addressed in this study, *e. g.* robustness of the translational machinery, may have caused evolutionary pressure leading to the measured rate constants. (iii) Neglecting the complexity of translation (mainly because details are experimentally unknown) in the model, *e. g.* other cognate tRNAs, cellular crowding, and cooperativity among ribosomes, may have caused apparently non-optimal rate constants.

In order to discriminate between these possibilities more experiments, involving also multiple cognate tRNA species, are necessary. In order to test if the translational machinery is optimized for other evolutionary goals, theoretical models for the robustness in genetic networks [168, 169, 170] could be applied and it could be probed both theoretically and in experiments whether cellular crowding and ribosome cooperativity has a significant effect on our results.

6 Perspectives

The main results of this thesis have already been outlined in the Summary chapter. We therefore conclude with perspectives and open questions left for future research.

While we have discussed optimal protocols yielding a minimal mean work for different dynamics and different potentials, it would be interesting to study the relation between optimal protocols for the mean work and optimal free energy calculations. In a broader context, the question whether (or more precisely under which circumstances) the Jarzynski estimate for the free energy difference is better than other free energy calculation methods is still open. However, in order to answer this question conclusively, it is necessary to define an "optimal" strategy for free energy calculations via the Jarzynski relation, combining different strategies from path sampling to optimal protocols. This combined strategy then must include a practical computational scheme to exploit protocol singularities for free energy calculations.

Additionally, it should be studied whether optimal protocols can also improve the reconstruction of free energy landscapes. There are few systematic studies on how to optimize the reconstruction of free energy landscapes from either experiments or simulations. Ultimately, a combined optimal strategy to extract the mobility and the free energy as a function of a reaction coordinate may become very helpful in the construction of effective Langevin dynamics from molecular dynamics simulations.

Beyond the application to free energy calculations, the classification of optimal protocols is of great theoretical interest. For Hamiltonian and Schrödinger dynamics, the question whether the adiabatic work can be achieved in an arbitrarily short time is still open. For Langevin dynamics, systematic studies identifying optimal protocols for anharmonic potentials could probe our conjecture that jumps and singularities generically occur in the optimal protocol.

In this thesis, we only considered optimal protocols for transitions between equilibrium states. For transitions between nonequilibrium steady states, the Jarzynski relation can be generalized to the so called Hatano-Sasa relation. Quite naturally, the question arises whether the features found for optimal protocols between equilibrium states will persist for transitions between nonequilibrium steady states. First of all, however, one has to identify the proper quantity to optimize in such a situation. A minimization of the total entropy production would require the system to be in the steady state with least entropy production for most of the transition time.

For a stochastic heat engine similar to a macroscopic Carnot engine, we have shown that the efficiency at maximum power is given by a simple, quite universal expression. Even though we derived the result using the concept of stochastic thermodynamics, one might expect that under appropriate conditions a "thermodynamic limit" exists, bridging the gap between the mesoscopic system discussed here and macroscopic heat engines. However, such a limit would require underdamped Langevin dynamics in order to include inertia effects which are important for a macroscopic Carnot engine.

For simple molecular motor models, we have found that a transition state near the initial position leads to a high efficiency at maximum power. If future experiments confirmed the indication that myosin motors have a transition state near the initial position for the main motor step (corresponding to an almost force-independent forward rate), it would be tempting to speculate whether evolutionary pressure for efficiency and large power has led to this characteristic. For a more comprehensive answer to this question, however, other evolutionary goals like speed, robustness, and high processivity should be considered. Likewise, the dependence of our results on the interaction between single motor domains needs to be explored in future work.

For a recently introduced scheme of the translation process, we have studied optimal performance regarding error rate and protein production rate. More generally, it would be interesting which evolutionary goals have led to the combined process of gene expression from the DNA template to proteins. Therefore, it is necessary to combine our study with complementary approaches for the transcription process, where proofreading is performed by "backtracks" of the RNA-Polymerase [171, 172].

A Solution of the underdamped optimization problem (case study II)

In this appendix, we give a detailed analysis of the numerical solution of the optimization problem. In order to minimize the integral in Eq. (3.70), the constraint [Eq. (3.72)] is included in an effective Lagrangian $\mathcal{L}_{\text{eff}} \equiv \mathcal{L} - \alpha(\tau)\mathcal{G}$ through a Lagrange multiplier $\alpha(\tau)$. Then the Euler-Lagrange equations whose solutions minimize the integral in Eq. (3.70) are obtained from

$$\frac{\partial \mathcal{L}_{\text{eff}}}{\partial w} + \frac{d^2}{d\tau^2}\frac{\partial \mathcal{L}_{\text{eff}}}{\partial \ddot{w}} = \frac{d}{d\tau}\frac{\partial \mathcal{L}_{\text{eff}}}{\partial \dot{w}}, \qquad \frac{\partial \mathcal{L}_{\text{eff}}}{\partial z} = \frac{d}{d\tau}\frac{\partial \mathcal{L}_{\text{eff}}}{\partial \dot{z}}, \tag{A.1}$$

which, together with the constraint $\mathcal{G} = 0$, define a system of three differential equations for w, z and α. By defining the useful new variable

$$\mu \equiv zw - \frac{m^2}{4}\dot{w}^2 \tag{A.2}$$

we can write the initially cumbersome differential equations (A.1) after a tedious manipulation in the following reduced form

$$\begin{aligned}
\ddot{w} &= \frac{\dot{w}^2}{2w} - \frac{2}{m^2}\frac{\mu}{w} + 2Tw\alpha + \frac{2T}{m}, && \text{(A.3)}\\
\dot{\mu} &= -\frac{2\gamma}{m}\mu + 2\gamma T w, && \text{(A.4)}\\
\dot{\alpha} &= \frac{2\gamma}{m}\alpha + \frac{1}{m}\frac{\dot{w}}{w^2}. && \text{(A.5)}
\end{aligned}$$

These equations have no analytical solution but they can easily be solved numerically for given initial conditions $w(0^+)$, $\dot{w}(0^+)$, $\mu(0^+)$ and $\alpha(0^+)$. It is important to note that some of these initial conditions are not fixed by the initial equilibrium conditions $w(0) = T/\lambda_i$, $\dot{w}(0) = 0$, $\ddot{w}(0) = 0$, $z(0) = mT$, but can be realized by additional discontinuities in the respective quantities at the boundaries. If such discontinuities do not change the value of the integral in Eq. (3.70), they do not affect the optimization of the integral via the Euler-Lagrange equations and hence the respective initial conditions should (in a first step) be treated as free parameters. Since the Langrangian does not depend on

$\ddot{w}(\tau)$, discontinuities in $\dot{w}(\tau)$ and $\ddot{w}(\tau)$ can occur at the boundaries. However, a jump in the mean squared position $w(\tau)$ would affect the integral in Eq. (3.70) and thus $w(\tau)$ must be chosen to be continuous at the boundaries, enforcing $w(0^+) = w(0) \equiv w_0 = T/\lambda_i$. Likewise, discontinuities in $z(\tau)$ can occur at the boundaries. However, the initial values $z(0^+)$ and $\dot{w}(0^+)$ are related by the constraint $\mathcal{G} = 0$. Integrating this constraint

$$\lim_{\epsilon \to 0} \int_{\tau-\epsilon}^{\tau+\epsilon} d\tau' \mathcal{G} = 0 \tag{A.6}$$

leads to

$$[wz]_{\tau^-}^{\tau^+} = \frac{m^2}{4} \left[\dot{w}^2\right]_{\tau^-}^{\tau^+}. \tag{A.7}$$

When applied at $\tau = 0$ it yields

$$\frac{T}{\lambda_i}[z(0^+) - mT] = \frac{m^2}{4}\dot{w}^2(0^+). \tag{A.8}$$

We consider a (possible) discontinuity through the parameter s_1 in

$$z(0^+) \equiv mTs_1. \tag{A.9}$$

With Eq. (A.8), the jump in the derivative of w at the initial time as a function of s_1 becomes

$$\dot{w}(0^+) = \pm 2T\sqrt{\frac{s_1 - 1}{m\lambda_i}}. \tag{A.10}$$

In the case in which $\lambda_i < \lambda_f$, the correct sign is the negative one. Note that the last equation implies $s_1 > 1$, so that at the initial time and given the equilibrium initial distribution, it is not possible to have a decrease in the mean squared momentum. From Eqs. (A.8) and (A.2) we also find

$$\mu(0^+) = mT^2/\lambda_i. \tag{A.11}$$

Secondly, we define a new free parameter s_2 in

$$\dot{y}(0^+) \equiv Ts_2, \tag{A.12}$$

which, from the evolution equation (3.68), directly yields $\ddot{w}(0^+) = \frac{2T}{m}s_2$. Then, writing Eq. (A.3) at $\tau = 0^+$ and inserting the above values, the initial value of the Lagrange multiplier needed to solve the Euler-Lagrange equations is

$$\alpha(0^+) = \frac{\lambda_i}{mT}(s_2 - s_1 + 1). \tag{A.13}$$

Last, from the evolution equations (3.66)-(3.68) we find the relative value of the initial jump in the protocol as a function of s_1 and s_2:

$$\frac{\Delta\lambda_i}{\lambda_i} \equiv \frac{\lambda(0^+) - \lambda_i}{\lambda_i} = s_1 - s_2 - 1 + \gamma\sqrt{\frac{s_1 - 1}{m\lambda_i}}. \tag{A.14}$$

At the end of the process, the value of $z(\tau)$ is allowed to jump again. Recalling Eq. (A.7) applied now at the final time $\tau = t$ and isolating $z(t)$, we obtain

$$z(t) = z(t^-) + \frac{m^2}{4}\frac{\dot{w}(t)^2 - \dot{w}(t^-)^2}{w(t)}. \tag{A.15}$$

Every quantity on the right hand side of the last equation except for $\dot{w}(t)$ is fixed by the solution of the Euler-Lagrange equation. The minimum value for $z(t)$, which leads to the minimal contribution to the work in Eq. (A.18), is reached for $\dot{w}(t) \equiv s_3 = 0$.

For a comparison of the present case with its overdamped analogue as discussed in Chapter 3.2, one can formally integrate the differential equations for μ and α and plug them into Eq. (A.3) to obtain the following integro-differential equation for w,

$$\left(\ddot{w} - \frac{\dot{w}^2}{2w}\right) = \frac{2T}{m}\left[f(\tau)\mathcal{A} - \frac{\mathcal{B}}{f(\tau)} + f(\tau)(1 + s_2 - s_1)\right] \tag{A.16}$$

where $f(\tau) \equiv \frac{w(\tau)}{w_0}e^{2\gamma\tau/m}$ and

$$\mathcal{A} = 1 - \frac{2\gamma}{m}\int_0^\tau \frac{1}{f(\tau')}d\tau', \qquad \mathcal{B} = 1 + \frac{2\gamma}{m}\int_0^\tau f(\tau')d\tau'. \tag{A.17}$$

In the overdamped limit, the Euler-Lagrange equation is given by $\ddot{w} - \dot{w}^2/2w = 0$. Including inertia leads to nonvanishing terms on the right hand side of Eq. (A.16). However, taking the corresponding overdamped limit $\tilde{m} \to 0$ in Eq. (A.16) yields the overdamped Euler-Lagrange equation only after optimizing the parameters s_1 and s_2.

Combining Eqs. (3.66)-(3.68), the work W [Eq. (3.62)] can be written as

$$W = \left[\frac{\lambda w}{2} + \frac{z}{2m}\right]_0^t - \frac{\gamma T}{m}t + \frac{\gamma}{m^2}\int_0^t d\tau z. \tag{A.18}$$

To calculate the integral, we insert the solution of the Euler-Lagrange equations for z, which depends on s_1 and s_2. Then, we need to insert the boundary values for w and z at $\tau = 0$ and $\tau = t$. In a last step, the work is optimized with respect to the free parameters s_1 and s_2.

Bibliography

[1] C. Bustamante, J. Liphardt, and F. Ritort, “The nonequilibrium thermodynamics of small systems,” Physics Today **58(7)**, 43 (2005).

[2] U. Seifert, “Stochastic thermodynamics: Principles and perspectives,” Eur. Phys. J. B **64**, 423–431 (2008).

[3] F. Jülicher, A. Ajdari, and J. Prost, “ Modeling molecular motors,” Rev. Mod. Phys. **69**, 1269 (1997).

[4] R. D. Astumian and P. Hänggi, “Brownian motors,” Physics Today **55(11)**, 33 (2002).

[5] K. Sekimoto, “Kinetic characterisation of heat bath and the energetics of thermal ratchet models,” J. Phys. Soc. Jpn. **66**, 1234–1237 (1997).

[6] K. Sekimoto, “Langevin equation and thermodynamics,” Prog. Theor. Phys. Supp. **130**, 17 (1998).

[7] U. Seifert, “Entropy production along a stochastic trajectory and an integral fluctuation theorem,” Phys. Rev. Lett. **95**, 040602 (2005).

[8] T. Schmiedl, T. Speck, and U. Seifert, “Entropy production for mechanically or chemically driven biomolecules,” J. Stat. Phys. **128**, 77 (2007).

[9] C. Jarzynski, “Nonequilibrium equality for free energy differences,” Phys. Rev. Lett. **78**, 2690 (1997).

[10] C. Jarzynski, “Equilibrium free-energy differences from nonequilibrium measurements: A master-equation approach,” Phys. Rev. E **56**, 5018 (1997).

[11] E. Schöll-Paschinger and C. Dellago, “A proof of Jarzynski’s nonequilibrium work theorem for dynamical systems that conserve the canonical distribution,” J. Chem. Phys. **125**, 054105 (2006).

[12] S. Mukamel, "Quantum extension of the Jarzynski relation : Analogy with stochastic dephasing," Phys. Rev. Lett. **90**, 170604 (2003).

[13] V. Blickle, T. Speck, L. Helden, U. Seifert, and C. Bechinger, "Thermodynamics of a colloidal particle in a time-dependent nonharmonic potential," Phys. Rev. Lett. **96**, 070603 (2006).

[14] D. J. Evans, E. G. D. Cohen, and G. P. Morriss, "Probability of second law violations in shearing steady states," Phys. Rev. Lett. **71**, 2401 (1993).

[15] G. Gallavotti and E. G. D. Cohen, "Dynamical ensembles in nonequilibrium statistical mechanics," Phys. Rev. Lett. **74**, 2694 (1995).

[16] G. E. Crooks, "Entropy production fluctuation theorem and the nonequilibrium work relation for free energy differences," Phys. Rev. E **60**, 2721 (1999).

[17] G. E. Crooks, "Path-ensemble averages in systems driven far from equilibrium," Phys. Rev. E **61**, 2361 (2000).

[18] G. Hummer and A. Szabo, "Free energy reconstruction from nonequilibrium single-molecule pulling experiments," Proc. Natl. Acad. Sci. U.S.A. **98**, 3658 (2001).

[19] T. Hatano and S. Sasa, "Steady-state thermodynamics of Langevin systems," Phys. Rev. Lett. **86**, 3463 (2001).

[20] T. Speck and U. Seifert, "Restoring a fluctuation-dissipation theorem in a nonequilibrium steady state," Europhys. Lett. **74**, 391 (2006).

[21] F. Douarche, S. Joubaud, N. B. Garnier, A. Petrosyan, and S. Ciliberto, "Work fluctuation theorems for harmonic oscillators," Phys. Rev. Lett. **97**, 140603 (2006).

[22] T. Taniguchi and E. G. D. Cohen, "Inertial effects in nonequilibrium work fluctuations by a path integral approach," J. Stat. Phys. **130**, 1–26 (2008).

[23] R. Kawai, J. M. R. Parrondo, and C. V. den Broeck, "Dissipation: The phase-space perspective," Phys. Rev. Lett. **98**, 080602 (2007).

[24] S. Vaikuntanathan and C. Jarzynski, "Escorted free energy simulations: Improving convergence by reducing dissipation," Phys. Rev. Lett. **100**, 190601 (2008).

[25] W. De Roeck and C. Maes, "Quantum version of free-energy-irreversible-work relations," Phys. Rev. E **69**, 026115 (2004).

[26] J. Teifel and G. Mahler, "Model studies on the quantum Jarzynski relation," Phys. Rev. E **76**, 051126 (2007).

[27] P. Reimann, "Brownian motors: noisy transport far from equilibrium," Phys. Rep. **361**, 57 (2002).

[28] K. Sekimoto, F. Takagi, and T. Hondou, "Carnot's cycle for small systems: Irreversibility and cost of operations," Phys. Rev. E **62**, 7759 (2000).

[29] J. M. R. Parrondo and B. J. D. Cisneros, "Energetics of Brownian motors: a review," Applied Physics A **75**, 179 (2002).

[30] A. Parmeggiani, F. Jülicher, A. Ajdari, and J. Prost, "Energy transduction of isothermal ratchets: Generic aspects and specific examples close to and far from equilibrium," Phys. Rev. E **60**, 2127 (1999).

[31] T. Hondou and K. Sekimoto, "Unattainability of Carnot efficiency in the Brownian heat engine," Phys. Rev. E **62**, 6021 (2000).

[32] C. van den Broeck, "Carnot efficiency revisited," Adv. Chem. Phys. **135**, 189–201 (2007).

[33] U. Seifert, "Fluctuation theorem for a single enzym or molecular motor," Europhys. Lett. **70**, 36 (2005).

[34] A. W. C. Lau, D. Lacoste, and K. Mallick, "Non-equilibrium fluctuations and mechanochemical couplings of a molecular motor," Phys. Rev. Lett. **99**, 158102 (2007).

[35] S. Velasco, J. M. M. Roco, A. Medina, and A. C. Hernandez, "Feynman's ratchet optimization: maximum power and maximum efficiency regimes," J. Phys. D **34**, 1000–1006 (2001).

[36] M. Asfaw and M. Bekele, "Energetics of a simple microscopic heat engine," Phys. Rev. E **72**, 056109 (2005).

[37] Z. C. Tu, “Efficiency at maximum power of Feynman’s ratchet as a heat engine,” J. Phys. A: Math. Gen. **41**, 312003 (2008).

[38] J. M. R. Parrondo, G. Harmer, and D. Abbott, “New paradoxical games based on Brownian ratchets,” Phys. Rev. Lett. **85**, 5226 (2000).

[39] P. Amengual, A. Allison, R. Toral, and D. Abbott, “Discrete-time ratchets, the Fokker-Planck equation and Parrondo’s paradox,” Proc. Roy. Soc. London A **460**, 2269 (2004).

[40] L. Dinis, “Optimal sequence for Parrondo games,” Phys. Rev. E **77**, 021124 (2008).

[41] M. B. Tarlie and R. D. Astumian, “Optimal modulation of a Brownian ratchet and enhanced sensitivity to a weak external force,” Proc. Natl. Acad. Sci. U.S.A. **95**, 2039–2043 (1998).

[42] S. J. Lade, “The optimal driving waveform for overdamped, adiabatic rocking ratchets,” J. Phys. A: Mathematical and Theoretical **41**, 275103 (2008).

[43] S. M. Bezrukov, A. M. Berezhkovskii, and A. Szabo, “Diffusion model of solute dynamics in a membrane channel: Mapping onto the two-site model and optimizing the flux,” J. Chem. Phys. **127**, 115101 (2007).

[44] F. Berger, T. Schmiedl, and U. Seifert, “Optimal potentials for temperature ratchets,” arXiv:0807.4644, (2008).

[45] F. J. Cao, L. Dinis, and J. M. R. Parrondo, “Feedback control in a collective flashing ratchet,” Phys. Rev. Lett. **93**, 040603 (2004).

[46] E. M. Craig, N. J. Kuwada, B. J. Lopez, and H. Linke, “Feedback control in flashing ratchets,” Annalen der Physik **17**, 115 (2008).

[47] A. Ashkin, J. Dziedzic, J. Bjorkholm, and S. Chu, “Observation of a single-beam gradient force optical trap for dielectric particles,” Opt. Lett. **11**, 288 (1986).

[48] V. Blickle, T. Speck, C. Lutz, U. Seifert, and C. Bechinger, “Einstein relation generalized to nonequilibrium,” Phys. Rev. Lett. **98**, 210601 (2007).

[49] V. Blickle, T. Speck, U. Seifert, and C. Bechinger, "Characterizing potentials by a generalized Boltzmann factor," Phys. Rev. E **75**, 060101 (2007).

[50] T. Speck, V. Blickle, C. Bechinger, and U. Seifert, "Distribution of entropy production for a colloidal particle in a nonequilibrium steady state," EPL **79**, 30002 (2007).

[51] R. W. Zwanzig, "High-temperature equation of state by a perturbation method. 1. nonpolar gases," J. Chem. Phys. **22**, 1420–1426 (1954).

[52] D. A. Hendrix and C. Jarzynski, "A "fast growth" method of computing free energy differences," J. Chem. Phys. **114**, 5974 (2001).

[53] G. Hummer, "Fast-growth thermodynamic integration: Error and efficiency analysis," J. Chem. Phys. **114**, 7330 (2001).

[54] M. R. Shirts, E. Bair, G. Hooker, and V. S. Pande, "Equilibrium free energies from nonequilibrium measurements using maximum-likelihood methods," Phys. Rev. Lett. **91**, 140601 (2003).

[55] P. Maragakis, M. Spichty, and M. Karplus, "Optimal estimates of free energies from multistate nonequilibrium work data," Phys. Rev. Lett. **96**, 100602 (2006).

[56] J. Liphardt, S. Dumont, S. B. Smith, I. Tinoco Jr, and C. Bustamante, "Equilibrium information from nonequilibrium measurements in an experimental test of Jarzynski's equality," Science **296**, 1832 (2002).

[57] D. Collin, F. Ritort, C. Jarzynski, S. Smith, I. Tinoco, and C. Bustamante, "Verification of the crooks fluctuation theorem and recovery of RNA folding free energies," Nature **437**, 231 (2005).

[58] D. D. L. Minh, "Free-energy reconstruction from experiments performed under different biasing programs," Phys. Rev. E **74**, 061120 (2006).

[59] C. F. Narambuena, D. M. Beltramo, and E. P. M. Leiva, "Polyelectrolyte adsorption on a charged surface. Free energy calculation from monte carlo simulations using Jarzynski equality," Macromolecules **41**, 8267–8274 (2008).

[60] S. Park and K. Schulten, “Calculating potentials of mean force from steered molecular dynamics simulations,” J. Chem. Phys. **120**, 5946 (2004).

[61] O. Braun, A. Hanke, and U. Seifert, “Probing molecular free energy landscapes by periodic loading,” Phys. Rev. Lett. **93**, 158105 (2004).

[62] G. Hummer and A. Szabo, “Free energy surfaces from single-molecule force spectroscopy,” Acc. Chem. Res. **38**, 504–513 (2005).

[63] D. D. L. Minh, “Multidimensional potentials of mean force from biased experiments along a single coordinate,” J. Phys. Chem. B **111**, 4137–4140 (2007).

[64] A. Imparato, S. Luccioli, and A. Torcini, “Reconstructing the free-energy landscape of a mechanically unfolded model protein,” Phys. Rev. Lett. **99**, 168101 (2007).

[65] S. Luccioli, A. Imparato, and A. Torcini, “Free-energy landscape of mechanically unfolded model proteins: Extended Jarzinsky versus inherent structure reconstruction,” Phys. Rev. E **78**, 031907 (2008).

[66] D. D. L. Minh and J. A. McCammon, “Springs and speeds in free energy reconstruction from irreversible single-molecule pulling experiments,” J. Phys. Chem. B **112**, 5892–5897 (2008).

[67] N. C. Harris, Y. Song, and C. H. Kiang, “Experimental free energy surface reconstruction from single-molecule force spectroscopy using Jarzynski’s equality,” Phys. Rev. Lett. **99**, 068101 (2007).

[68] R. W. Friddle, “Experimental free energy surface reconstruction from single-molecule force spectroscopy using Jarzynski’s equality - comment,” Phys. Rev. Lett. **100**, 019801 (2008).

[69] N. C. Harris, Y. Song, and C. H. Kiang, “Experimental free energy surface reconstruction from single-molecule force spectroscopy using Jarzynski’s equality - reply,” Phys. Rev. Lett. **100**, 019802 (2008).

[70] C. Micheletti, G. Bussi, and A. Laio, “Optimal Langevin modeling of out-of-equilibrium molecular dynamics simulations,” J. Chem. Phys. **129**, 074105 (2008).

[71] J. Gottschall and J. Peinke, “On the definition and handling of different drift and diffusion estimates,” New J. Phys. **10**, 083034 (2008).

[72] R. Hegger and G. Stock, “Multidimensional Langevin modeling of biomolecular dynamics,” J. Chem. Phys. **130**, 034106 (2009).

[73] J. Gore, F. Ritort, and C. Bustamante, “Bias and error in estimates of equilibrium free-energy differences from nonequilibrium measurements,” Proc. Natl. Acad. Sci. U.S.A. **100**, 12564 (2003).

[74] C. Jarzynski, “Rare events and the convergence of exponentially averaged work values,” Phys. Rev. E **73**, 046105 (2006).

[75] F. M. Ytreberg and D. M. Zuckerman, “Single-ensemble nonequilibrium path-sampling estimates of free energy differences,” J. Chem. Phys. **120**, 10876 (2004).

[76] E. Atilgan and S. X. Sun, “Equilibrium free energy estimates based on nonequilibrium work relations and extended dynamics,” J. Chem. Phys. **121**, 10392 (2004).

[77] D. Wu and D. A. Kofke, “Rosenbluth-sampled nonequilibrium work method for calculation of free energies in molecular simulation,” J. Chem. Phys. **122**, 204104 (2005).

[78] W. Lechner, H. Oberhofer, and C. Dellago, “Equilibrium free energies from fast-switching trajectories with large time steps,” J. Chem. Phys. **124**, 044113 (2006).

[79] A. M. Hahn and H. Then, “Using bijective maps to improve free energy estimates,” Phys. Rev. E **79**, 011113 (2009).

[80] D. D. L. Minh, “Inverting the nonequilibrium path sampling problem,” arXiv:0901.3369v1, (2009).

[81] D. D. L. Minh and A. B. Adib, “Optimized free energies from bidirectional single-molecule force spectroscopy,” Phys. Rev. Lett. **100**, 180602 (2008).

[82] H. Oberhofer, C. Dellago, and P. L. Geissler, “Biased sampling of nonequilibrium trajectories: Can fast switching simulations outperform conventional free energy calculation methods?,” J. Phys. Chem. B **109**, 6902 (2005).

[83] F. M. Ytreberg, R. H. Swendsen, and D. M. Zuckerman, “Comparison of free energy methods for molecular systems,” J. Chem. Phys. **125**, 184114 (2006).

[84] W. Lechner and C. Dellago, “On the efficiency of path sampling methods for the calculation of free energies from non-equilibrium simulations,” J. Stat. Mech.: Theor. Exp.,P04001 (2007).

[85] G. M. Torrie and J. P. Valleau, “Non-physical sampling distributions in Monte-Carlo free-energy estimation - umbrella sampling,” J. Comput. Phys. **23**, 187–199 (1977).

[86] F. G. Wang and D. P. Landau, “Efficient, multiple-range random walk algorithm to calculate the density of states,” Phys. Rev. Lett. **86**, 2050–2053 (2001).

[87] P. Maragakis, F. Ritort, C. Bustamante, M. Karplus, and G. E. Crooks, “Bayesian estimates of free energies from nonequilibrium work data in the presence of instrument noise,” arXiv:0707.0089v1, (2007).

[88] J. C. Schön, “A thermodynamic distance criterion of optimality for the calculation of free energy changes from computer simulations,” J. Chem. Phys. **105**, 10072 (1996).

[89] M. de Koning, “Optimizing the driving function for nonequilibrium free-energy calculations in the linear regime: A variational approach,” J. Chem. Phys. **122**, 104106 (2005).

[90] W. P. Reinhardt and J. E. Hunter, “Variational path optimization and upper and lower bounds to free energy changes via finite time minimization of external work,” J. Chem. Phys. **97**, 1599 (1992).

[91] J. E. Hunter, W. P. Reinhardt, and T. F. Davis, “A finite-time variational method for determining optimal paths and obtaining bounds on free energy changes from computer simulations,” J. Chem. Phys. **99**, 6856 (1993).

[92] G. M. Wang, E. M. Sevick, E. Mittag, D. J. Searles, and D. J. Evans, “Experimental demonstration of violations of the second law of thermodynamics for small systems and short time scales,” Phys. Rev. Lett. **89**, 050601 (2002).

[93] D. M. Carberry, J. C. Reid, G. M. Wang, E. M. Sevick, D. J. Searles, and D. J. Evans, "Fluctuations and irreversibility: An experimental demonstration of a second-law-like theorem using a colloidal particle held in an optical trap," Phys. Rev. Lett. **92**, 140601 (2004).

[94] E. H. Trepagnier, C. Jarzynski, F. Ritort, G. E. Crooks, C. J. Bustamante, and J. Liphardt, "Experimental test of Hatano and Sasa's nonequilibrium steady-state equality," Proc. Natl. Acad. Sci. U.S.A. **101**, 15038 (2004).

[95] M. Sotomayor and K. Schulten, "Single-molecule experiments in vitro and in silico," Science **316**, 1144–1148 (2007).

[96] C. Jarzynski, "Hamiltonian derivation of a detailed fluctuation theorem," J. Stat. Phys. **98**, 77–102 (2000).

[97] S. X. Sun, "Generating generalized distributions from dynamical simulation," J. Chem. Phys. **118**, 5769 (2003).

[98] A. E. Allahverdyan and T. M. Nieuwenhuizen, "Minimal-work principle and its limits for classical systems," Phys. Rev. E **75**, 051124 (2007).

[99] A. Engel and R. Nolte, "Failure of Jarzynski identity for a simple quantum system," EPL **79**, 10003 (2007).

[100] P. Talkner, E. Lutz, and P. Hänggi, "Fluctuation theorems: Work is not an observable," Phys. Rev. E **75**, 050102 (2007).

[101] G. E. Crooks, "On the Jarzynski relation for dissipative quantum dynamics," J. Stat. Mech.: Theor. Exp.,P10023 (2008).

[102] M. Esposito, U. Harbola, and S. Mukamel, "Nonequilibrium fluctuations, fluctuation theorems, and counting statistics in quantum systems," arXiv:0811.3717, (2008).

[103] S. Deffner and E. Lutz, "Nonequilibrium work distribution of a quantum harmonic oscillator," Phys. Rev. E **77**, 021128 (2008).

[104] P. Talkner, B. P. S, and H. P, "Statistics of work performed on a forced quantum oscillator," Phys. Rev. E **78**, 011115 (2008).

[105] Y. B. Band, O. Kafri, and P. Salamon, "Finite-time thermodynamics - optimal expansion of a heated working fluid," J. Appl. Phys. **53**, 8 (1982).

[106] H. Then and A. Engel, “Computing the optimal protocol for finite-time processes in stochastic thermodynamics,” Phys. Rev. E **77**, 041105 (2008).

[107] C. Dellago, private communication (unpublished).

[108] In Ref. [104], Talkner et al. discuss the case of a time-dependent, spatially constant force acting on a quantum harmonic oscillator. This additional force tilts the potential and leads to both a moving potential minimum and a lowering of the potential. This situation is slightly different from the moving harmonic potential where the minimum of the potential is only moved horizontally. However, both Hamiltonians can be transferred into each other by adding a term proportional to the square of the force.

[109] S. H. Shi, A. Woody, and H. Rabitz, “Optimal-control of selective vibrational-excitation in harmonic linear-chain molecules,” J. Chem. Phys. **88**, 6870–6883 (1988).

[110] R. S. Judson and H. Rabitz, “Teaching lasers to control molecules,” Phys. Rev. Lett. **68**, 1500–1503 (1992).

[111] Y. J. Yan, R. E. Gillilan, R. M. Whitnell, K. R. Wilson, and S. Mukamel, “Optical control of molecular-dynamics - Liouville-space theory,” J. Phys. Chem. **97**, 2320–2333 (1993).

[112] R. J. Gordon and S. A. Rice, “Active control of the dynamics of atoms and molecules,” Annu. Rev. Phys. Chem. **48**, 601–641 (1997).

[113] O. Mazonka and C. Jarzynski, cond-mat/9912121 (unpublished).

[114] F. L. Curzon and B. Ahlborn, “Efficiency of a Carnot engine at maximum power output,” Am. J. Phys. **43**, 22 (1975).

[115] K. H. Hoffmann, J. Burzler, A. Fischer, M. Schaller, and S. Schubert, “Optimal process paths for endoreversible systems,” J. Noneq. Thermodyn. **28**, 233–268 (2003).

[116] C. van den Broeck, “Thermodynamic efficiency at maximum power,” Phys. Rev. Lett. **95**, 190602 (2005).

[117] B. J. de Cisneros and A. C. Hernández, “Collective working regimes for coupled heat engines,” Phys. Rev. Lett. **98**, 130602 (2007).

[118] R. P. Feynman, R. B. Leighton, and M. Sands, *The Feynman Lectures on Physics* (Addison-Wesley, Reading, MA, 1966).

[119] M. Büttiker, “Transport as a consequence of state-dependent diffusion,” Z. Phys. B **68**, 161 (1987).

[120] R. Landauer, “Motion out of noisy states,” J. Stat. Phys. **53**, 233 (1988).

[121] M. Asfaw and M. Bekele, “Current, maximum power and optimized efficiency of a Brownian heat engine,” Eur. Phys. J. B **38**, 457 (2004).

[122] A. Gomez-Marin and J. M. Sancho, “Tight coupling in thermal Brownian motors,” Phys. Rev. E **74**, 062102 (2006).

[123] M. Esposito, K. Lindenberg, and C. Van den Broeck, “Thermoelectric efficiency at maximum power in a quantum dot,” arXiv:0808.0216, (2008).

[124] M. Esposito, K. Lindenberg, and C. van den Broeck, “Universality of efficiency at maximum power,” arXiv:0901.2600v1, (2009).

[125] Y. M. Blanter and M. Büttiker, “Rectification of fluctuations in an underdamped ratchet,” Phys. Rev. Lett. **81**, 4040 (1998).

[126] S. Duhr and D. Braun, “Thermophoretic depletion follows Boltzmann distribution,” Phys. Rev. Lett. **96**, 168301 (2006).

[127] S. Duhr and D. Braun, “Why molecules move along a temperature gradient,” Proc. Natl. Acad. Sci. U.S.A. **103**, 19678–19682 (2007).

[128] F. M. Weinert, J. A. Kraus, T. Franosch, and D. Braun, “Microscale fluid flow induced by thermoviscous expansion along a traveling wave,” Phys. Rev. Lett. **100**, 164501 (2008).

[129] P. Reimann, R. Bartussek, R. Haussler, and P. Hänggi, “Brownian motors driven by temperature oscillations,” Phys. Lett. A **215**, 26–31 (1996).

[130] I. M. Sokolov and A. Blumen, “Non-equilibrium directed diffusion and inherently irreversible heat engines,” J. Phys. A: Math. Gen. **30**, 3021–3027 (1997).

[131] I. M. Kulic, R. Thaokar, and H. Schiessel, “A DNA ring acting as a thermal ratchet,” J. Phys.: Condens. Matter **17**, S3965–S3978 (2005).

[132] C. Jarzynski and O. Mazonka, “Feynman’s ratchet and pawl: An exactly solvable model,” Phys. Rev. E **59**, 6448–6459 (1999).

[133] C. van den Broeck, R. Kawai, and P. Meurs, “Microscopic analysis of a thermal Brownian motor,” Phys. Rev. Lett. **93**, 090601 (2004).

[134] J. Howard, *Mechanics of Motor Proteins and the Cytoskeleton* (Sinauer, New York, 1. ed., 2001).

[135] N. J. Carter and R. A. Cross, “Mechanics of the kinesin step,” Nature **435**, 308 (2005).

[136] A. D. Mehta, R. S. Rock, M. Rief, J. A. Spudich, M. S. Mooseker, and R. E. Cheney, “Myosin-V is a processive actin-based motor,” Nature **400**, 590 (1999).

[137] A. E. M. Clemen, M. Vilfan, J. Jaud, J. S. Zhang, M. Barmann, and M. Rief, “Force-dependent stepping kinetics of myosin-V,” Biophys. J. **88**, 4402–4410 (2005).

[138] J. C. M. Gebhardt, A. E. M. Clemen, J. Jaud, and M. Rief, “Myosin-V is a mechanical ratchet,” Proc. Natl. Acad. Sci. U.S.A. **103**, 8680–8685 (2006).

[139] R. Yasuda, H. Noji, K. Kinosita, and M. Yoshida, “F1-ATPase is a highly efficient molecular motor that rotates with discrete 120 degree steps,” Cell **93**, 1117 (1998).

[140] D. Okunoa, R. Fujisawaa, R. Iinoa, Y. Hirono-Harab, H. Imamuraa, and H. Noji, “Correlation between the conformational states of F1-ATPase as determined from its crystal structure and single-molecule rotation,” Proc. Natl. Acad. Sci. U.S.A. **105**, 20722–20727 (2008).

[141] R. D. Astumian and M. Bier, “Fluctuation driven ratchets - molecular motors,” Phys. Rev. Lett. **72**, 1766–1769 (1994).

[142] M. E. Fisher and A. B. Kolomeisky, “The force exerted by a molecular motor,” Proc. Natl. Acad. Sci. U.S.A. **96**, 6597 (1999).

[143] R. Lipowsky, “Universal aspects of the chemomechanical coupling for molecular motors,” Phys. Rev. Lett. **85**, 4401 (2000).

[144] M. E. Fisher and A. B. Kolomeisky, “Simple mechanochemistry describes the dynamics of kinesin molecules,” Proc. Natl. Acad. Sci. U.S.A. **98**, 7748–7753 (2001).

[145] A. B. Kolomeisky and M. E. Fisher, “A simple kinetic model describes the processivity of myosin-V,” Biophys. J. **84**, 1642–1650 (2003).

[146] S. Liepelt and R. Lipowsky, “Kinesin’s network of chemomechanical motor cycles,” Phys. Rev. Lett. **98**, 258102 (2007).

[147] J. Howard, “Protein power strokes,” Curr. Biol. **16**, R517 (2006).

[148] R. Lipowsky and S. Liepelt, “Chemomechanical coupling of molecular motors: Thermodynamics, network representations, and balance conditions,” J. Stat. Phys. **130**, 39–67 (2008).

[149] F. J. Kull, E. P. Sablin, R. Lau, R. J. Fletterick, and R. D. Vale, “Crystal structure of the kinesin motor domain reveals a structural similarity to myosin,” Nature **380**, 550–555 (1996).

[150] D. Tsygankov and M. E. Fisher, “Mechanoenzymes under superstall and large assisting loads reveal structural features,” Proc. Natl. Acad. Sci. U.S.A. **104**, 19321–19326 (2007).

[151] B. Alberts, D. Bray, A. Johnson, J. Lewis, M. Raff, K. Roberts, and P. Walter, *Molecular Biology of the Cell* (Garland (New York), 2002).

[152] J. M. Ogle and V. Ramakrishnan, “Structural insights into translational fidelity,” Annu. Rev. Biochem. **74**, 129–177 (2005).

[153] J. J. Hopfield, “Kinetic proofreading: A new mechanism for reducing errors in biosynthetic processes requiring high specificity,” Proc. Natl. Acad. Sci. U.S.A. **71**, 4135 (1974).

[154] J. Ninio, “Kinetic amplification of enzyme discrimination,” Biochimie **57**, 587 (1975).

[155] R. C. Thompson and A. M. Karim, “The accuracy of protein-biosynthesis is limited by its speed - high fidelity selection by ribosomes of aminoacyl-transfer RNA ternary complexes containing GTP[gamma-s],” Proc. Natl. Acad. Sci. U.S.A. **79**, 4922 (1982).

[156] M. Ehrenberg and C. G. Kurland, “Costs of accuracy determined by a maximal growth rate constraint,” Q. Rev. Biophys. **17**, 45 (1984).

[157] C. G. Kurland and M. Ehrenberg, “Growth-optimizing accuracy of gene expression,” Annu. Rev. Biophys. Biophys. Chem. **16**, 291 (1987).

[158] K. B. Gromadski and M. V. Rodnina, “Kinetic determinants of high-fidelity tRNA discrimination on the ribosome,” Mol. Cell **13**, 191 (2004).

[159] H. Zouridis and V. Hatzimanikatis, “A model for protein translation: Polysome self-organization leads to maximum protein synthesis rates,” Biophys. J. **92**, 717 (2007).

[160] D. Andrieux and P. Gaspard, “Nonequilibrium generation of information in copolymerization processes,” Proc. Natl. Acad. Sci. U.S.A. **105**, 9516–9521 (2008).

[161] M. Ehrenberg and C. Blomberg, “Thermodynamic constraints on kinetic proofreading in biosynthetic pathways,” Biophys. J. **31**, 333 (1980).

[162] M. A. Savageau and R. R. Freter, “Energy cost of proofreading to increase fidelity of transfer ribonucleic acid aminoacylation,” Biochemistry **18**, 3486 (1979).

[163] T. Pape, W. Wintermeyer, and M. Rodnina, “Induced fit in initial selection and proofreading of aminoacyl-tRNA on the ribosome,” EMBO Journal **18**, 3800 (1999).

[164] H. S. Zaher and R. Green, “Quality control by the ribosome following peptide bond formation,” Nature **457**, 161–166 (2009).

[165] T. L. Hill, *Free Energy Transduction and Biochemical Cycle Kinetics*, 2nd ed. (Dover, 1989).

[166] J. Schnakenberg, “Network theory of microscopic and macroscopic behavior of master equation systems,” Rev. Mod. Phys. **48**, 571 (1976).

[167] K. B. Gromadski, T. Daviter, and M. V. Rodnina, “A uniform response to mismatches in codon-anticodon complexes ensures ribosomal fidelity,” Mol. Cell **21**, 369 (2006).

[168] N. Barkai and S. Leibler, “Robustness in simple biochemical networks,” Nature **387**, 913–917 (1997).

[169] A. Becskei and L. Serrano, "Engineering stability in gene networks by autoregulation," Nature **405**, 590–593 (2000).

[170] H. Kitano, "Biological robustness," Nat. Rev. Genet. **5**, 826–837 (2004).

[171] E. A. Galburt, S. W. Grill, A. Wiedmann, L. Lubkowska, J. Choy, E. Nogales, M. Kashlev, and C. Bustamante, "Backtracking determines the force sensitivity of RNAP II in a factor-dependent manner," Nature **446**, 820–823 (2007).

[172] M. Depken, private communication (unpublished).

List of publications

Stochastic Thermodynamics is a very active and competitive research field. Therefore, some results of this thesis have already been published, as listed in the following.

- T. Schmiedl and U. Seifert. Optimal finite-time processes in stochastic thermodynamics. *Phys. Rev. Lett.*, **98**, 108301 (2007).
- T. Schmiedl and U. Seifert. Efficiency at maximum power: An analytically solvable model for stochastic heat engines. *EPL*, **81**, 20003 (2008).
- A. Gomez-Marin, T. Schmiedl, and U. Seifert. Optimal protocols for minimal work processes in underdamped stochastic thermodynamics. *J. Chem. Phys.*, **129**, 024114 (2008).
- T. Schmiedl and U. Seifert. Efficiency of molecular motors at maximum power. *EPL*, **83**, 30005 (2008).
- T. Schmiedl, E. Dieterich, P. Dieterich, and U. Seifert. Optimal protocols for Hamiltonian and Schrödinger dynamics. *arXiv:0902.2182* (2009).

Lebenslauf

Persönliche Daten:

Name	Tim Schmiedl
Geburtstag	31.01.1982
Geburtsort	Zweibrücken

Schulbildung:

1988-1991	Hermann-Hedenus-Grundschule Erlangen
1991-1992	Haidenhof-Grundschule Passau
1992-2001	Maristengymnasium Fürstenzell
2001	Abitur, Maristengymnasium Fürstenzell

Studium:

2001-2002	Fernstudium “Früheinstieg ins Physikstudium”, Universität Kaiserslautern
2002-2006	Diplomstudium Physik, Universität Stuttgart
10/2003	Vordiplom Physik
02/2006	Diplom Physik Diplomarbeit : “Fluktuationstheorien für chemische Reaktionen”
2006-2009	Promotion bei Prof. Dr. U. Seifert, Universität Stuttgart

Acknowledgement

I am grateful for the help of many people who contributed to the completion of this thesis. First and foremost, I want to thank my supervisor Prof. Dr. Udo Seifert for his competent advice and his skilled direction of research as well as for numerous discussions about fundamental and practical issues. Particularly, I acknowledge his profound committment to excellence in scientific research. I want to thank Prof. Dr. Günter Mahler for writing the second report on my dissertation and the very interesting discussion on the definition of work for quantum systems. I am indebted to Anja Steinhauser for her obliging and unbureaucratic help in all administrative and semi-administrative subjects. During my dissertation, the atmosphere at the institute has always been very comfortable and I want to thank all present and former colleagues. Particularly, I want to acknowledge

- Dr. Alex Gomez-Marin for the fruitful collaboration during his stay at our institute.
- Florian Berger for the fruitful and very pleasant collaboration during his diploma thesis.
- Dr. Peter Graf, Roman Bedau, and Stefan Leitenberger for the administration of the computer network and particularly for their permanent readiness to help me with all sorts of computer problems.
- Dr. Reimar Finken and Steffen Keßler for their help with mathematical questions and numerous discussions about physical problems.
- Dr. Reimar Finken and Stefan Leitenberger for their optimal proofreading of parts of the manuscript.